A Szilikátipari Tudományos Egyesület lapja

építőanyag

Journal of Silicate Based and Composite Materials

A TARTALOMBÓL:

2021/1

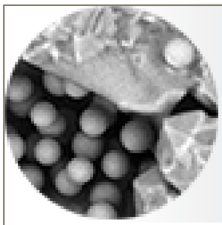

We are pleased to announce the organization of

ec-siliconf2

THE 2ND EUROPEAN CONFERENCE ON SILICON AND SILICA BASED MATERIALS

to be held in Hotel Palota in Miskolc-Lillafüred, Hungary, in October 4-8, 2021

The **ec-siliconf2** conference will be held in the wonderful palace of **Hotel Palota** in the exceptionally beautiful environment of **Beech Mountain** in **Miskolc-Lillafüred** in **Hungary**.
In 2019 in the previous conference scientists had participated from **21** countries of **Asia, Europe, North- and South America** and **Africa**.

THE CONFERENCE SESSIONS

SESSION 1: Silicon and silica in inorganic and molecular chemistry
SESSION 2: Metallic silicon and silicon as an alloying agent
SESSION 3: Silicon (Si) and silica ($SiO2$) in medicine, therapy and health
SESSION 4: Silicon in micro and nanoelectronics and devices
SESSION 5: Silicon and silica in functional materials
SESSION 6: Silicon and silica in polymers
SESSION 7: Silicon and silica in ceramics and composites
SESSION 8: Silicon and silica in construction materials and glass
SESSION 9: Silicon and silica in biological systems and technologies
SESSION 10: Silicon and silica in smart materials and technologies
SESSION 11: Silicon and silica in minerals and rocks
SESSION 12: Testing and characterization methods, tools and errors
SESSION 13: Other results in research and development of silicon and silica and materials contain of them
SESSION 14: Other results in processing and application of silicon and silica and materials contain of them
SESSION 15: Miscellaneous in silicon and silica materials science

Registration abstract submission, and further information are available in:
www.ec-siliconf.eu

építőanyag

2021/1

Journal of Silicate Based and Composite Materials

TARTALOM

CONTENT

A finomkerámia-, üveg-, cement-, mész-, beton-, tégla- és cserép-, kő- és kavics-, tűzállóanyag-, szigetelőanyag-iparágak szakmai lapja
Scientific journal of ceramics, glass, cement, concrete, clay products, stone and gravel, insulating and fireproof materials and composites

Szerkesztőbizottság ▪ Editorial board
Prof. Dr. GÖMZE A. László – elnök/president
GYURKÓ Zoltán – főszerkesztő/editor-in-chief
Dr. habil. BOROSNYÓI Adorján – vezető szerkesztő/senior editor
WOJNÁROVITSNÉ Dr. HRAPKA Ilona – örökös tiszteletbeli felelős szerkesztő/honorary editor-in-chief
TÓTH-ASZTALOS Réka – tervezőszerkesztő/design editor

Tagok ▪ Members
Prof. Dr. Parvin ALIZADEH, Dr. Benchaa BENABED, BOCSKAY Balázs, Prof. Dr. CSŐKE Barnabás, Prof. Dr. Emad M. M. EWAIS, Prof. Dr. Katherine T. FABER, Prof. Dr. Saverio FIORE, Prof. Dr. David HUI, Prof. Dr. GÁLOS Miklós, Dr. Viktor GRIBNIAK, Prof. Dr. Kozo ISHIZAKI, Dr. JÓZSA Zsuzsanna, KÁRPÁTI László, Dr. KOCSERHA István, Dr. KOVÁCS Kristóf, Prof. Dr. Sergey N. KULKOV, Dr. habil. LUBLÓY Éva, MATTYASOVSZKY ZSOLNAY Eszter, Dr. MUCSI Gábor, Dr. Salem G. NEHME, Dr. PÁLVÖLGYI Tamás,Prof. Dr. Tomasz SADOWSKI, Prof. Dr. Tohru SEKINO, Prof. Dr. David S. SMITH, Prof. Dr. Bojja SREEDHAR, Prof. Dr. SZÉPVÖLGYI János, Prof. Dr. SZŰCS István, Prof. Dr. Yasunori TAGA, Dr. Zhifang ZHANG

Tanácsadó Testület ▪ Advisory board
FINTA Ferenc, KISS Róbert, Dr. MIZSER János

A folyóiratot referálja · The journal is referred by:

A folyóiratban lektorált cikkek jelennek meg.
All published papers are peer-reviewed.
Kiadó · Publisher: Szilikátipari Tudományos Egyesület (SZTE)
Elnök · President: ASZTALOS István
1034 Budapest, Bécsi út 120.
Tel.: +36-1/201-9360 ▪ E-mail: epitoanyag@szte.org.hu
Tördelő szerkesztő · Layout editor: NÉMETH Hajnalka
Címlapfotó · Cover photo: GYURKÓ Zoltán

Hirdetési árak 2021 ▪ ADVERTISING RATES 2021:

B2 borító színes · cover colour	76 000 Ft	304 EUR
B3 borító színes · cover colour	70 000 Ft	280 EUR
B4 borító színes · cover colour	85 000 Ft	340 EUR
1/1 oldal színes · page colour	64 000 Ft	256 EUR
1/1 oldal fekete-fehér · page b&w	32 000 Ft	128 EUR
1/2 oldal színes · page colour	32 000 Ft	128 EUR
1/2 oldal fekete-fehér · page b&w	16 000 Ft	64 EUR
1/4 oldal színes · page colour	16 000 Ft	64 EUR
1/4 oldal fekete-fehér · page b&w	8 000 Ft	32 EUR

Az árak az áfát nem tartalmazzák. · Without VAT.

A hirdetési megrendelő letölthető a folyóirat honlapjáról.
Order-form for advertisement is avaliable on the website of the journal.

WWW.EPITOANYAG.ORG.HU
EN.EPITOANYAG.ORG.HU

Online ISSN: 2064-4477
Print ISSN: 0013-970x
INDEX: 2 52 50 ▪ 73 (2021) 1–38

Az SZTE támogató tagvállalatai
Supporting companies of SZTE

3B Hungária Kft. ▪ Akadémiai Kiadó Zrt. ▪ ANZO Kft.
Baranya-Tégla Kft. ▪ Berényi Téglaipari Kft.
Beton Technológia Centrum Kft. ▪ Budai Tégla Zrt.
Budapest Keramia Kft. ▪ CERLUX Kft.
COLAS-ÉSZAKKŐ Bányászati Kft. ▪ Daniella Ipari Park Kft.
Electro-Coord Magyarország Nonprofit Kft.
Fátyolüveg Gyártó és Kereskedelmi Kft.
Fehérvári Téglaipari Kft.
Geoteam Kutatási és Vállalkozási Kft.
Guardian Orosháza Kft. ▪ Interkerám Kft.
KK Kavics Beton Kft. ▪ KŐKA Kő- és Kavicsbányászati Kft.
KTI Nonprofit Kft. ▪ Kvarc Ásvány Bányászati Ipari Kft.
Lighttech Lámpatechnológiai Kft.
Maltha Hungary Kft. ▪ Messer Hungarogáz Kft.
MINERALHOLDING Kft. ▪ MOTIM Kádkő Kft.
MTA Természetíudományi Kutatóközpont
O-I Hungary Kft. ▪ Pápateszéri Téglaipari Kft.
Perlit-92 Kft. ▪ Q & L Tervező és Tanácsadó Kft.
QM System Kft. ▪ Rákosy Glass Kft.
RATH Hungária Tűzálló Kft. ▪ Rockwool Hungary Kft.
Speciálbau Kft. ▪ SZIKKTI Labor Kft.
Taurus Techno Kft. ▪ Tungsram Operations Kft.
Witeg-Kőporc Kft. ▪ Zalakerámia Zrt.

Vol. 73, No. 1

Effects of poly-sal polymer and barite addition on rheological properties of algerian bentonite

Ilyes BACHIR BELMEHDI ▪ Laboratory of Petroleum Equipment's Reliability and Materials, Faculty of Hydrocarbons and Chemistry, University M'Hamed Bougara of Boumerdes, Algeria
Abderrahmane MELLAK ▪ Laboratory of Hydrocarbons Physical Engineering, Faculty of Hydrocarbons and Chemistry, University of M'Hamed Bougara Boumerdes, Algeriat ▪ a.mellak@univ-umbb.dz
Larbi HAMMADI ▪ Laboratory of Rheology, Transport and Treatment of the Complex Fluids, University of Science and Technology, Mohamed Boudiaf Oran, Algeria

Érkezett: 2020. 04. 17. ▪ Received: 17. 04. 2020. ▪ https://doi.org/10.14382/epitoanyag-jsbcm.2021.1

Abstract
In this paper, we investigate the effect of Poly-Sal polymer and barite on the rheological properties of bentonite of Maghnia (western Algeria). The modified Cross model is used to fit the stationary flow curves of bentonite at different concentrations of Poly-Sal add in base bentonite (4%) and the generalized model of Kelvin-Voigt is successfully applied to fit the creep and recovery data and to analyze the viscoelastic properties of the mixture Bentonite-Barite. Finally, the thixotropic behavior studied of the mixture Bentonite-Barite at constant temperature is analyzed by using a structural kinetic model (SKM) in order to account for the time dependent effect. It is demonstrated that the increase in quantity of barite in base bentonite induces a restructuring and reorganization of the particles of the bentonite at the microstructural level.

Keywords: bentonite, barite, Poly-Sal, structural parameter, thixotropy, viscoelasticity

Ilyes BACHIR BELMEHDI
He is petroleum Engineer . Preparing the Phd thesis on the rheology of clay-polymer systems, at the Faculty of Hydrocarbons and Chemistry, M'Hamed Bougara University of Boumerdes, Algeria.

Abderrahmane MELLAK
He is the Director of the Hydrocarbon Physics Engineering Laboratory (LGPH) at the Faculty of Hydrocarbons and Chemistry of the University of Boumerdès in Algeria. He is a Research Professor and his research focuses mainly on energy, the rheology of complex fluids, oil and gas drilling, materials, as well as the environment. He is Director of several doctoral theses including the thesis of Ilyes Bachir Belmahdi.

Larbi HAMMADI
He is Doctor of Science in Hydraulics (University of Science and Technology of Oran) and Engineer in Mechanical Engineering. Since 2002, he is Researcher Professor at the University of Science and Technology of Oran (USTOMB) where he exercised many teaching activities. He is actually the director of Laboratory of Rheology, Transport and Complex Fluids Treatment (LRTTFC) Oran Algeria.

1. Introduction

The Bentonite represents an important clay material for a multitude of processes and industrial applications due to the exceptional properties of its dispersion in water [1] and their significant influences on the drilling process of oil and gas wells [2-3]. They are found, in particular, as a texturing agent, in cosmetics, as drilling muds in the petroleum industry [4-5-6] or as a sealant in civil engineering [7-8]. The bentonite is also employed as a thickener in waterproofing of hydraulic structures (dams, large reservoirs, etc...). They are also used for stabilization of the oil-water emulsions [9-10-11].

Despite their potential usefulness, applications of bentonite have been limited because of some reasons, namely their swelling [12] and evolution with time. In order to widen the use of bentonite and improve their sorption properties many additives have been added in bentonite such the electrolytes, polymers [13-14] and barite [15-16].

In addition, the knowledge of the rheological properties of bentonite suspension and bentonite additives is important in industry applications in order to provide information for design and process evaluation, control, storage stability and the degree of bentonite-additive interactions. It is noted that the rheological behavior of bentonite dispersions depends on different factors such as the type and concentration of bentonite, the size of bentonite particles, the pH and the concentration of the additives in dispersions.

The effect of sodium carboxymethylcellulose, xanthan gum and sodium dodecyl sulfate on rheological proprieties of bentonite was studied [17]. It was shown; for the three additives; that the apparent viscosities of the solutions increase with increasing concentrations. Other authors [18], has investigated the effect of polyethylene Oxide (PEO) and shear rate on rheological properties of bentonite suspensions. The authors demonstrated that when polyethylene oxide (PEO) was added to bentonite clay, the yield stress and fluid consistency index of the mixture increased. The effect of the temperature on the rheological properties of a complex bentonite-sodium carboxymethylcellulose was investigated [19]. They observed that in the liquid like regime the viscosity of the fluids decreased as the temperature increased, and in the solid-like regime, they observed; at low shear stresses; the Brownian effect dominates the hydrodynamic one. An increase of temperature generates an increase of the Brownian motion. Recently, the effect of Hydroxyethyl cellulose on rheological proprieties of Algerian bentonite was studied [20]. A significant increase in the rheological properties of the mixture bentonite–HEC with the increase in HEC concentration has been shown. The impact of barite on structural recovery behavior of bentonite was studied [15]. It has been clearly demonstrated that the structural recovery of mixture bentonite-barite is time-dependent and their yield stress increases with time of rest and quantity of barite add in bentonite. The authors also used the Leong and Nguyen–Boger models in order to model the structural recovery behavior of barite-loaded bentonite suspensions. The impact of barite and ilmenite mixture on enhancing the drilling muds has been investigated [21]. The study showed that the rheological properties of barite/ilmenite mixture give comparable results as barite and has the potential to be used as alternative weighting material especially in a heavier drilling mud.

From the literature different rheological properties of the mixtures bentonite-sodium carboxymethylcellulose, bentonite-xanthan gum, bentonite- polyethylenean Oxide and bentonite- Hydroxyethyl cellulose have been investigated and analyzed by various models [18, 20, 22-25]. However, as far as we know only a few studies focused on the rheological behavior of bentonite-barite but no study done on rheological behavior of the mixture bentonite-Poly-sal. Although this polymer is designed to reduce the fluid losses and can be used in drilling fluids to increase the viscosity. For this reason the knowledge of the rheological characteristics of the mixtures bentonite-Poly-sal polymer and bentonite-barite plays a fundamental role in flows and performance of transport technologies such as losses of linear and singular energy, non-flow zones, recirculation time, and operation of drilling fluids.

The objective of this paper is, mainly, to study the effect of Poly-sal polymer on the rheological properties of a bentonite in a steady state and on the other hand to study the effect of barite on the viscoelastic and thixotropic properties of bentonite. In order to provide useful information for the proper design of pipes and the selection of pumps during use of bentonite-Poly-sal and bentonite-barite in drilling fluids or in others application.

2. Theoretical time dependent modeling

In order to model the structural evaluation of the bentonite-barite, we applied the structural kinetic model (SKM) [26], which has been successfully employed for starch pastes and concentrated suspensions of minerals. In this study, the kinetic structural approach assumes that the change in the rheological behavior is associated with shear-induced breakdown of the internal structure in the bentonite-barite system.

The structured state of the thixotropic structure at any time t and under an applied shear rate can be represented by the structural parameter (λ):

$$\lambda = \lambda(t, \dot{\gamma}) \tag{1}$$

Which $\lambda(t, \dot{\gamma})$ is defined as:

$$\lambda(t, \dot{\gamma}) = \frac{\eta - \eta_e}{\eta_0 - \eta_e} \tag{2}$$

Where η_0 is the initial apparent viscosity at t=0 (structured state), and η_e is the equilibrium apparent viscosity as t → ∞ (non-structured state). Note that, both η_0 and η_e are functions of the applied shear rate only [27]. The structural parameter λ ranged from an initial value of unity for zero shear time to an equilibrium λ_e valuelower than the unity. The rate of structural breakdown can be expressed as:

$$-\frac{d\lambda}{dt} = k(\lambda - \lambda_e)^n \tag{3}$$

Where $k = k(\dot{\gamma})$ is the rate constant and is the order of the structure breakdown reaction. At a constant applied shear rate, integration of (3) from t=0 to t yields:

$$(\lambda - \lambda_e)^{1-n} = (n-1)kt + (\lambda_0 - \lambda_e)^{1-n} \tag{4}$$

Substituting (2) into (4) yields for a constant shear rate:

$$\left(\frac{\eta - \eta_e}{\eta_0 - \eta_e}\right)^{1-n} = (n-1)kt + 1 \tag{5}$$

3. Materials and methods

3.1 Materials and sample preparation

3.1.1 Materials

The polymer used in this work is the Poly-sal, it's designed to provide filtration control in all types of water-based drilling fluids. This non-ionic, natural polymer is effective in all make-up waters, including high salinity and high hardness brines such as NaCl, KCl, $MgCl_2$, $CaCl_2$ and complex brines. The Poly-sal polymer used in this work was supplied from Company Algeria. The Table 1 presented the physical properties of the Poly-sal used in this study.

Physical appearance	Tan granular powder
Specific gravity	1.5
pH	7.0
Solubility in water	Soluble
Bulk density	561 kg/m³

Table 1 Typical physical properties of the Poly-sal used in this study
1. táblázat A tanulmányban használt Poly-sal fizikai tulajdonságai

The clay used in this study is the bentonite of Maghnia (west of Algeria). The main components of this bentonite sample are: SiO_2 (61.78%), Al_2O_3 (17.15%), Fe_2O_3 (3,82%), MgO (3.56%), CaO (0.26%). The specific surface of bentonite and barite used in this study are 1.05 m²/g and 2.84 m²/g respectively. *Fig. 1* shows the particle size distribution of bentonite and barite suspensions measured by the light scattering technique with a Malvern Instruments Mastersizer 2000 system. In order to avoid the formation of aggregates during the measurements, the sample was submitted to ultrasound excitation. We observed in *Fig. 1* the particle sizes of bentonite ranging between 1 and 138 μm were found with a symmetric distribution centered at about 46 μm and particle sizes of barite ranging between 1 and 138 μm were found with a symmetric distribution centered at about 25 μm. We also observed that the maximum volume of bentonite is greater than the maximum volume of barite which means that the bentonite is more swelling compared to barite.

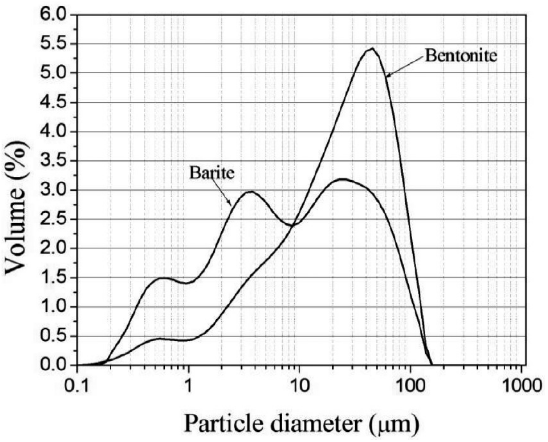

Fig. 1 Particle size distribution of bentonite and barite
1. ábra A bentonit és barit szemcseméret eloszlása

3.1.2 Sample preparation

Given that the way of preparation has a great influence on the final state of suspensions, thus on the rheological behavior, all tests were carefully carried out under equal conditions to allow for comparison of the results.

3.1.2.1 Effect of Poly-sal

For each mixture, the base bentonite suspension has the same mass concentration (4 wt%). The bentonite powder was dispersed in the required amount of distilled water without any chemical additives. The homogenization was performed under continuous magnetic agitation for 24 hours. The additives at different concentrations (0.2; 0.4; 0.6; 0.8 and 1 wt%) were then added to the base suspensions, afterwards, the mixtures obtained were subjected to a continuous agitation for 24 hours. An average pH ranging between 9.6 and 11.5 was measured.

3.1.2.2 The effect of barite

The mixture bentonite-barite used in this study contain in proportion by weight 0, 1, 2, 3 and 4 g barite to bentonite. The based bentonite mixture consists of 4% wt solid (i.e. 4 g bentonite and 96 g water). In the preparation of the mixture with 1 ratio of barite to bentonite, the mixture compositions consist of 96 g water, 4 g bentonite and 4 g barite. For the 0.75 barite to bentonite ratio the composition is 96 g water, 4 g bentonite and 3 g barite. For the 0.5 ratio, the composition is 4 g bentonite, 2 g barite and 96 g water. For the 0.25 ratio, the composition is 4 g bentonite, 1 g barite and 96 g water. For the 0 ratio the composition is 4 g bentonite, 0 g barite and 96 g water.

3.2 Experimental set up

The rheological measurements were performed by using a torque controlled Rhéometer (RS600 from Thermo-Fischer), equipped with a cone-plate geometry (diameter: 60mm; angle: 2°; gap: 105 µm). It has a Peltier temperature control system that allows having a very quick response to any change in temperature. In order to prevent changes in composition during measurements due to water evaporation, a solvent trap was placed around the measuring device.

3.1.2 Experimental methods

3.1.2.1 Steady shear measurements

For study the effect of Poly-sal on the flow properties of bentonite, the sample was pre-sheared at a frequency of $500 s^{-1}$ for 60 seconds in the measuring device in order to avoid any memory effect. After pre-shearing the sample has kept at rest for 600 seconds prior to measurements in order to permit the material recovering its initial structure partially at least. After kept rest of 600 seconds a continuous ramp of shear stress has been applied. The imposed shear stress range depends on the mass concentration of Poly-sal added in base bentonite (4%). In this study for the concentration of Poly-sal less than 1%, a continuous ramp of shear stress, which is ranging from 0 to 3.5 Pa applied during 600 seconds. For the concentrations greater or equal to 1% a continuous ramp of shear stress, which is ranging from 0 to 4 Pa applied during 600 seconds.

3.1.2.2 Creep-recovery measurements

Creep and recovery tests are carried out as follows: After a rest time of 600 seconds prior to the measurements, a constant shear stress τ=0.5 was applied to the simples and the compliance (J) was recorded as a function of creep time; at t = 180 seconds the stress τ was set to zero and the recoverable part of compliance was measured as a function of the recovery time equal at 180 seconds.

4. Results and discussion

4.1 Effect of Poly-sal on the flow properties of bentonite

The bentonite dispersions were prepared with 4% solid content in desalted water and the Poly-sal concentrations ranging between 0 and 1%. *Fig. 2* shows the flow curves of mixtures bentonite 4% at different concentrations of Poly-sal. Experimental data were fitted to the modified Cross model (Eq. (6)) [28], which has been successfully employed for weak gel systems.

$$\tau = \tau_0 + \eta_\infty \dot{\gamma} + \frac{(\eta_0 - \eta_\infty)\dot{\gamma}}{1+(\lambda_c \dot{\gamma})^m} \qquad (6)$$

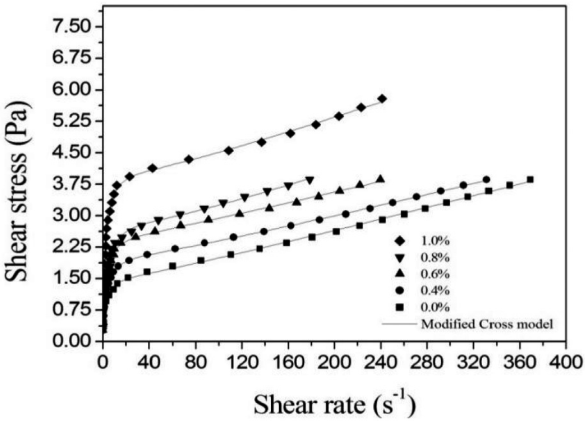

Fig. 2 Shear stress as a function of shear rate at different mass concentrations of Poly-sal add (0, 0.4, 0.6, 0.8 and 1%) in 4% of bentonite. The solid lines correspond to the curve fitting to Eq. (6)

2. ábra Nyírófeszültség a nyírási sebesség függvényében különböző Poly-sal adagolás add (0, 0,4, 0,6, 0,8 és 1%) mellett 4% bentonitban. A folytonos vonalak a (6)-os egyenlethez tartoznak

It is clear that the shear stress of the bentonite–Poly-sal systems increased with the increase in the Poly-sal T content. *Fig. 3* and *4* shows the variation of the parameters of the modified Cross model for bentonite–Poly-sal mixtures systems as a function of different concentration of Poly-sal added in base bentonite (4%) at 20 °C. We observe in *Fig. 3* and *4*, a rapid increase in the yield stress , zero shear rate viscosity and the infinite shear rate viscosity with the increase of Poly-sal concentration, this increase of yield stress, zero shear rate viscosity and the infinite shear rate viscosity is related to the adsorption of Poly-sal by the bentonite. This adsorption makes the specific surface higher and causes an increase of interaction between the bentonite particles. The increase in the yield stress causes an increase in the friction and an increase in the viscosity of the mixture due to the interaction between the solid particles and viscous effects [18]. In this case, the interactions between the clay particles and polymer intensify lead to difficult movements in the dispersing medium. In fact, the presence of Poly-sal in the mixture allows reinforcement of the rigidity and the consistency of the mixture because of the structural nature of the Poly-sal.

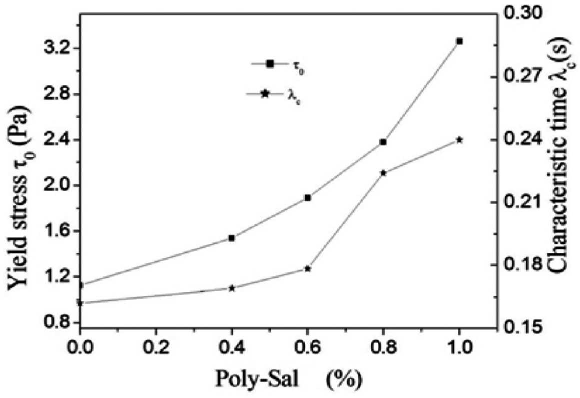

Fig. 3 *Variation of yield stress and characteristic time of mixture bentonite base (4%)-Poly-sal at different concentration of Poly-sal (0, 0.4, 0.6 , 0.8 and 1%)*

3. ábra *A folyási feszültség és a bentonite(4%)-Poly-sal keverék karakterisztikus idejének változása - a Poly-sal különböző koncentrációjában (0, 0,4, 0,6, 0,8 és 1%)*

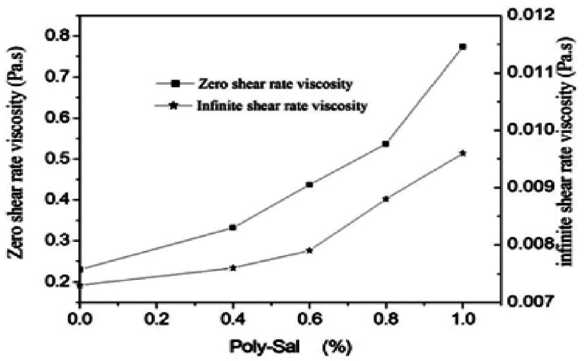

Fig. 4 *Variation of zero shear rate viscosity η_0 and the infinite shear rate viscosity η_∞ of mixture bentonite base (4%)-Poly-sal at different concentration of Poly-sal (0, 0.4, 0.6 , 0.8 and 1%)*

4. ábra *A nulla nyírósebességű viszkozitás valamint a végtelen nyírósebességű viszkozitás a bentonite(4%)-Poly-sal keverék karakterisztikus idejének függvényében - a Poly-sal különböző koncentrációjában (0, 0,4, 0,6, 0,8 és 1%)*

4.2 Effect of barite on the viscoelastic properties of bentonite

After a rest time (time during which the sample is left at rest in geometry) of 600 seconds, in the creep phase, the samples were subjected to constant stress at 0.5 Pa and at constant temperature (20±0.2 °C). In the recovery phase, the applied stress was suddenly removed and the sample recovery was registered for an additional period of 180 seconds. *Fig. 8* shows the values of compliance $(t) = \frac{\gamma}{\tau}$, as a function of time, for the creep experiments corresponding to the bentonite –barite mixtures studied for ration barite to base bentonite (4%) range between 0 and 1, in a time interval between 0 and 180 seconds. For the interval of time between 180 seconds and 360 seconds, we have represented the corresponding recovery. An increase of the elastic compliance (increase of the elastic modulus $(G = \frac{1}{J})$) with the increase of quantity of barite added in the based bentonite (4%), indicating an increase of the viscoelastic properties of mixtures barite-bentonite. In other word, the creep deformation decreases with increasing the barite in bentonite and the time necessary to reach a constant deformation during recovery, after removal of the shear stress decreases.

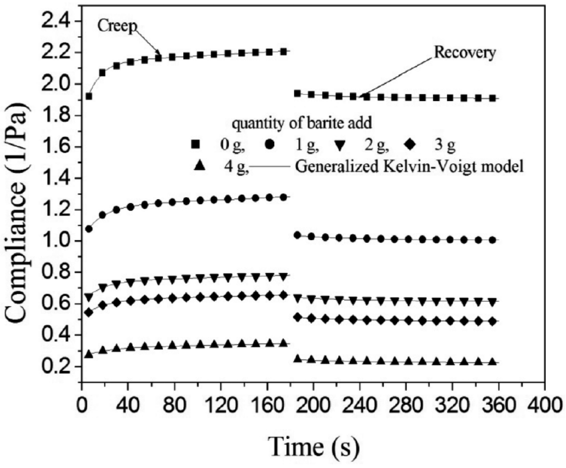

Fig. 5 *Compliance versus time in creep and recovery test at different ratio of quantity added in base bentonite (0, 1, 2, 3 and 4 g). The solid lines correspond to the curve fitting to Generalized Kelvin–Voigt model*

5. ábra *A megfelelőség az idő függvényében kúszási és a visszanyerési teszt során a hozzáadott bentonite mennyiségének (0, 1, 2, 3 és 4 g) függvényében. A folytonos vonalak megfelelnek a Generalized Kelvin – Voigt modellhez illeszkedő görbének*

The elastic properties were defined by correlating the results with the well-known viscoelastic models of Burger model or Generalized Kelvin-Voigt model [29-30] based on the association in the series of the Maxwell model and the Kelvin–Voigt model.

The creep curves are described by:

$$J_F = J_0 + \frac{t}{\mu_0} + \sum_{i=1}^{N} J_i \left[- \exp\left(-\frac{t}{\theta_i}\right)\right] \tag{7}$$

$$\theta_i = \frac{J_i}{\eta_i} \tag{8}$$

Whereas the recovery strain is given by:

$$J_R = \frac{t_1}{\mu_0} + \sum_{i=1}^{N} J_i \left[\exp\left(\frac{t_1}{\theta_i}\right) - 1\right] \exp\left(-\frac{t}{\theta_i}\right) \tag{9}$$

where J_0 is the purely elastic contribution (or the instantaneous elastic compliance), μ_0 is the purely viscous contribution, represented by the despot of the Maxwell model, i.e., the uncoupled or residual steady-state viscosity obtained from the creep curve at long times when the compliance curve is linear, J_i is the contribution to retarded elastic compliance, θ_i is the retarded time, η_i is the retarded viscosity and t_1 is the time where the stress is applied for $t \le t_1$ and removed at $t = t_1$. The fitting parameters are detailed in *Table 2*. The column $G_0 = \frac{1}{J_0}$ represents the instantaneous elastic modulus of the Maxwell unit at t = 0; that is the instantaneous elastic response of the system and the column $G_1 = \frac{1}{J_1}$, J_1 is the elastic modulus of Kelvin–Voigt. The latter represents the contributions of the retarded elastic region to the total compliance. The strong increase is observed in G_0 and G_1 when the quantity of barite is changed between 0 and 4 g cause the manifestation of the shift from viscous to elastic behavior and an increase of the viscoelastic properties in that range of barite.

	Creep			Recovery		
Barite	$G_0\ (Pa)$	$G_1\ (Pa)$	$\mu_0\ (Pa.s)$	$G_1\ (Pa)$	$\mu_0\ (Pa\ s)$	$\theta_1\ (s)$
0	0.56	2.88	2364.69	28.49	94.32	55.36
1	0.99	4.88	2872.69	29.07	179.31	56.26
2	1.66	7.28	3906.40	43.48	799.49	61.12
3	1.95	9.43	4550.02	35.71	293.26	60.65
4	3.88	16.13	6899.11	34.60	369.50	59.99

Table 2 Fitting parameters of the creep–recovery data in Fig. 5, with N = 1in Eqs. (7) and (9)

2. táblázat A kúszás-helyreállítási adatok illesztési paraméterei; (7) és (9) egyenletekben N=1 esetén

It has the meaning of viscosity of the system in the Newtonian regime, whereas it also shows a clear increasing trend as the quantity of barite in the based bentonite (4%) increases. This increasing of viscosity could be the interactions between bentonite-barite mixture particles and the enhancement of Brownian motion. At high quantity of barite added in based bentonite, the applied stress of 0.5 Pa is not sufficient to break particle-to-particle bonds, and the mixtures (Bentonite-Barite) do not flow. For lower quantity of barite values such resistance to flow is not so large, and this explains the values of and in this case the retarded deformation, related to the breaking and reconstruction of weak links between the particles. The characteristic relaxation time associated with these breaking/reconstruction processes is. Although this time does not show a definite trend when estimated from creep data.

4.3. Apparent viscosity evolution under constant shear rate and determination of the structural parameter of mixtures barite-bentonite

Figs. 6 and *7* show the time dependence of apparent viscosity for constant shear rates (0.5 s^{-1} and 0.8 s^{-1}) at different quantities of barite (0, 1, 2, 3 and 4 g) added in base bentonite (4%) fitted with the second-order SKM (see Eq. (5)).

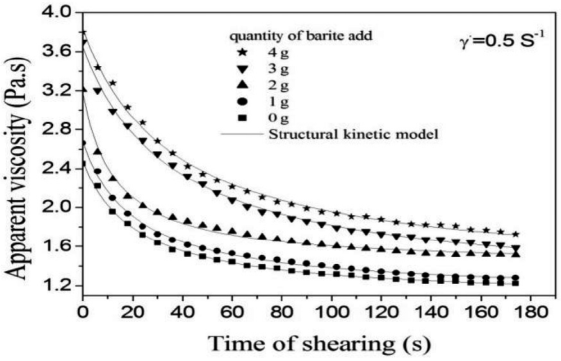

Fig. 6 Apparent viscosity data of barite-bentonite mixtures as a function of shearing time at 20°C for different quantities of barite added in bentonite (4%) and for constant shear 0.5 s-1. The solid line corresponds to curve fitting to Eq. (5) where n=2

6. ábra A barit-bentonit keverékek látszólagos viszkozitási adatai a nyírási idő függvényében 20 ° C-on különböző mennyiségű barit esetén, 4%-os bentonite adagolás és állandó nyírási sebesség (0,5 s-1) mellet. A folytonos vonal megfelel az (5)-ös egyenletre illeszkedő görbének n = 2 esetén

A good concordance was found between the model fitted results (solid line) and the experimental transient apparent viscosity data for all quantities of barite added in base bentonite (4%) and for the both shear rates applied.

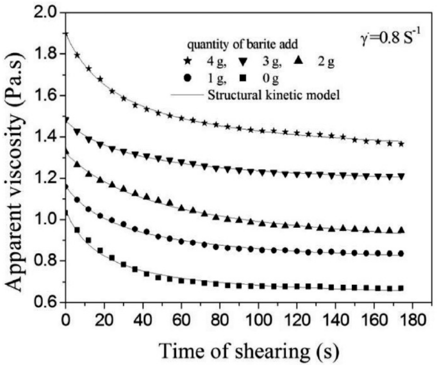

Fig. 7 Apparent viscosity data of barite-bentonite mixtures as a function of shearing time at 20°C for different quantities of barite added in bentonite (4%) and for constant shear 0.8 s^{-1}. The solid line corresponds to curve fitting to Eq. (5) where n=2

7. ábra A barit-bentonit keverékek látszólagos viszkozitási adatai a nyírási idő függvényében 20 ° C-on különböző mennyiségű barit esetén, 4%-os bentonite adagolás és állandó nyírási sebesség (0,8 s^{-1}) mellet. A folytonos vonal megfelel az (5)-ös egyenletre illeszkedő görbének n = 2 esetén

For all studied quantities of barite added in base bentonite and for both shear rates, the viscosity decreases significantly with shearing time, particularly in the initial stages of shearing. After approximately 140 seconds shearing periods for shear rate of 0.5 s^{-1} applied on the mixtures and after approximately 100 seconds of shearing periods for shear rate of 0.8 s^{-1} applied in the mixtures, the viscosity tends to an equilibrium value. Therefore the equilibrium state of mixtures barite-bentonite depends on the shear rate applied to the system. *Fig. 8* shown the variation of the rate constant k and the equilibrium structural parameter λ_e as a function of the quantity of barite added in base bentonite (4%) and for both shear rates applied.

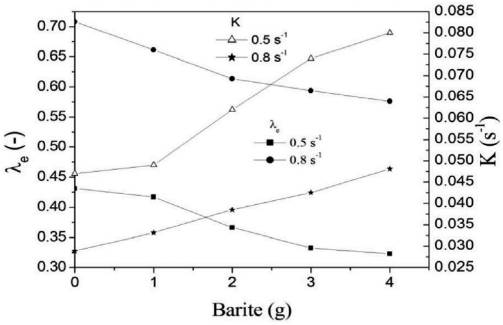

Fig. 8 the variation of the rate constant k and equilibrium structural parameter as a function of the quantity of barite added in base bentonite (4%) and for both shear rates applied

8. ábra A k sebességi állandó és az egyensúlyi szerkezeti parameter változása a barit mennyiségének (4%) függvényében, mindkét alkalmazott nyírási sebesség esetén

The rate *k* constant k can be considered as a measure of the rate of the structural breakdown, i.e. the degree of thixotropy. On the other hand, the ratio of equilibrium to initial viscosity can be considered as an equilibrium structural parameter $\lambda_e = \frac{\eta}{\eta}$. We observed in *Fig. 6* an increase of the degree of thixotropy with increase of the quantity of barite in bentonite. This increase in the degree of thixotropy leads to an increase in the yield stress and the apparent viscosity of the mixtures bentonite-barite.

As it is shown in *Fig. 9* structural parameter changes are most significant during the initial shear period after which nearly constant values are reached.

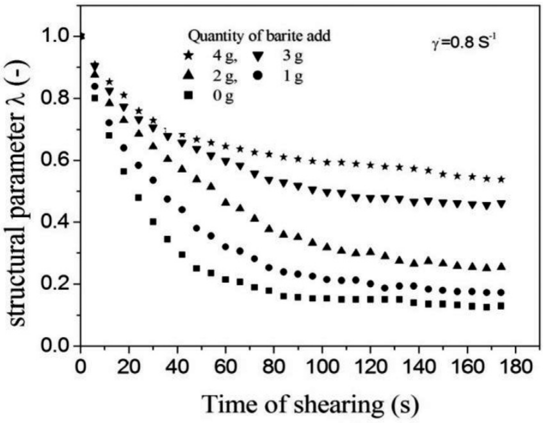

Fig. 9 Structural parameter as a function of time at 20°C for different quantities of barite adds in bentonite for shear rate of 0.8 s^{-1}

9. ábra A szerkezeti parameter a nyírási idő függvényében, 20 °C-on, különböző barit adagolás mellett 0,8 s^{-1}-es nyírási sebesség mellett

We also find that the structural parameter of mixture suspension (bentonite-barite) increases with increasing the quantity of barite added in bentonite. This behavior could be explained by the deflocculating of mixtures particles in the water at high quantity of barite added (4 g). The applied stress of 0.8 s^{-1} is not sufficient to break particle-to-particle bonds. The mixture in this case developed a network structure which leads to enhance the organization of particles in the mixtures at the microstructural level [31].

5. Conclusions

The effect of Poly-sal polymer on the stationary behavior of bentonite and the effect of barite on the viscoelastic and thixotropic behavior of bentonite were studied. The stationary flow curves of bentonite at different concentration of Poly-sal add in base bentonite (4%) was successfully modeled using The Modified Cross model. the generalized model of Kelvin-Voigt is successfully applied to fit the creep and recovery data and to analyze the viscoelastic properties of mixture bentonite-barite.

The addition of Poly-sal in a concentration range between 0 and 1% to 4% of bentonite leads to an increase in the yield stress τ_0, zero shear rate viscosity η_0 and the infinite shear rate viscosity η_∞ with dose of Poly-sal. The increase of these parameters is related to the interaction between the solid particles and the viscous effects. The increase of the modified Cross model parameters causes an increase in the friction and an increase in the viscosity of the mixture.

The increase of quantity of barite in bentonite suspensions causes an increase of the viscoelastic behavior of the system and the structure of particle-to-particle bonds. in order to avoid the problems related to the structure of particle-to-particle bonds of bentonite, caused by high concentration of barite, during the process of pumping, we propose the addition of an electrolyte as a third additive i.e., bentonite-barite- electrolyte. The effect of barite on the break-down behavior of the bentonite suspension was examined. The time dependent viscosity decreased rapidly with shearing time and reached a steady state. The structural kinetic model (SKM) for viscosity decay with time at the constant shear rate was applied successfully to analyze the time-dependent behavior of bentonite-barite mixtures. The rate of structure breakdown (degree of thixotropy) increases with increasing quantity of barite added to based bentonite.

References

[1] Vryzas, Z. – Kelessidis, VC. – Nalbantian, L. – Zaspalis, V. – Gerogiorgis, DI. – Wubulikasimu, Y. (2017): Effect of temperature on the rheological properties of neat aqueous Wyoming sodium bentonite dispersions. Applied Clay Science, Vol. 136, pp. 26-36, ISSN: 0169-1317, https://doi.org/10.1016/j.clay.2016.11.007.

[2] Y., Ren et al., (2019): Adsorption of imidazolium-based ionic liquid on sodium bentonite and its effects on rheological and swelling behaviors. Applied Clay Science, Vol. 182, pp. 105248, ISSN: 0169-1317, https://doi.org/10.1016/j.clay.2019.105248.

[3] Mellak, Abderrahmane (2019): Mathematical modelling: case of Haoud Berkaoui. Epitoanyag-Journal of Silicate Based & Composite Materials, Vol. 71, No. 1.

[4] Kok, MV. (2011): A rheological characterization and parametric analysis of a bentonite sample. Energy Sources, Part A: Recovery, Utilization and Environmental Effects. 33(4): 344-348.

[5] Işçi, E. – Turutoğlu, S. İ. (2011): Stabilization of the mixture of bentonite and sepiolite as a water based drilling fluid. Journal of Petroleum Science and Engineering, Vol. 76, Issues: 1–2, pp. 1-5, ISSN 0920-4105. https://doi.org/10.1016/j.petrol.2010.11.021.

[6] Coussot, P. – Tabuteau, H. – Château, X. – Tocquer, L. – Ovarlez, G. (2006): Aging and solid or liquid behavior in pastes. Journal of Rheology. Vol. 50, pp. 975– 94, https://doi.org/10.1122/1.2337259.

[7] Lam, C. – Jefferis, S. A. – Suckling, T. P. – Troughton, V. M., (2015): Effects of polymer and bentonite support fluids on the performance of bored piles. Soils and Foundations, Vol. 55, Issue 6, pp. 1487-1500, ISSN 0038-0806, https://doi.org/10.1016/j.sandf.2015.10.013.

[8] Besq, A. – Malfoy, C. – Pantet, A. – Monnet, P. – Righi, D. (2003): Physicochemical characterisation and flow properties of some bentonite muds. Applied Clay Science, Vol. 23, Issues 5–6, pp. 275-286, ISSN 0169-1317, https://doi.org/10.1016/S0169-1317(03)00127-3.

[9] Hempoonsert, J. – Tansel, B. – Laha, S. (2010): Effect of temperature and pH on droplet aggregation and phase separation characteristics of flocs formed in oil–water emulsions after coagulation. Colloids and Surfaces A: Physicochemical and Engineering Aspects. Vol. 353, Issue 1, pp. 37-42, ISSN 0927-7757, https://doi.org/10.1016/j.colsurfa.2009.10.016.

[10] Abend, S. – Bonnke, N. – Gutschner, U. – Lagaly, G. (1998): Stabilization of emulsions by heterocoagulation of clay minerals and layered double hydroxides. Colloid & Polymer Science. Vol. 276, pp. 730-737, https://doi.org/10.1007/s003960050303.

[11] Abderrahmane, Mellak (2007): Caracterisations rhéologiques des coulis de ciments spécifiques aux formations salifères.Lebanese Science Journal, Vol. 8, No (2), pp.115-125.

[12] Barast, G. – Razakamanantsoa, A. R. – Djeran-Maigre, I. – Nicholson, T. – Williams, D. (2016): Swelling properties of natural and modified bentonites by rheological description. Applied Clay Science, Vol. 142, pp. 60-68, ISSN 0169-1317, https://doi.org/10.1016/j.clay.2016.01.008.

[13] Abu-Jdayil, B. – Ghannam, M. (2014): The modification of rheological properties of sodium bentonite-water dispersions with low viscosity CMC polymer effect. Energy Sources, Part A: Recovery, Utilization, and Environmental Effects. Vol. 36, pp. 1037-1048,

[14] Menezes, R. R. – Marques, L. N. – Campos, L. A. – Ferreira, H. S. – Santana, L. N. L. – Neves, G. A., (2010): Use of statistical design to study the influence of CMC on the rheological properties of bentonite dispersions for water-based drilling fluids. Applied Clay Science. Vol. 49, Issues 1–2, pp. 13-20, ISSN 0169-1317, https://doi.org/10.1016/j.clay.2010.03.013.

[15] Yap, J. – Leong, Y. K. – Liu, J. (2011): Structural recovery behavior of barite-loaded bentonite drilling muds. Journal of Petroleum Science and Engineering. Vol. 78, Issue 2, pp. 552-558, ISSN 0920-4105, https://doi.org/10.1016/j.petrol.2011.06.010.

[16] Asghari, I. – Esmaeilzadeh, F. (2013): Manipulation of key parameters in RESS process for attapulgite particles utilizing in drilling mud and investigation on its rheological characteristics. Journal of Petroleum

Science and Engineering. Vol. 112, pp. 359-369, ISSN 0920-4105, https://doi.org/10.1016/j.petrol.2013.09.013.

[17] Benchabane, A. – Bekkour, K., 2006: Effects of anionic additives on the rheological behavior of aqueous calcium montmorillonite suspensions. Rheologica Acta. Vol. 45, No (4), pp. 425-434, https://doi.org/10.1007/s00397-005-0063-1

[18] Hammadi, L. – Boudjenane, N. – Belhadri, M. (2014): Effect of polyethylene oxide (PEO) and shear rate on rheological properties of bentonite clay. Applied Clay Science. Vol. 99, pp. 306-311, ISSN: 0169-1317, https://doi.org/10.1016/j.clay.2014.07.016.

[19] Azouz, K. B. – Bekkour, K. – D., Dupuis (2016): Influence of the temperature on the rheological properties of bentonite suspensions in aqueous polymer solutions. Applied Clay Science. Vol. 123, pp. 92-98, ISSN: 0169-1317, https://doi.org/10.1016/j.clay.2016.01.016.

[20] Ouaer, H. – Gareche, M. (2019): Hydroxyethyl cellulose as a rheology modifier for water-based drilling fluids formulated with Algerian bentonite. Journal of the Brazilian Society of Mechanical Sciences and Engineering Vol. 41:123, https://doi.org/10.1007/s40430-019-1627-9

[21] Abdou, M. I. – Al-Sabagh, A. M. – Ahmed, Hany El-Sayed – Fadl, A. M. (2018): Impact of barite and ilmenite mixture on enhancing the drilling mud weight. Egyptian Journal of Petroleum, Vol. 27, Issue 4, pp. 955-967, ISSN: 1110-0621, https://doi.org/10.1016/j.ejpe.2018.02.004.

[22] Benyounes, K. – Mellak, A. – Benchabane, A. (2010): The effect of carboxymethylcellulose and xanthan on the rheology of bentonite suspensions. Energy Sources, Part A: Recovery, Utilization, and Environmental Effects. Vol. 32, pp. 1634-1643.

[23] Kelessidis, V. C. – Poulakakis, E. – Chatzistamou, V. (2011) : Use of Carbopol 980 and carboxymethyl cellulose polymers as rheology modifiers of sodium-bentonite water dispersions. Applied clay science, Applied Clay Science, Vol. 54, Issue 1, pp. 63-69, ISSN: 0169-1317, https://doi.org/10.1016/j.clay.2011.07.013.

[24] Shaikh, S. M. – Nasser, M. S. – Hussein, I. – Benamor, A. – Onaizi, S. A. – Qiblawey, H. (2017): Influence of Polyelectrolytes and Other Polymer Complexes on the Flocculation and Rheological Behaviors of Clay Minerals: A Comprehensive Review. Separation and Purification Technology. Separation and Purification Technology, Vol. 187, pp. 137-161, ISSN: 1383-5866, https://doi.org/10.1016/j.seppur.2017.06.050.

[25] Benslimane, A. – Bahlouli, I. M. – Bekkour, K. – Hammiche, D. (2016): Thermal gelation properties of carboxymethyl cellulose and bentonite-carboxymethyl cellulose dispersions: Rheological considerations, Applied Clay Science, Vol. 132–133, pp. 702-710, ISSN: 0169-1317, https://doi.org/10.1016/j.clay.2016.08.026.

[26] Nguyen, Q. D. – Jensen, C. T. – Kristensen, P. G. (1998): Experimental and modelling studies of the flow properties of maize and waxy maize starch pastes. Chemical Engineering Journal. Vol. 70, Issue 2, pp. 165-171, ISSN: 1385-8947, https://doi.org/10.1016/S0923-0467(98)00081-5.

[27] Abu-Jdayil, B. (2003): Modelling the time-dependent rheological behavior of semisolid foodstuffs. Journal of food engineering. Vol. 57, pp. 97-102, ISSN: 0260-8774, https://doi.org/10.1016/S0260-8774(02)00277-7.

[28] Grassi, M. – Lapasin, R. – Pricl, S. (1996): A study of the rheological behavior of scleroglucan weak gel systems. Carbohydrate Polymers, Vol 29, Issue 2, pp. 169-181, ISSN: 0144-8617, https://doi.org/10.1016/0144-8617(95)00120-4.

[29] Hammadi, L. – Ponton, A. (2017): Rheological Investigation of Vase of Dam: Effects of Aging Time, Shear Rate, and Temperature. Applied Rheology. Vol. 27, No 1, pp. 21-29.

[30] Dolz, M. – Hernández, M. J. – Delegido, J. (2008): Creep and recovery experimental investigation of low oil content food emulsions. Food Hydrocolloids. Vol. 22, pp. 421-427.

[31] Wang, Q. – Cui,Y.J – Tang, A. M. – Barnichon, J. D. – Saba, S. – Ye, W. M. (2013): Hydraulic conductivity and microstructure changes of compacted bentonite/sand mixture during hydration. Engineering Geology vol. 164, pp. 67-76.

Ref.:

Bachir Belmehdi, Ilyes – **Mellak**, Abderrahmane – **Hammadi**, Larbi:

Effects of poly-sal polymer and barite addition on rheological properties of algerian bentonite

Építőanyag – Journal of Silicate Based and Composite Materials, Vol. 73, No. 1 (2021), 2–8. p.

https://doi.org/10.14382/epitoanyag-jsbcm.2021.1

Kinetics and products composition of catalytic hydration of ethylene oxide in the presence of layered double hydroxides

Eleonora BUTENKO ▪ Azov Sea State Technical University; Ukraine ▪ butenkoeo@rambler.ru
Elena KAPUSTINA ▪ Environmental Protection Agency; Cincinnati, USA ▪ kapustinalena@gmail.com
Alexey KAPUSTIN ▪ Miami University; Oxford, USA ▪ kapustinlesha@gmail.com

Érkezett: 2020. 05. 19. ▪ Received: 19. 05. 2020. ▪ https://doi.org/10.14382/epitoanyag-jsbcm.2021.2

Abstract

The reaction of ethylene oxide hydration proceeds under acid and basic catalysis. Using of heterogeneous catalysts allows to adjust the length of the chain. The kinetics of the selective hydration of ethylene oxide in aqueous solution in the presence of layered double hydroxides as heterogeneous catalysts was studied. It was shown that the molecular weight distribution of the reaction products depends on the concentration of active sites on the catalyst surface as well as the inner structure of the catalysts.

Keywords: layered double hydroxide, ethylene oxide, catalysis, kinetics
Kulcsszavak: réteges kettős hidroxid, etilén-oxid, katalízis, kinetika

Prof. Eleonora BUTENKO
Donetsk National University – M.Sc.Chemical faculty, June 2007, Specialization: Analytical Chemistry, Donetsk, Ukraine. Pryazovskyi State Technical – Ph.D. Environmental Safety, October 2011, Protection of water bodies using synthetic anionic clays, Kharkov, Ukraine. Pryazovskyi State Technical University – Head of Department of Chemical Technology and Engineering, 2018 – present, Mariupol, Ukraine.

Dr. Elena KAPUSTINA
Mendeleev University of Chemical Technology – M.Sc. Chemical Engineering, May 1981, Specialization: Technology of solid fuels, Moscow, Russia. Mendeleev University of Chemical Technology – Ph.D. Chemical Engineering, December 1986, Carbon technology and coal processing, Moscow, Russia. Pryazovskyi State Technical University – Research Associate, August 1986-2014, Department of Chemical Technology and Engineering, Mariupol, Ukraine. Environmental Protection Agency, Researcher, Water Department, 2015-present, Cincinnati, USA.

Prof. Alexey KAPUSTIN
Mendeleev University of Chemical Technology – M.Sc. Chemical Engineering, May 1981, Specialization: Catalysis, Moscow, Russia. Mendeleev University of Chemical Technology – Ph.D. Chemical Engineering, January1985, Catalysis, Moscow, Russia. Mendeleev University of Chemical Technology – Doctor of Science (Chemistry), December 1996, Catalysis, Moscow, Russia. Pryazovskyi State Technical University – Research Associate, September 1985-2015, Department of Chemical Technology and Engineering, Mariupol, Ukraine. Miami University – Professor, 2015-present, Oxford, USA.

1. Introduction

The hydration of ethylene oxide is the basis of the industrial method of ethylene glycol production. The hydration reaction proceeds as a series-parallel route, which leads to the formation of glycol homologue derivatives:

$$H_2O \xrightarrow[k_0]{C_2H_4O} HOCH_2CH_2OH \xrightarrow[k_1]{C_2H_4O} HO(CH_2CH_2O)_2H \xrightarrow[k_2]{C_2H_4O} \text{i.t.d.} \qquad (1)$$

where k_0, k_1, k_2 are the rate constants of consecutive steps.

The reaction (1) proceeds under acidic, basic and nucleophilic catalytic conditions [1-2]; at temperatures above 120 °C it proceeds at a fairly high rate and in the absence of catalysts.

Currently, in industry ethylene glycol is produced by a non-catalytic reaction via adjusting the product composition by the ratio of ethylene oxide - water in the initial mixture.

Since the ratio of the rate constants of successive stages of the reaction (1) is unfavorable towards the formation of ethylene glycol – the distribution coefficient for the non-catalytic reaction $b=k_1/k_0$ according to various sources is 1.9-2.8 [3-4] – a 15-20-fold molar (or 6-9-fold mass) excess of water relative to ethylene oxide is employed.

One of the options to raise the selectivity of the ethylene glycol formation and, consequently, reduce the amount of excess water is to use catalysts that accelerate only the first stage of reaction (1).

The kinetics and reaction mechanism of α-oxide hydration under homogeneous catalysis with salts have been studied in detail.

Amine compounds were investigated for catalytic hydration of ethylene oxide to monoethylene glycol. A good correlation between catalyst performance and its acidity/basicity was established. While both strong acidic and basic catalyst accelerate reaction rate they are not selective toward monoethylene glycol formation.

Selective hydration of ethylene oxide by inorganic salt system as homogeneous catalysts was studied. The highest monoethylene glycol selectivity was obtained with 99 % conversion of ethylene oxide, even at low water/ethylene oxide ration.

The kinetics of selective hydration of ethylene and propylene oxides in concentrated aqueous solutions is studied during homogeneous catalysis by sodium bicarbonate. The mathematical model of the process with determined parameters adequately describing the rate of the reaction and products distribution is developed. [3-5].

The goal of the present work was to study the kinetics of the hydration reaction of ethylene oxide in the presence of layered double hydroxides (LDH) [6].

2. Materials and methods

LDHs were prepared by adding $Mg(NO_3)_2 \cdot 6H_2O$ and $Al(NO_3)_3 \cdot 9H_2O$ in de-ionized water. After complete dissolution, the above solution was added dropwise to a vigorously stirred Na_2CO_3 solution in the de-ionized water. Freshly prepared 1 M NaOH solution was then added dropwise to the above solution to maintain constant pH of 11. The resultant gel was aged by stirring at 85 °C for 24 hours. The precipitate was then separated from the solution by centrifugation, washed several times with de-ionized water and dried in vacuum. All these reactions were carried out in an inert atmosphere.

X-ray diffraction patterns revealed that well-crystallized hydrotalcite-like compounds were obtained and no other phase was identified. The X-ray diffraction for these samples typically consist of anionic clay having molecular formula $Mg_6Al_2(OH)_{16}CO_3$.

Basic properties of LDHs catalysts were determined with a Hammett indicator titration method in the presence of Bromothymol Blue ($pK_a = 7.2$).

The special technique was used in order to investigate acidic and basic properties by means of titration with Hammett indicators. A sample of LDH and a magnetic stirrer were inserted into a small glass, which was then put on a magnetic stirring device and filled with benzene. After that, a glass cylinder divided by porous separator, with a standard sample, was inserted into the small glass.

After the Hammett indicator was added into benzene the changes in color could be seen on the surface of the standard sample.

Catalytic activity was studied in the reaction of hydration of ethylene and propylene oxide. 1 g of LDH was carried out into a 5 ml glass ampoule under a nitrogen stream, and 10 ml of a-oxide was introduced. The ampoule was frozen by liquid nitrogen, seal after the degassing and kept into a bath with the device for shaking. The product was washed with acetone and analyzed by chromatography.

Kinetic studies were carried out with Mg-Al-LDH formed with acetate, as the sample with the largest specific surface area. Beforehand, the catalyst was converted to its basic form.

It should be noted that the most effective catalysts for the hydration of α-oxides are LDH in their basic form [6-8].

3. Results and discussion

The activity of LDH as heterogeneous catalysts is determined by the number of basic sites, as well as their availability, which correlates with the specific surface area (*Fig. 1*).

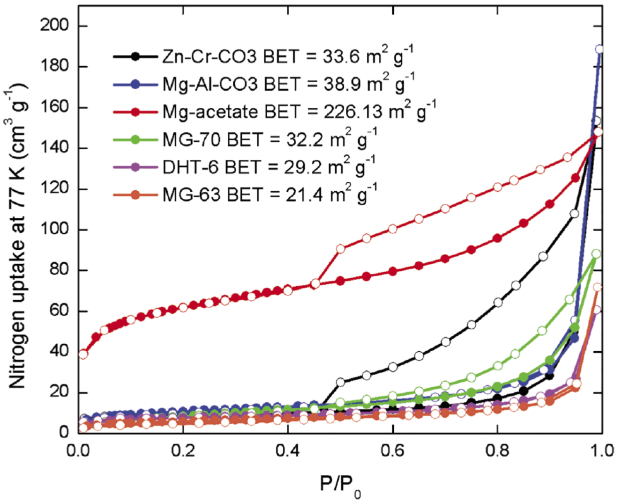

Fig. 1 Specific surface area of some LDHs
1. ábra LDH-k fajlagos felülete

The obtained kinetic data showed that at a concentration of the LDH basic sites of 0.5 mol/l, the distribution coefficient $b=k_1/k_0$ decreases by 10 or more times to 0.1-0.2. This makes it possible to obtain ethylene glycol with high selectivity at molar ratios of water-ethylene oxide close to one.

The mechanism of catalytic hydration of α-oxide with anions is the nucleophilic addition of the catalyst anion (A^-) to the α-oxide molecule:

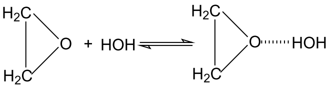

(2)

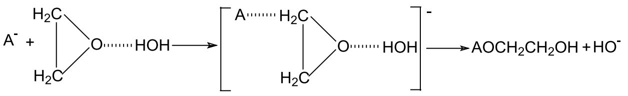

(3)

And the further hydrolysis of the intermediate ester to produce glycol and catalyst regeneration:

$$AOCH_2CH_2OH + HO^- \longrightarrow A^- + HOCH_2CH_2OH \quad (4)$$

The rate-limiting step in most cases is the stage of formation of the intermediate ester according to reaction (III). In dilute aqueous solutions the reaction rate is described by the following kinetic equation:

$$r = k\,[C_2H_4O]\,[A^-] \quad (5)$$

To implement the catalytic process of hydration of concentrated solutions of ethylene oxide, it is necessary to establish a kinetic model of reaction (3) suitable for the quantitative description of a heterogeneous catalytic process in a wide range of concentrations of water and ethylene glycol.

Our kinetic experiments showed that the immobilization of anions on heterogeneous carriers does not change the form of kinetic equation (5) and its parameters. To describe the heterogeneous catalytic reaction, it is sufficient to change the concentration of the heterogeneous catalyst $[A^-]$ in equation (5) by the number of active sites per unit volume of the reaction mass.

Such a model can be constructed taking into account the results of experiments on homogeneous catalytic hydration.

To establish such a module one can assume a trimolecular mechanism of the ring opening of the oxide cycle (2, 3), which is also adequate to describe the non-catalytic hydration reaction and the polyglycol formation reaction:

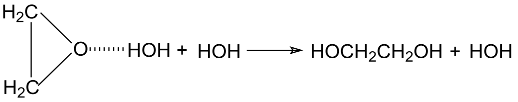

(6)

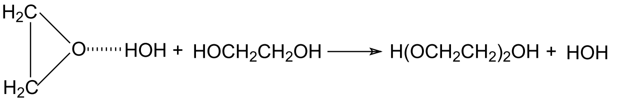

(7)

In concentrated aqueous solutions of glycols, it must be taken into account that ethylene oxide solvates in equilibrium (2) not only with water, but also with glycols. The effective concentration of proton donor substances that activate the oxide cycle due to the formation of hydrogen bond can be denoted as [SH]:

$$[SH] = [H_2O] + p\Sigma[Gly_i] \quad (8)$$

where $\Sigma[Gly_i]$ is the sum of the concentrations of ethylene glycol and all polyglycols; p is the parameter characterizing the efficiency of solvation of ethylene oxide.

Assuming that equilibrium (2) is quickly established and shifted to the left, equation (5) for concentrated glycol solutions takes the following form:

$$r = k_{cat}\,[A^-]\,[C_2H_4O]\,[SH] \qquad (9)$$

Taking into account that the non-catalytic reactions of ethylene oxide (1) proceeding in parallel with the mechanism (6, 7), we can obtain the general kinetic equation for the consumption of ethylene oxide in concentrated solutions during nucleophilic catalysis:

$$-\,d[C_2H_4O]/dt = (k_0([H_2O]+b\Sigma[Gly_i])+k_{ct}[A^-])\,([H_2O]+p\Sigma[Gly_i])[C_2H_4O] \qquad (10)$$

In equation (10), the known equality of the rate constants of the consecutive steps of reaction (1) was taken into account, starting from the second one, i.e. $b=k_1/k_0= k_2/k_0= k_3/k_0\ldots$

The parameters of equation (10) were determined using Mg-Al-acetate as a catalyst.

Initially in order to refine the distribution coefficient b, a series of experiments was carried out to determine the product composition of non-catalytic hydration of ethylene oxide in the range of ethylene oxide - water molar ratios β of 0.1-0.4. The experiments were carried out in an autoclave at 90 °C until the complete conversion of ethylene oxide. The amount of mono-, di- and triethyleneglycol in the reaction products was determined via gas-liquid chromatography. The results are shown in *Table 1*.

β	Monoglycol, %		Diglycol, %		Triglycol, %	
0.1	**Exp.**	**Calc.**	**Exp.**	**Calc.**	**Exp.**	**Calc.**
0.2	22.74	21.74	3.82	3.38	0.36	0.29
0.3	31.91	32.63	10.11	10.87	1.80	2.04
0.4	35.03	35.20	15.83	16.09	4.04	4.16

Table 1 The product composition of the non-catalytic hydration of ethylene oxide (b = 2.1)
1. táblázat Az etilén-oxid nem katalitikus hidratálásának termékösszetétele (b = 2,1)

According to the equation (10), the rates of formation of ethylene glycol (Gly_1) and polyglycols (Gly_i) in the absence of a catalyst ($k_{cat}\,[A^-] = 0$) is described according to the equation (11):

$$-\,d[Gly_1]/dt = k_0([H_2O]-b[Gly_1])([H_2O]+p\Sigma[Gly_i])[C_2H_4O]$$
$$-\,d[Gly_i]/dt = k_0b([Gly_{i-1}] - [Gly_i])([H_2O]+p\Sigma[Gly_i])[C_2H_4O] \qquad (11)$$

Dividing equation (11) by equation (10) and taking into account that $k_{cat}[A^-]=0$, one can obtain the equations (12, 13) to estimate the product composition shown in Table 1:

$$d[Gly_1]/d[C_2H_4O] = ([H_2O] - b[Gly_1])/([H_2O]+ b([H_2O]_0 - [H_2O])) \qquad (12)$$

$$d[Gly_i]/d[C_2H_4O]=b([Gly_{i-1}] - [Gly_i])/([H_2O] +b([H_2O]_0 - [H_2O])) \qquad (13)$$

Processing the experimental data summarized in Table 1 using the obtained equations (12 and 13) allowed for the calculation of the value b=2.1±0.1 – at this value, the best agreement between the calculated and experimental values is observed.

In order to determine the remaining unknown parameters of equation (10), a series of kinetic experiments were carried out with varying concentrations of LDH catalyst, water, ethylene glycol, and temperature. The reaction rate was measured by the pressure drop of ethylene oxide vapor over the reaction mixture. The initial concentration of ethylene oxide was in the range of 0.5-1.0 mol/l and water in a mixture of ethylene glycol-water from 20 to 80 wt. %. The experimental conditions provided the first-order kinetics for ethylene oxide.

The experimental values of the first-order rate constant were calculated as the slope in coordinates lnP vs. time, where P is the partial pressure of ethylene oxide.

The first-order rate constants are shown in *Table. 2*, calculated using the equation (14):

$$K= (k_0([H_2O]+bS[Gly_i])+k_{cat}[HCO_3^-])([H_2O]+pS[Gly_i]) \qquad (14)$$

C_{cat}, mol/l	Temperature					
	70 °C		80 °C		90 °C	
	$K_{exp.}$	$K_{calc.}$	$K_{exp.}$	$K_{calc.}$	$K_{exp.}$	$K_{calc.}$
	Water					
0	3.63	3.65	8.07	8.14	16.76	17.39
0.1	5.41	5.46	13.04	12.49	27.81	27.30
0.3	8.46	9.08	21.41	21.15	47.98	47.07
0.5	1.20	1.27	30.65	29.79	64.08	66.78
	Water – 80 %, ethylene glycol – 20 %					
0	3.17	3.34	7.66	7.46	15.62	15.94
0.1	6.03	5.02	11.71	11.47	25.74	25.09
0.3	8.19	8.36	19.84	19.48	45.67	43.35
0.5	10.20	11.70	25.54	27.46	60.60	61.55
	Water – 60 %, ethylene glycol – 40 %					
0	2.84	3.03	6.62	6.77	13.43	14.45
0.1	4.38	4.56	10.75	10.44	22.50	22.82
0.3	7.13	7.62	19.41	17.75	49.93	39.52
0.5	9.59	10.67	25.99	25.05	55.71	56.16
	Water – 40 %, ethylene glycol – 60 %					
0	2.47	2.71	5.54	6.06	10.79	12.93
0.1	4.29	4.10	9.31	9.37	19.66	20.49
0.3	6.60	6.86	16.17	15.97	33.32	35.56
0.5	8.91	9.61	23.41	22.56	45.23	50.58
	Water – 20 %, ethylene glycol – 80 %					
0	1.92	2.39	4.33	5.33	8.16	11.38
0.1	3.59	3.62	8.86	8.27	19.02	18.09
0.3	6.26	6.07	15.02	14.13	33.16	31.47
0.5	7.98	8.51	21.85	20.00	45.19	44.80

Table 2 The rate constants of the hydration of ethylene oxide, s^{-1}; 10^5
2. táblázat Az etilén-oxid hidratálásának sebességi állandói, s^{-1}; 10^5

The calculation of the parameters of equation (14), which provide an adequate description of the experimental data, results in the following values of $k_0=\exp(9.1-9355/T)$, $l^2/(mol^2\cdot s)$; $k_{cat}=\exp(18.2-10574/T)$, $l^2/(mol^2\cdot s)$; p=1.88.

The good agreement between the calculated and experimental values in *Table 3* confirms the sufficiency of the obtained model for describing the reaction rate and selectivity of the catalytic hydration of ethylene oxide and the possibility of its use in the development of an industrial process.

β	$[Gly_1]$, mol/L, exp.	$[Gly_1]$, mol/L, calc.	Reaction yield, %, exp.	Reaction yield, %, calc.
T=90 °C, C_{cat}=0.25 mol/L				
0.062	2.88	2.79	94.9	91.9
0.082	3.52	3.47	91.0	89.7
0.101	4.19	4.04	91.1	87.8
0.124	4.77	4.66	87.9	85.9
T=95 °C, C_{cat}= 0.2 mol/L				
0.039	1.94	1.90	97.1	95.1
0.072	3.15	3.11	91.1	89.9
0.098	3.98	3.92	88.7	87.3
0.131	4.8	4.75	84.8	83.9
0.178	5.72	5.72	80.3	80.3
0.220	6.32	6.38	76.5	77.2

Table 3 *Experimental and calculated concentrations and reaction yields of ethylene glycol at various molar ratios of ethylene oxide-water (b)*

3. táblázat *Kísérleti és számított etilén-glikol koncentrációk és reakció-hozamok az etilén-oxid-víz különböző mólarányainál*

5. Conclusions

LDHs are effective catalysts for industrial organic synthesis.

The activity of LDH is determined by the number of basic active sites on the surface, which, in turn, depends on the structure and chemical composition.

The use of LDHs as heterogeneous catalysts allows to move from homogeneous to heterogeneous catalysis, which reduces the environmental pollution effect.

References

[1] Tapio Salmi Ethylene oxide – kinetics and mechanism. Current Opinion in Chemical Engineering, 2012, V. 1-3, p. 321-327. https://doi.org/10.1016/j.coche.2012.06.002

[2] Georges, A. M. – Arturo, G. – Marc, E. L.: Kinetics of the reactions of ethylene oxide with water and ethylene glycols. Process Safety Progress, 2001, V. 20, p. 231-246. https://doi.org/10.1002/prs.680200405

[3] Butenko, E. – Kapustin, A. – Dan, O.: Propylene oxide polymerization in the presence of layered double hydroxides. Chemistry-Didactics-Ecology-Metrology, 2018, V. 23, N. 1-2, p. 137-142. https://doi.org/10.1515/cdem-2018-0009

[4] Butenko, E. – Kapustin, A.: Catalysis by Pillared Layered Double Hydroxides. Biomedical Journal of Scientific & Technical Research (BJSTR). 2019, V. 22, N1, p. 16289-16290 https://doi.org/10.26717/bjstr.2019.22.003681

[5] Butenko, E. – Kapustin, A.: Mercarbide Catalyst for Alcohol Ethoxylation. Journal of Siberian Federal University. Chemistry, 2020, V. 13, № 3, p. 330-339. https://doi.org/10.17516/1998-2836-0186

[6] Penaloza, David P.: Modified clay for the synthesis of clay-based nanocomposites. Epitoanyag, 2019, V. 71, N 1, p. 5-11. https://doi.org/10.14382/epitoanyag-jsbcm.2019.2

[7] Butenko, E.: Sorption reseaches on the removal of the bond ammonia from the wastewater. Epitoanyag, 2019, V. 71, N 3, p. 84-86. https://doi.org/10.14382/epitoanyag-jsbcm.2019.15

[8] Jinchang, Z. – Tiechun, L.: Facile synthesis of a highly effective layered double hydroxide catalyst and its application in the one-step ethoxylation of butyl acetate to oligo-ethylene glycol butyl ether acetates. Ind. Eng. Chem. Res. 2019, V. 58, p. 16320-16325. https://doi.org/10.1021/acs.iecr.9b01892

Ref.:

Butenko, Eleonora – **Kapustina**, Elena – **Kapustin**, Alexey: *Kinetics and products composition of catalytic hydration of ethylene oxide in the presence of layered double hydroxides*
Építőanyag – Journal of Silicate Based and Composite Materials, Vol. 73, No. 1 (2021), 9–12. p.
https://doi.org/10.14382/epitoanyag-jsbcm.2021.2

Infrared transmission and properties of glasses in the PbO–B_2O_3–SiO_2–GeO_2 system

Victor GOLEUS ▪ Department of Ceramics and Glass,
Ukrainian State University of Chemical Technology ▪ holvik22@gmail.com
Yurii HORDIEIEV ▪ Department of Ceramics and Glass,
Ukrainian State University of Chemical Technology ▪ yuriihordieiev@gmail.com

Érkezett: 2020. 06. 30. ▪ Received: 30. 06. 2020. ▪ https://doi.org/10.14382/epitoanyag-jsbcm.2021.3

Goleus Victor IVANOVYCH
head of the department of Ceramics and Glass of Ukrainian State University of Chemical Technology, Doctor of Technical Science, Professor. Author and co-author of more than 150 papers, 2 monographs, 50 author's certificates and patents. Scientific interests: studying the conditions of glass formation, the relationship between the chemical structure, oxide composition and physical and chemical properties borosilicate and other oxide glass; development of mathematical models for describing the properties of glasses depending on their oxide composition

Hordieiev Yurii SERGEEVICH
PhD Student of the department of Ceramics and Glass of Ukrainian State University of Chemical Technology. Author and co-author of more than 18 papers, 2 author's certificates and patents.

Abstract

A study of transparent materials for infrared emission is conditioned by the need for development and improvement of the optical and optoelectronic devices for space, aviation and medical purposes. Easily fusible optical glasses working in the near- and mid-infrared spectral region being characterized by a high refractive index are of great scientific and practical interest. The objective of these studies was to study influence of the chemical composition on the infrared transmission and properties of glasses in the PbO–B_2O_3–SiO_2–GeO_2 system. Conducted studies have testified to the fact that the transmission cutoff of glasses in the infrared region varies from 2.7 to 5.5 μm depending on the content of basic glass forming oxides B_2O_3, SiO_2 and GeO_2. The additive of fluoride to the compositions of glasses under study makes for the expansion of the transmission cutoff of infrared rays and the decrease in the intensity of absorption bands of the hydroxyl groups.

Keywords**:** lead glasses, oxyfluoride glasses, infrared transmission, refractive index, absorption
Kulcsszavak: ólomüveg, oxifluorid üvegek, infravörös átvitel, törésmutató, abszorpció

1. Introduction

Easily fusible glasses based on heavy metal oxides (PbO, Bi_2O_3, TeO_2, GeO_2 and others) are characterized by a number of valuable properties making these materials attractive and promising for many areas of applied optics. The important properties among them are: high refractive index; low softening point (makes it possible to make complex-shape articles by the extrusion or moulding); wide range of spectral transmission (from the near ultraviolet to the middle infrared band). The glasses, which are characterized by a high transmission in the near- and mid-infrared spectral region (up to λ = 5.5 μm), are of special scientific and practical interest [1–6]. This is due to the fact that some windows of the atmospheric spectral transparency are in this region, which is critically important when transferring the emission over large distances, especially for the aeronautical and aerospace engineering.

However, regardless of the prospects, a high level of optical losses, first of all conditioned by the impurity absorption of hydroxyl groups in the near- and mid-infrared spectral region, still prevents wide use of easily fusible glasses in the infrared optics [6–10]. The nature of the influence exerted by these impurities on the optical properties of glasses is firstly determined by the chemical composition and structure of initial glass.

The objective of these studies is to examine the influence of the chemical composition on the infrared transmission and properties of glasses in the PbO–B_2O_3–SiO_2–GeO_2 system.

2. Materials and methods

Finely ground quartz sand, high purity and chemically pure chemical reagents (H_3BO_3, $BaCO_3$, ZnO, Pb_3O_4, La_2O_3, Al_2O_3, and GeO_2) were used to prepare batches of test glasses, which chemical composition is set forth in *Table 1*.

Glass No.	Content of components, mol %					
	PbO	B_2O_3	SiO_2	GeO_2	ZnO+BaO	La_2O_3+Al_2O_3
PbB2	53.9	34	0	12.1	0	0
PbSi1	49.6	0	31.9	11.3	7.2	0
PbGe1	40	0	0	60	0	0
PbGe2	52	0	0	32	0	16

Table 1 Chemical composition of oxide glasses
1. táblázat Oxid üvegek kémiai összetétele

The glasses were melted in platinum crucibles with a volume of 50 ml in an electric furnace with the silicon carbide heating elements at a temperature of 1050 °C within 60 minutes. The samples of glasses for the determination of their properties were manufactured by the glass melt casting into the steel moulds followed by their muffle furnace annealing at a temperature of 320 °C.

The properties of glasses were determined according to the standard procedures: the density (d) of glasses by hydrostatic weighing according to GOST 9553–74; the thermal coefficient of linear expansion (TCLE) in the temperature range of 20-200 °C and the glass transition temperature (t_g) with the quartz dilatometer according to GOST 10978–2014.

The refractive index of the glasses have been measured with ellipsometric method [11]. The ellipsometric measurements were carried out at seven different incident angles (for error minimization) using LEM-3M ellipsometer equipped with low-intensity He-Ne laser (λ = 632.8 nm).

The transmission spectra of plane-parallel glass samples 2.0 mm thick were measured at room temperature with Spectrometer Thermo-Nicolet Avatar 370 FT–IR (in the range of 2500–25000 nm wavelengths at a pitch of 1 nm).

3. Results and Discussion

3.1 Research of properties of glasses in the PbO–B_2O_3–SiO_2–GeO_2 oxide system

Experimentally established values of the properties of oxide glasses are set forth in *Table 2*.

Glass No.	Refractive index (at λ=632.8 nm)	Density d, (g/cm³)	Glass transition temperature t_g, (°C)	Thermal expansion coefficient $\alpha \cdot 10^7$, (K^{-1})
PbB2	1.970	6.22	375	103
PbSi1	1.937	6.28	380	95
PbGe1	1.952	6.24	400	88
PbGe2	1.979	6.15	390	94

Table 2 Properties of oxide glasses
2. táblázat Oxid üvegek tulajdonságai

Depending on the content of basic glass forming oxides B_2O_3, SiO_2, and GeO_2, the glasses have different transmission cutoff and transparency in the infrared region (*Fig. 1*). A wavelength, at which the transmittance of glass 2 mm thick is greater than 50 % and 0 %, accordingly, is taken as the transmission cutoff ($\lambda_{50\%}$) and transparency ($\lambda_{0\%}$) in the infrared region.

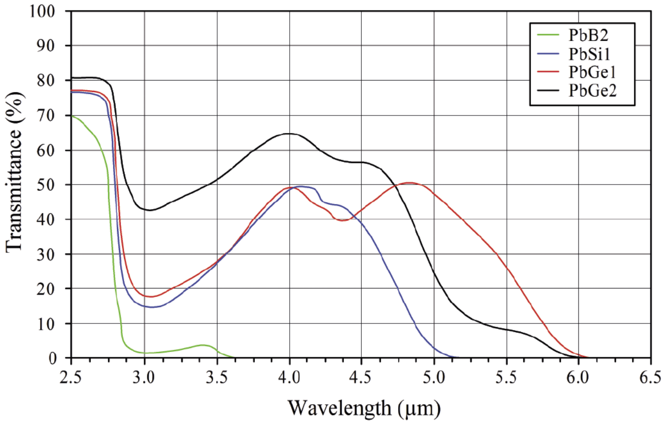

Fig. 1 IR transmission spectra of oxide glasses (2mm thick)
1. ábra Oxid üvegek (2 mm vastagságú) infravörös spektruma

The PbB2 glass (*Fig. 1*) having B_2O_3 in its content is characterized by a low transparency in the infrared region ($\lambda_{0\%}$ = 3.5 μm). The transmission cutoff of this glass is limited by a 2.7 μm wavelength; in the following, there begins a strong absorption band of free hydroxyl groups present in the glass.

Complete replacement of B_2O_3 with SiO_2 makes it possible to expand transparency of the PbSi1 glass up to $\lambda_{0\%}$ = 5.0 μm. However, due to the absorption bands in the 2.8–3.2 μm and 4.25 μm region, which are associated with the stretch vibration of free and tightly bound hydroxyl groups, the transmission cutoff of the PbSi1 glass ends in the region $\lambda_{50\%}$ = 2.7 μm.

The PbGe1 and PbGe2 glasses based on the glass forming oxide GeO_2, which are transparent up to $\lambda_{0\%}$ = 6.0 μm, have a high transparency in the infrared region. The transmission cutoff of these glasses ends in the region of absorption bands of free and tightly bound hydroxyl groups in the glass structure, which absorption maximum is in the region of 3.0 and 4.3 μm wavelengths, accordingly.

The analysis of IR transmission spectra of glasses in the PbO–B_2O_3–SiO_2–GeO_2 system has proved that all glasses have a limited infrared transmission cutoff up to $\lambda_{50\%}$ = 2.7 μm due to the absorption bands in the 2.8–3.2 μm and 4.25 μm region, which are associated with the stretch vibration of free and tightly bound –OH groups.

The removal of hydroxyl groups from the glass structure is a rather complicated technological task, which requires the creation of special glass melting conditions. The optical glasses with the minimum amount of impurities of –OH groups are obtained: when glass melting in vacuum or dry atmosphere; when glass melt bubbling with dry oxygen or nitrogen; when fluoride or chloride additives are introduced to the glass batch [6–10].

3.2 Study of influence of fluoride additives on the infrared transmission and properties of glasses in the PbO–B_2O_3–SiO_2–GeO_2 system

After a number of experiments carried out by us, we managed to attain high level of transparency and expand the transmission cutoff of oxide glasses with the help of fluoride glass dehydration technique [12]. The dehydration mechanism of this technique is based on a chemical reaction, which is going in the glass melt:

$$-OH_{melt} + F^-_{melt} \rightarrow -O^-_{melt} + HF\uparrow \qquad (1)$$

The study of influence of fluoride additives on the degree of dehydration of test glasses was conducted on the compositions (PbB2, PbSi1 and PbGe1) with different content of basic glass forming oxides. Lead, barium and zinc oxides were replaced with fluorides so that when fluorine was replaced with oxygen in the glass, its chemical composition (*Table 3*) corresponded to the initial glass composition (*Table 1*). Experimentally established values of the properties of glasses are set forth in *Table 4*.

Glass No.	Content of components, mol %					
	PbO	B_2O_3	SiO_2	GeO_2	ZnO+BaO	F^-
PbBF2	52.3	34	0	12.1	0	1.6
PbSiF1	48.2	0	31.9	11.3	7	1.6
PbSiF2	47	0	31.9	11.3	6.8	3
PbGeF1	38.4	0	0	60	0	1.6
PbGeF2	37	0	0	60	0	3

Table 3 Chemical composition of oxyfluoride glasses
3. táblázat Oxifluorid üvegek kémiai összetétele

Glass No.	Refractive index (at λ=632.8 nm)	Density d, (g/cm³)	Glass transition temperature t_g, (°C)	Thermal expansion coefficient $\alpha \cdot 10^7$, (K^{-1})
PbBF2	1.934	6.21	335	105
PbSiF1	1.920	6.26	360	97
PbSiF2	1.911	6.22	340	100
PbGeF1	1.936	6.24	365	92
PbGeF2	1.921	6.20	315	95

Table 4 Properties of oxyfluoride glasses
4. táblázat Oxifluorid üvegek tulajdonságai

The introduction of a small amount of fluorine additives to the composition of oxide glasses makes for a sharp decrease in the refractive index, density and glass transition temperature thereof as well as the increase of the TCLE and decrease in the glass colour intensity (*Fig. 2*).

Fig. 2 Samples of oxide and oxyfluoride glasses
2. ábra Oxid- és oxifluorid-üveg minták

Depending on the nature of the basic glass forming oxide in the composition of test glass, the introduction of fluorine additives exerts different influence on the change in the intensity of absorption bands of the hydroxyl groups.

When fluorine is introduced to the composition of the PbB2 glass (*Fig. 3*), there has been observed a decrease in content of free hydroxyl groups in the glass as evidenced by a decrease in the intensity of absorption band with the maximum in the 2.9 μm region and its shift to the longwave region.

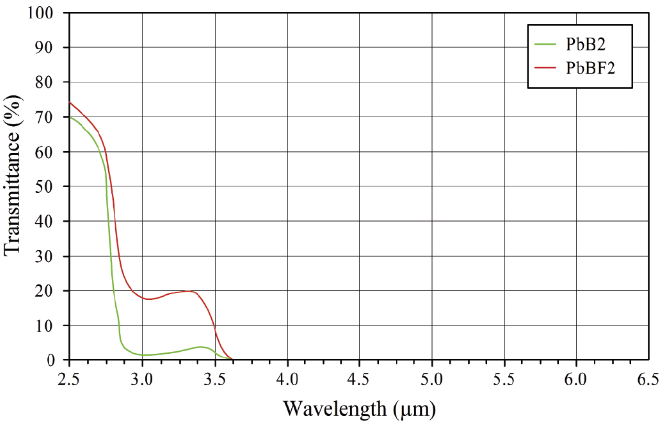

Fig. 3 IR transmission spectra of PbB2 and PbBF2 glasses (2mm thick)
3. ábra PbB2 és PbBF2 üvegek (2 mm vastagságú) infravörös spektruma

The transparency of glasses containing B_2O_3 in their composition completely ends in the region $\lambda_{0\%} = 3.6$ μm. The authors of different works [13–15] relate limited infrared transparency of glasses based on the B_2O_3 to the high vibrational frequencies associated of the B–O bonds.

The introduction of fluorine to the composition of the PbSi1 glass (*Fig. 4*, line PbSiF1) leads to the decrease in the intensity of absorption bands of free and tightly bound hydroxyl groups with the maximum in the 3.0 μm and 4.25 μm wavelength region. Further increase of fluorine content in the glass does not exert influence on the intensity of absorption bands of the hydroxyl groups (*Fig. 4*, line PbSiF2), however, leads to a significant decrease in the refractive index, density and glass transition temperature (Table 4). The transparency of glasses based on glass forming oxide SiO_2 completely ends in the region $\lambda_{0\%} = 5.0$ μm.

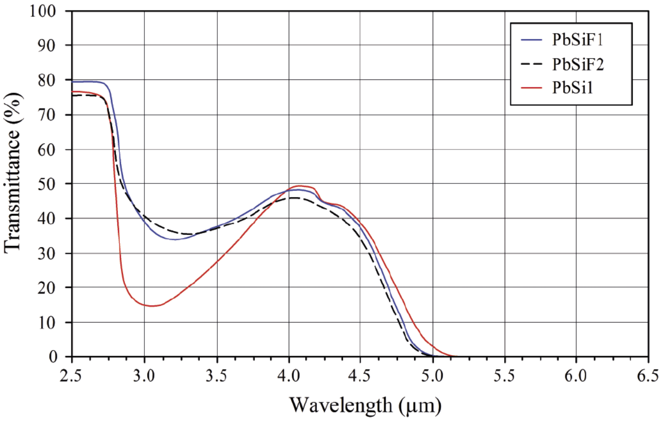

Fig. 4 IR transmission spectra of PbSi1, PbSiF1 and PbSiF2 glasses (2mm thick)
4. ábra PbSi1, PbSiF1 és PbSiF2 üvegek (2 mm vastagságú) infravörös spektruma

We managed to attain a high level of transparency and expand the transmission cutoff by introduction of a small amount of fluorine additives to the composition of the PbGe1 glass (*Fig. 5*) wherein GeO_2 is the glass forming oxide. The introduction of F^- anion to the composition of the PbGe1 glass makes for the expansion of its transmission cutoff in the infrared region up to $\lambda_{50\%} = 5.5$ μm and also increases its transparency up to $\lambda_{0\%} = 6.2$ μm.

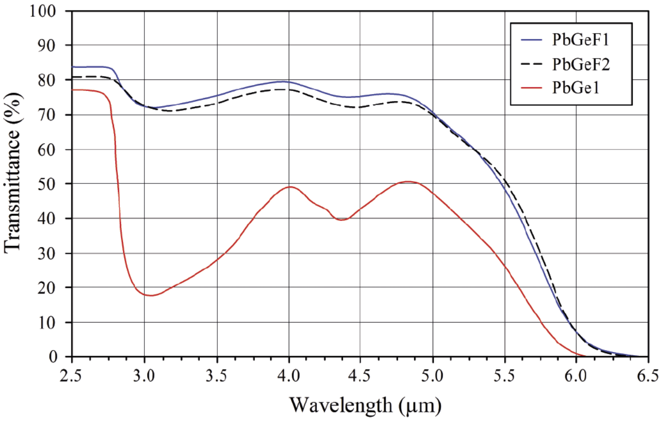

Fig. 5 IR transmission spectra of PbGe1, PbGeF1 and PbGeF2 glasses (2mm thick)
5. ábra PbGe1, PbGeF1 és PbGeF2 üvegek (2 mm vastagságú) infravörös spektruma

Further increase of fluorine content in the glass (*Fig. 5*, line PbGeF2) does not exert significant influence on the intensity of absorption bands of the hydroxyl groups and the transmission cutoff of glass, however, leads to a decrease in the refractive index, density and glass transition temperature.

4. Conclusions

The influence of chemical composition on the physicochemical properties of glasses in the $PbO–B_2O_3–SiO_2–GeO_2$ system is experimentally established. It is shown that the transmission cutoff of research glasses in the infrared region varies from 2.7 to 5.5 μm depending on the content and nature of the basic glass forming oxide. It is noted the efficiency of use of fluoride additives in the composition of oxide glasses in order to decrease the impurity absorptions of the hydroxyl groups in the infrared region.

References

[1] Munasinghe, H. T. – Winterstein-Beckmann, A. – Schiele, C. – Manzani, D. – Wondraczek, L. – Afshar, S. – Monro T. M.: Ebendorff-Heidepriem, H. (2013). Lead-germanate glasses and fibers: a practical alternative to tellurite for nonlinear fiber applications. Optical Materials Express. Vol. 3, No. 9, pp. 1488–1503, https://doi.org/10.1364/OME.3.001488

[2] Goleus, V. I. – Hordieiev, Y. S. (2018): Calculation of optical constants of glasses in the $PbO–B_2O_3–SiO_2–GeO_2$ oxide system. Voprosy Khimii i Khimicheskoi Tekhnologii. No. 5, pp. 92–96.

[3] Tao, G. – Ebendorff-Heidepriem, H. – Stolyarov, A. M. – Danto, S. – Badding, J. V. – Fink, Y. – Ballato, J. – Abouraddy, A. F. (2015): Infrared fibers. Advances in Optics and Photonics. Vol. 7, No. 2, pp. 379–458, https://doi.org/10.1364/AOP.7.000379

[4] Chung, J. – Watanabe, Y. – Yananba, Y. – Nakatsuka, Y. – Inoue, H. (2020): Novel gallate-based oxide and oxyfluoride glasses with wide transparency, high refractive indices, and low dispersions. Journal of the American Ceramic Society, Vol. 103, No. 1, pp. 167–175, https://doi.org/10.1111/jace.16701

[5] Hordieiev, Y. – Goleus, V. – Dimitrov, Ts. – Amelina, A. (2018): Development of optical glass for mid-infrared transmission. Proceedings of the University of Ruse. Vol. 57, 10–13.

[6] Kobayashi, K. (2003): Development of infrared transmitting glasses. Journal of non-crystalline solids, 316 (2–3), pp. 403–406, https://doi.org/10.1016/S0022-3093(02)01907-5

[7] Massera, J. – Haldeman, A. – Jackson, J. – Rivero-Baleine, C. – Petit, L. – Richardson, K. (2011): Processing of Tellurite-Based Glass with Low OH Content. Journal of the American Ceramic Society. Vol. 94, No. 1, pp. 130–136, https://doi.org/10.1111/j.1551-2916.2010.04031.x

[8] Jiang, X. – Lousteau, J. – Shen, S. – Jha, A. (2009): Fluorogermanate glass with reduced content of OH-groups for infrared fiber optics. Journal of non-crystalline solids. Vol. 355, No. 37–42, pp. 2015–2019, https://doi.org/10.1016/j.jnoncrysol.2009.04.069

[9] Richards, B. D. O. – Jha, A. – Jose, G. – Jiang, X. (2011): Oxide glasses for mid-infrared lasers. Proc. of SPIE. Vol. 8039, 80390R, https://doi.org/10.1117/12.886722

[10] Wang, W. C. – Zhou, B. – Xu, S. H. – Yang, Z. M. – Zhang, Q. Y. (2019):Recent advances in soft optical glass fiber and fiber lasers. Progress in Materials Science. Vol. 101, pp. 90–171, https://doi.org/10.1016/j.pmatsci.2018.11.003

[11] Krupych, O. – Martynyuk-Lototska, I. – Say, A. – Boyko, V. – Goleus, V. – Hordieiev, Y. – Vlokh, R. (2020): Characterization of $PbO–B_2O_3–GeO_2–La_2O_3$ and $PbO–B_2O_3–SiO_2–ZnO$ glasses: refractive, acoustic, photo-elastic and acousto-optic properties. Ukrainian Journal of Physical Optics, Vol. 21, No. 1, pp. 47–56, https://doi.org/ 10.3116/16091833/21/1/47/2020

[12] Tatarintsev, B. V. – Yakhkind, A. K. (1976): Dehydration of Tellurite Glasses by a Fluoride. Process. Fiz. Khim. Stekla, Vol. 2, No. 4, pp. 356–361.

[13] Golubeva, O. Y. – Pavinich, V. F. (2005): IR spectroscopic study of water in the structure of binary alkali borate glasses. Glass Phys Chem, Vol. 31, pp. 155–161, https://doi.org/10.1007/s10720-005-0037-5

[14] Donald, I. W. – McMillan, P. W. (1978): Infra-red transmitting materials. Part 2 Non-crystalline materials. Journal of Materials Science, Vol. 13, No. 11, pp. 2301–2312, https://doi.org/10.1007/BF00808042

[15] ElBatal, F. H. – Marzouk, M. A. – Abdel ghany, A. M. (2011): Gamma rays interaction with bismuth borate glasses doped by transition metal ions. Journal of materials science. Vol. 46, No. 15, pp. 5140–5152, https://doi.org/10.1007/s10853-011-5445-4

Ref.:

Goleus, Victor– **Hordieiev**,Yurii: *Infrared transmission and properties of glasses in the $PbO–B_2O_3–SiO_2–GeO_2$ system*
Építőanyag – Journal of Silicate Based and Composite Materials, Vol. 73, No. 1 (2021), 13–16. p.
https://doi.org/10.14382/epitoanyag-jsbcm.2021.3

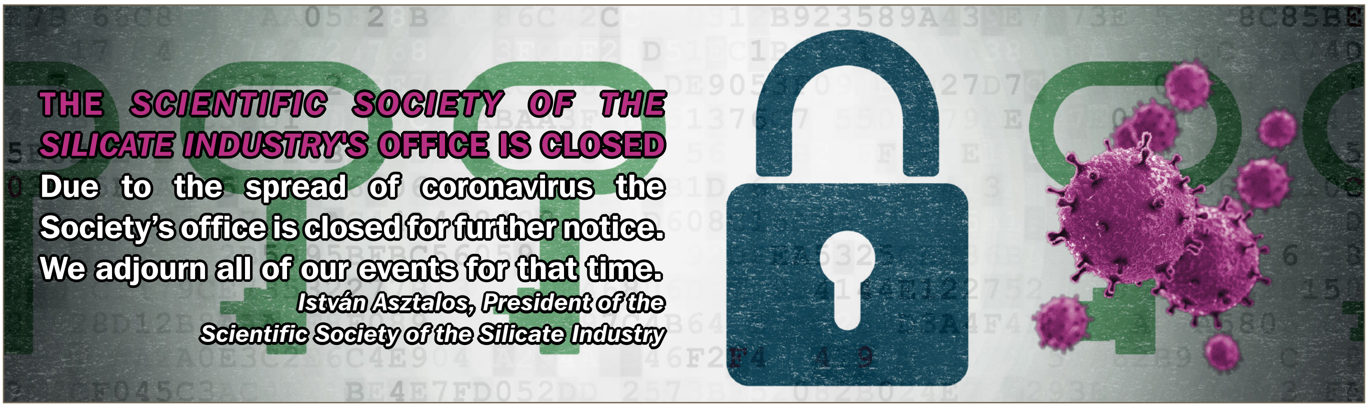

Durability against carbonation of concrete formulated with partial replacement of cement with marble powder

Ahmed MERAH
Lecturer (MCA), Civil engineering department, Amar Telidji University of Laghouat; Research professor; Civil Engineering department, Faculty of Civil Engineering and Architecture, Amar Telidji University of Laghouat
Research topics including mainly: concrete durability, concrete carbonation, anti-carbonation materials.

Benharzallah KROBBA
PhD, Assistant professor at the Department of Civil Engineering, University of Laghouat, Algeria. His research interests include, formulation of cement reparation mortars, concrete durability, the use of local materials as the dune sand in concrete.

AHMED MERAH ▪ University AmmarTelidji of Laghouat , Faculty of Civil Engineering and Architecture, Research Laboratory of Civil Engineering (LRGC), Laghouat, Algeria. ▪ a.merrah@lagh-univ.dz and ahmed-merrah@gmail.com

BENHARZALLAH KROBBA ▪ University AmmarTelidji of Laghouat , Faculty of Civil Engineering and Architecture, Structural Rehabilitation and Materials Laboratory (SREML), Laghouat, Algeria ▪ b.krobba@yahoo.fr and h.kroba@lagh-univ.dz

Érkezett: 2020. 06. 10. ▪ Received: 10. 06. 2020. ▪ https://doi.org/10.14382/epitoanyag-jsbcm.2021.4

Abstract

The first objective of this study is the use of marble waste powder as a partial replacement for cement (CEM I 42.5) in concrete. Furthermore, the phenomenon of carbonation significantly influences the durability of reinforced concrete structures, in this context, the second objective of this work is the study of the effect of accelerated carbonation on the durability of concretes formulated with cement. Containing marble powder with different percentages. To achieve this objective, four concrete mixes containing 0%, 10%, 15% and 30% marble powder as a cement replacement by weight were prepared. These concrete mixes were subjected to accelerated carbonation to study their durability against this phenomenon. The series of tests is carried out to study the effect of replacing 10%, 20% and 30% of the cement with marble powder on the depth of carbonation and the compressive strength and compare it with traditional concrete. The result of the present study indicates that the depth of carbonation increases with the increase in the rate of replacement of the cement with marble powder (10% to 30%) and that the resistance to compression decreases slightly with the increase in the replacement. the compressive strength of the concrete remains within the acceptable range recommended by the regulations used in Algeria.

Keywords: waste, marble powder, concrete durability, carbonation depth, compressive strength, environment
Kulcsszavak: hulladék, márványpor, beton tartóssága, karbonátosodási mélység, nyomószilárdság, környezet

1. Introduction

The consumption of fossil fuels releases trace gases in the atmosphere that affect the climate, such as methane, Sulphur dioxide, nitrogen and carbon dioxide. The latter being responsible for half of the greenhouse effect [1]. The global carbon dioxide (CO_2) content of the atmosphere reaches the symbolic and significant threshold of 400 parts per million (ppm) for the first time in 2015 and set new records in 2016 [2].

Concrete is the most widely used composite material in the world, given its high strength and stability. This material is mainly composed of cement, aggregates, water and possibly additives, all the components of this material are available in nature with the exception of the cement which requires fossil energy for production which is the main source of pollution air. The cement industry generates enormous quantities of carbon dioxide and thus participates in increasing the concentration of CO_2 in the air. This concentration can reach 1% and to produce a ton of cement, the cement industry releases a ton of CO_2 [3].

Moreover, the country of Algeria contains several marble quarries that generate marble powder who leads to an environmental problem, in this approach fits our study, which consists in the use of this waste as partial substitution with Portland cement. In this context, two objectives are to be expected, the first consists in limiting the CO_2 on emissions due to the manufacture of cement, the second consists in minimizing the effects on the environment by the use of marble powder as a partial replacement for the cement, in this axe of research several researchers have carried out several studies on the effect of this partial replacement of cement with marble powder, among these researchers, [4] conducted a study on the possibility of using marble powder in self-placing concrete as a partial replacement for cement, the results of this study showed that the optimal percentage of replacement is around 50% which leads to an increase in compressive strength . [5-6] studies the effect of the use of marble powder as a partial replacement of cement on the concrete properties, the results obtained shown that the use of marble powder improves workability, compressive and tensile strength. [7-10] studied the effect of different percentage of substitution of cement by marble powder on compressive strength, the results of this research shown that the optimal rate of replacement of cement by powder marble is up to 10%. In the same way, [11-12] concluded that an optimum of 15% replacement leads to an improvement in strength and durability of concrete.

In the same way other researchers continued to explore this field, [13] concluded that the marble powder incorporated in concrete shows increase in mechanical properties at 15% replacement by weight of cement for lower w/b ratios 0.35 and 0.40, and for w/b ratio 0.45 the strength increases only up to 10% replacement. In their study, [14] found out that the use of waste marble in the conventional or self-compacting concrete can improve durability properties of the concrete.

In their study, [15] show that waste marble can be used into concrete to improve its strength and permeation properties, with the maximum improvement obtained at 40% replacement level. In [16] it was concluded that the maximum percentage of partial replacement of marble powder in cement don't exceed 20%.

The studies cited in this work in the field of partial replacement of cement with marble dust conclude that the replacement of the cement must not exceed 20% of marble dust in order to have acceptable compressive strength of the concrete. High levels of marble dust increase the capillarity of concrete.

On the other hand, many environmental phenomena influence the durability of reinforced concrete structures. Among these phenomena, we can cite the concrete carbonation which is one of the main factors of degradation of unprotected reinforced concrete structures, and those exposed to high concentrations of carbon dioxide (such as road tunnels). This causes corrosion of the reinforcements, causing the concrete to lose its alkalinity and consequently causes the reduction of the service life of reinforced concrete structures. carbon dioxide gas penetrates through the open porosity of concrete to react with interstitial water to give carbonic acid, this in turn reacts with portlandite $Ca(OH)_2$ (product responsible for the durability of the steels against corrosion while keeping an environment with a basic pH of the order of 13), this reaction produces calcium carbonate $CaCO_3$ which consumes the reserve of portlandite and putting steels without protection. Then, lead to disorders in the construction by swelling and cracking.

Several researchers have studied the effect of carbonation, on the durability of concretes formulated with substitution of cements with marble powder, in their study [17-18] shows that the depth of carbonation increases with the increase of the replacement.

In [19] it is shown that with 15% of partial replacement of the marble powder, the resistance for carbonation was improved. According to the experimental study, [20-21] also show that the depth of carbonations increased in case of use of powder marble.

In their review study, [22] show that the concrete carbonation depth depends on its porosity. Carbonation values also decrease with inclusion of marble powder and reported a similar trend to carbonation depth and water absorption by immersion for the chloride mitigation coefficient.

This paper presents a contribution in this area. this contribution consists on studying the durability of concrete formulated with a partial replacement of cement with marble powder who is the first objective, the second consist to study the effect of using marble powder as partially replace of cement on the durability of concrete against the phenomenon of concrete carbonation.

The result of this investigation indicates that the carbonation depth decreases with the increase of the replacement of cement with waste marble powder (10 % to 30%) and the compressive strength decreases slightly with the increase of replacement. the compressive strength remains within the acceptable range of M25 concrete.

2. Materials

2.1 Cement

The used cement is a Portland cement CEM I 42.5 produced in the locality of BISKRA in South East of Algeria, the cement density is 3.07 g/cm³, with the characteristics shows in *Table 1, 2* and *3*.

Elements	Content %	Norms
SO_3	2.30	(NA 237) < 3.5%
CL	0.028	(NA 5080) ≤ 0.1%
P.A.F	2.04	(NA 237) ≤ 5%
C_3S clinker	62	In accordance with Bogue
C_2S clinker	13	In accordance with Bogue
C_3A clinker	1.5	In accordance with Bogue
C_4AF clinker	17	In accordance with Bogue

Table 1 Mineralogic characteristics of used Cement CEM I 42.5
1. táblázat A felhasznált cement (CEM I 42.5) ásványtani jellemzői

Designation	Measures	Norms
Specific surface Blaine (cm^2/g)	3420	(NA231)
Start of taking (min)	180	(NA233) ≥60 min
Hot expansion (min)	0.5	≤10mm(NA232)
Consistence (%)	25.7	T(NA290)

Table 2 Physics proprieties of used cement CEM I 42.5
2. táblázat A használt cement (CEM I 42.5) fizikai tulajdonságai

Mechanical proprieties			
Compressive strength (MPa)	2 days	≥10	21
	28 days	62.5≥R≥42.5	49.5

Table 3 Mechanic proprieties of used cement CEM I 42.5
3. táblázat A használt cement mechanikai tulajdonságai (CEM I 42.5)

2.2 Powder marble

The used marble powder was a waste resulting from the cutting, shaping and lustration of marble stones. This powder was supplied by the company MCA (Marble Tile and Agglomarble installed in locality of Bordj Bou Arrérdj in Algeria). The physic and the chemical properties of the marble powder are given in *Table 4*.

Powder marble										
Component	SiO_2	Al_2O_3	Fe_2O_3	CaO	MgO	K_2O	Na_2O	SO_3	Cl^-	PAF
Content (%)	0.76	0.41	0.23	54.9	0.61	0.24	0.04	0.61	0.005	36.3

Table 4 Chemical properties of the marble powder
4. táblázat A márványpor kémiai tulajdonságai

2.3 Aggregates

The used sand is alluvial (0-5 mm) which produced by Oued M'zi quarry of Laghouat, Algeria, two classes of limestone aggregates (3-8 mm and 8-15 mm) were used in the concrete formulation which produced by the quarry (Laghouat).

The *Table 5* gives the physical proprieties of the used aggregates

Physical proprieties of the used aggregates	Standard	Aggregates		
		Sand	Gravel	
		0/5	3/8	8/15
Apparent density (g/cm³)	NF P 18-554	1.564	1.319	1.255
Absolute density (g/cm³)		2.6	2.65	2.65
Absorption coefficient (%)		1	1.5	1.5

Table 5 Physical proprieties of the used aggregates
5. táblázat A felhasznált adalékanyag fizikai tulajdonságai

The used sand has a particle size of 0–5 mm, apparent density of 1.56 g/cm³ and absolute density of 2.61 g/cm³. Two sizes of aggregates (3–8 mm), (8–15 mm) are used to formulate the concretes, these aggregates are characterized by a calcareous rock with a high calcium carbonate content (98% $CaCO_3$), their apparent densities are 1.32 g/cm³ and 1.26 g/cm³ respectively. Their absolute density is 2.6 g/cm³. The used water is tap water. It meets all the requirements of NFP 18-303 and EN 1008, taking into account the concentrations of suspended solids and dissolved salts.

3. Methods

3.1 Concrete formulation

The used concrete formulation method in the present study is DREUX GORISSE method.

The results of the concrete formulation were gives in *Table 6*:

S/G	W/C	Sand (S) (kg/m³)	Gravel (G) 3/8 (kg)
0.60	0.57	683.7	146.7
Gravel (G) 8/15 (kg)	**Cement (C) (CEM I) (kg)**	**Water (W)(l)**	**Slump test (cm)**
990.25	374.40	216.42	8

Table 6 Results of control concrete formulation (Legend: S: Sand, G: Gravels, W: Water, C: Cement)
6. táblázat A referencia beton tulajdonságai (S: homok, G: kavics, W: víz, C: cement)

Table 6 shows the results of the control concrete formulation. According to the synthesis of this results, the concrete formulation has the density, who is a normal concrete according the standard NF EN 12350-6 [28] (Normal concrete with a density between 2000 and 2600 kg/m³). From this control concrete formulation, three other concrete mixes were formulated by substituting different percentages (10%, 20% and 30%) of cement replace by weight with marble powder according to *Table 7*.

Concretes formulations	Cement (kg)	Marble powder (kg)
B1 (0% replacement)	374.4	0
B2 (10% replacement)	336.96	37.44
B3 (20% replacement)	299.52	74.88
B4 (30% replacement)	262.08	112.32

Table 7 Weights of Marble powder for different concrete formulations
7. táblázat Márványpor tömege a különböző betonkeverékekben

3.2 Confection and preservation of samples

Before mixing the concretes, the aggregates, previously washed and dried in an oven at 10 ± 5 °C for one day (24 h), then cooled in ambient air, then they are introduced, according to mass proportions already known. in parallel with the preparation of the concrete, the moulds (7×7×7 cm³) are prepared for the determination of the compressive strength and for the accelerated carbonation tests. All the samples are kept in the moulds for 24 hours in plastic film, after demoulding, they are immersed in water at T = 20 ± 0.5 °C according to standard NA 426 for 28 days and according to the recommendation of the AFPC AFREM [22] until the deadlines for the start of tests (*Fig. 1*).

Fig. 1 Samples conservation
1. ábra Minták tárolási módja

Fig. 2 Machine for compressive strength test
2. ábra A nyomószilárdság vizsgálatához használt eszköz

After 28 days of cure, the cubic samples (7×7×7 cm³) of prepared concrete will be subjected to two test campaigns, compression test and accelerated carbonation test.

3.3 Compressive strength test

In order to determinate the compressive strength of the four concrete formulations (B1, B2, B3 and B4) cubic samples

(7×7×7 cm^3) were used. The compressive strength for cubic samples of carbonated and control concrete samples were determinate at age 7, 14 and 28 days.

The compression resistance test was carried out on 7×7×7 cm^3 cubic samples according to NF P18-406. The hydraulic press used has a loading speed of 0.5 MPa / Sec with a capacity of 3000 kN. the rupture stress is given directly by the testing machine with an accuracy of 0.5 MPa (*Fig. 2*).

3.4 Accelerated carbonation test

The concrete carbonation is a very slow phenomenon in the atmosphere, the concentration of carbon dioxide is not very important (of the order of 0.3%) in the air, the effect of this phenomenon is manifested only after several years of exposure of reinforced concrete structures to this phenomenon, therefore, it is necessary to find a way to accelerate the carbonation of the cementitious material ensuring results representative of this natural phenomenon. This test is called accelerated carbonation test.

3.4.1 Accelerated carbonation test procedure according to AFPC-AFREM test protocol

The test consists in following the evolution of the thickness of the carbonated concrete preserved in an atmosphere rich in carbon dioxide (CO_2).

A.1. Equipment:

- **Ventilated oven:** controlled at 40 ± 2°C, located in a room with a temperature of 20 ± 2°C
- **Accelerated carbonation chamber:** the accelerated carbonation test consists in obtaining a gas mixture (50% CO_2 + 50% air) in the carbonation chamber (*Fig. 3*) with controlling the relative humidity which must be between 40 and 80%. To monitor the relative humidity, a hygrometer was used. The carbonation test is executed using a carbon dioxide (CO_2) incubator according to the AFPC-AFREM test protocol (1997) [22].

Fig. 3 Accelerated carbonation chamber
3. ábra Gyorsított karbonátosító kamra

To start the accelerated carbonation test, the samples must be preconditioned in two phases:

In the first phase, the samples were submitted to a cure in a humid environment (relative humidity greater than 95% or emerged into water) for 28 days according AFPC AFREM[22] then weighed, in order to determining the bulk density and the water content.

In the second phase, they are placed in an oven at 40 ± 2° C, for 48 hours, then weighed for second time [22]. The two faces of each sample must be covered with adhesive aluminium to guide the diffusion of CO_2, then the samples are subjected to accelerated carbonation in the carbonation chamber for 28 days (*Fig. 4* and *Fig. 5*) AFPC AFREM[22] while other control samples are stored in the laboratory to measure the compressive strength.

Fig. 4 Preparation of samples for accelerated carbonation test
4. ábra Minták előkészítése vizsgálathoz

Fig. 5 Samples into the chamber of carbonation
5. ábra Minták a karbonátosító kamrában

At the age 7, 14 and 28 days, concrete samples are weighed and removed from the carbonation chamber to measure the evolution of accelerated carbonation according to the experimental procedures of the AFPC AFREM 1997 recommendations [22]. To measure the concrete carbonated depth, the samples are cut in two parts and using the colour indicator recommended by the procedure of standard NF P18-458 the reading is made immediately. It colours the uncarbonated concrete in pink while the carbonated concrete does not change. The used PH indicator to reveal the carbonated concrete is a phenolphthalein solution (*Fig. 6*).

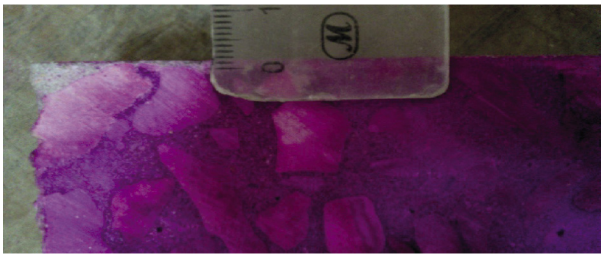

Fig. 6 Determination of Carbonation depth with phenolphthalein pulverisation
6. ábra Karbonátosodási mélység meghatározása fenoftalein oldattal

4. Results and discussions

4.1 Densities and water content of samples

In order to conduct the accelerated carbonation test and according to AFPC AFREM 97 [22] recommendations, in the first pre-conditioning phase, the bulk density and water content of the samples must be determined for the accelerated carbonation test.

Table 8 show the results of densities and water content for the four-concrete formulation

Concrete formulations	Densities (kg/m³)	Water content (%)
B1(0% replacement)	2537.63	2.37
B2(10% replacement)	2566.14	2.32
B3(10% replacement)	2602.85	2.32
B4(10% replacement)	2592.64	2.34

Table 8 Densities and water content for the four concrete formulations
8. táblázat A négy beton keverék sűrűsége valamint víztartalma

Table 8 show that the densities increases with the increase of substitution (cement with the powder marble) for the four concrete formulations. The water content of the all-concrete formulations have the same value, from these results, then, the accelerated carbonation test can be started according to AFPC AFREM 97 [22].

4.2 Effect of the replacement (cement by the powder marble) on the compressive strength for the four concretes formulations

At the age of 28 days, samples were tested with the compressive machine, the table 9 show the effect of the carbonation on the compressive strength of the control concrete and the other concretes with different percentages of replacements of cement with powder marble (10%, 20% and 30%)

Compressive strength (MPa)			
Formulation B1(control)	Formulation B2 (10% replacement)	Formulation B3 (20% replacement)	Formulation B4 (30% replacement)
59.2	55.4	52.9	46.4

Table 9 Compressive strength for different concrete formulations
9. táblázat A minták nyomószilárdsága

In *Fig. 7*, it is clearly shown that the compressive strength decreases with increasing percentage of substitution of cement with marble powder. This decrease is slightly (of the order of 11%) up to a percentage of 20% of substitution and it is important of the order of 22% for a substitution of 30%.

The obtained results for the compressive strength of concrete are in agreement with those obtained by [23]. The value of the compressive strength of 46 MPa corresponding to a substitution of cement with 30% of marble powder is acceptable for the realization of structural elements of reinforced concrete. This result will lower cost of making reinforced concrete structures, with condition to protecting the exposed concrete against carbonation.

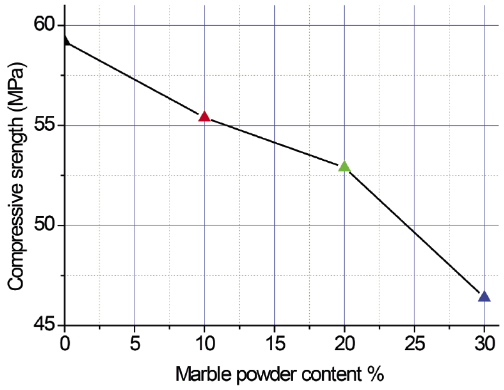

Fig. 7 Compressive strength with marble powder content
7. ábra Nyomószilárdság a márványpor tartalom függvényében

4.3 Effect of the carbonation on the gain mass for the four concrete formulations

The *Table 10* show the effect of the carbonation on the gain mass for the four concrete formulations at the different ages 7, 14 and 28 days.

Age (days)	Mass gain (g)			
	Concrete B1 (control)	Concrete B2 (10% replacement)	Concrete B3 (20% replacement)	Concrete B4 (30% replacement)
7	853.24	865.92	881.7	913.3
14	856.8	869.2	886.8	923.1
28	858.2	870.6	889.1	925.6

Table 10 Mass gain (g) for different concrete formulations
10. táblázat A betonkeverékek tömegnövekménye (g)

From *Table 10*, we draw the following curve (*Fig. 8*)

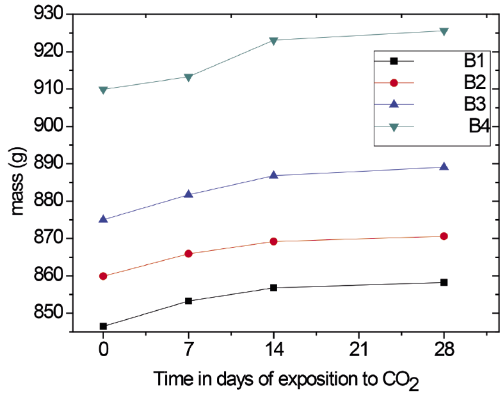

Fig. 8 Mass gain for the four concretes formulations
8. ábra A négy betonkeverék tömegnövekménye

Fig. 8 show that the carbonation increases the mass of samples with the increase of the substitution (cement by marble powder (10%, 20%, 30%). This increase is due mainly to the concrete carbonation who makes changes in the microstructure of carbonated concrete (replacement of portlandite by calcite).

4.4 Effect of the accelerated carbonation on the four concretes formulations.

The carbonate depth was determined, according to the AFPC-AFREM 97 procedure [22] with a phenolphthalein method described above, applied to the face of the cubic samples (7×7×7 cm^3) after cutting into two parts with the ages 7, 14 and 28 days. *Table 11* shows the evolution of the depth of carbonation at different ages for the four concrete formulations.

Age (days)	Carbonation depth (mm)			
	Concrete B1 (Control)	B2 (10% replacement)	B3(20% replacement)	B4(30% replacement)
7	1	3	4	6
14	2	5	7	8
28	3	6	7.5	9.5

Table 11 Evolution of carbonation depth at different ages for the four concrete formulations
11. táblázat A karbonátosodási mélység alakulása különböző életkorokban a négy betonkeverék esetében

From the *Table 11*, we draw the following curve (*Fig. 9*).

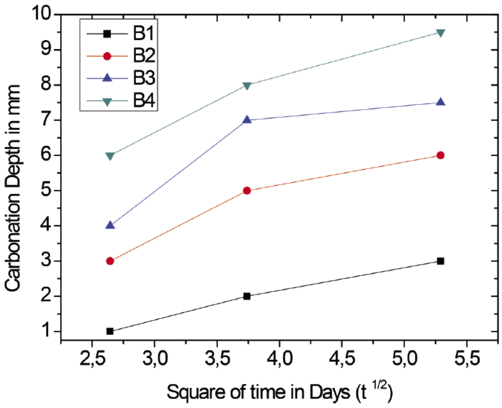

Fig. 9 Carbonation depth for the four concrete formulations
9. ábra Karbonotosodási mélység a négy betonkeverék esetén

According to the curve of the evolution of the carbonation depth with the square of time for the different concretes, we note that the depth of the carbonation increases with the substitution of cement by the marble powder (10%, 20%, 30%).

In addition, it can be seen from the previous curve (*Fig. 9*) that the evolution of the carbonation depth is relatively fast from 7 days to 14 days and stabilizes at almost constant values until the 28th days. This for all concretes (B1, B2, B3, B4). This result can be explained as follows:

During the 7 to 14-day period, the available amount of portlandite is larger, resulting in faster carbonation with calcite formation.

For the period between 14 and 28 days, the available amount of portlandite becomes low as it is consumed during the first period. This will reduce the carbonation rate.

This reduction is caused by clogging of pores caused by the formation of calcite which has a molar volume greater than the molar volume of portlandite.

On the other hand, it can be concluded that the depth of carbonation increases with the increase of the percentage of replacement of powder marble.

5. Conclusions

From this study, the following conclusions can be written

- The depth of carbonation increases with the time of exposure in the enclosure of accelerated carbonation.
- The increase in the substitution of cement by powdered marble increases the depth of carbonation. this is due to the replacement of cement by the marble powder which makes decreased, the rate of portlandite and consequently, it accelerates the consumption of this one by the reaction of carbonation.
- The increase in the mass of carbonate samples increases with the increase in the depth of carbonation, this is mainly due to the carbonation of portlandite giving rise to calcite denser than portlandite
- The compressive strength decreases with substitution of the cement by the marble powder. This decrease is slight and remains within values acceptable by Algerian standards.
- Partial replacement of cement with marble powder up to 30% can give a quality concrete (Acceptable compressive strength according to Algerian standards). Moreover, this replacement contributes to reducing the harmful effects of marble waste on the environment.
- To protect this concrete and make it durable against carbonation, it must be protected by an anti-carbonation coating.
- The optimal rate (30%) obtained by replacing cement with marble powder can reduce the carbon dioxide emission in the atmosphere by the production of CEM I cement by 25%.

References

[1] Retallack, G. J. – Conde, G .D. (2020): Deep time perspective on rising atmospheric CO_2. Global and Planetary Change 103177.
[2] Betts, R. A. – Jones, C. D. – Knight, J. R. – Keeling, R. F. – Kennedy, J. J. (2016): El Niño and a record CO_2 rise. Nature Climate Change 6, 806.
[3] Diet, A. – Schmitt, A. (1996): Electricity of France and renewable energies: this is part Solar systems (Review) 17–23.
[4] Sadek, D.M. – El-Attar, M.M. – Ali, H.A. (2016): Reusing of marble and granite powders in self-compacting concrete for sustainable development. Journal of Cleaner Production 121, 19–32. https://doi.org/10.1016/j.jclepro.2016.02.044
[5] Soliman, N. M. (2013): Effect of using marble powder in concrete mixes on the behaviour and strength of RC slabs. International Journal of Current Engineering and Technology 3, 1863–1870.
[6] Aliabdo, A. A. – Elmoaty, A. E. M. A. – Auda, E. M. (2014): Re-use of waste marble dust in the production of cement and concrete. Construction and building materials 50, 28–41. https://doi.org/10.1016/j.conbuildmat.2013.09.005
[7] Kumar, R. – Kumar, S. K. (2015): Partial replacement of cement with marble dust powder. International Journal of Engineering Research and Applications 5, 106–114.
[8] Vaidevi, C. (2013): Study on marble dust as partial replacement of cement in concrete. Indian journal of engineering 4, 14–16.
[9] Rodrigues, R. – De Brito, J. – Sardinha, M. (2015): Mechanical properties of structural concrete containing very fine aggregates from marble cutting sludge. Construction and Building Materials 77, 349–356. https://doi.org/10.1016/j.conbuildmat.2014.12.104
[10] Ergün, A. (2011): Effects of the usage of diatomite and waste marble powder as partial replacement of cement on the mechanical properties

of concrete. Construction and building materials 25, 806–812. https://doi.org/10.1016/j.conbuildmat.2010.07.002

[11] Singh, M. – Srivastava, A. – Bhunia, D. (2019): Long term strength and durability parameters of hardened concrete on partially replacing cement by dried waste marble powder slurry. Construction and Building Materials 198, 553–569. https://doi.org/10.1016/j.conbuildmat.2018.12.005

[12] Singh, M. – Srivastava, A. – Bhunia, D. (2017): An investigation on effect of partial replacement of cement by waste marble slurry. Construction and Building Materials 134, 471–488. https://doi.org/10.1016/j.conbuildmat.2016.12.155

[13] Singh, M. – Srivastava, A. – Bhunia, D. (2019): Analytical and experimental investigations on using waste marble powder in concrete. Journal of Materials in Civil Engineering 31, 04019011. https://doi.org/10.1061/(ASCE)MT.1943-5533.0002631

[14] Ulubeyli, G. C. – Bilir, T. – Artir, R. (2016): Durability properties of concrete produced by marble waste as aggregate or mineral additives. Procedia engineering 161, 543–548.

[15] Vardhan, K. – Siddique, R. – Goyal, S. (2019): Strength, permeation and micro-structural characteristics of concrete incorporating waste marble. Construction and Building Materials 203, 45–55. https://doi.org/10.1016/j.conbuildmat.2019.01.079

[16] Ashish, D. K. (2018): Feasibility of waste marble powder in concrete as partial substitution of cement and sand amalgam for sustainable growth. Journal of Building Engineering 15, 236–242. https://doi.org/10.1016/j.jobe.2017.11.024

[17] Ashish, D. K. (2019): Concrete made with waste marble powder and supplementary cementitious material for sustainable development. Journal of cleaner production 211, 716–729. https://doi.org/10.1016/j.jclepro.2018.11.245

[18] Gameiro, F. – De Brito, J. – da Silva, D. C. (2014): Durability performance of structural concrete containing fine aggregates from waste generated by marble quarrying industry. Engineering Structures 59, 654–662 https://doi.org/10.1016/j.engstruct.2013.11.026

[19] Singh, M. – Choudhary, K. – Srivastava, A. – Sangwan, K.S. – Bhunia, D. (2017): A study on environmental and economic impacts of using waste marble powder in concrete. Journal of Building Engineering 13, 87–95. https://doi.org/10.1016/j.jobe.2017.07.009

[20] Rana, A. – Kalla, P. – Csetenyi, L. J. (2015) Sustainable use of marble slurry in concrete. Journal of Cleaner Production 94, 304–311. https://doi.org/10.1016/j.jclepro.2015.01.053

[21] Kumar, A. – Thakur, A. (2018): A State of Art Review: On Usage of Waste Marble Powder In Concrete Production.

[22] Rougeau, P. : AFREM crossover test results, Accelerated carbonation test, CERIB, 1997.

[23] Tayeh, B. A. (2018): Effects of marble, timber, and glass powder as partial replacements for cement. Journal of Civil Engineering and Construction 7, 63–71. https://doi.org/10.32732/jcec.2018.7.2.63

Ref.:
Merah, Ahmed – **Krobba**, Benharzallah: *Durability against carbonation of concrete formulated with partial replacement of cement with marble powder*
Építőanyag – Journal of Silicate Based and Composite Materials, Vol. 73, No. 1 (2021), 17–23. p.
https://doi.org/10.14382/epitoanyag-jsbcm.2021.4

Synthesis and characterization of iron-doped $GdMnO_3$ multiferroic ceramics

Jamal Eldin F. M. IBRAHIM ▪ Institute of Ceramics and Polymer Engineering,
University of Miskolc, Hungary ▪ jamalfadoul@gmail.com
Ayhan MERGEN (deceased ▪ Marmara University, Turkey.
Umut PARLAK ▪ Peter Grünberg Institute, Research Centre Jülich, Germany
▪ umut.parlak@marmara.edu.tr
Emese KUROVICS ▪ Institute of Ceramics and Polymer Engineering,
University of Miskolc, Hungary ▪ fememese@uni-miskolc.hu
Mohammed TIHTIH ▪ Institute of Ceramics and Polymer Engineering,
University of Miskolc, Hungary ▪ medtihtih@gmail.com
László A. GÖMZE ▪ Institute of Ceramics and Polymer Engineering,
University of Miskolc, Hungary ▪ IGREX Engineering Service Ltd, ▪ femgomze@uni-miskolc.hu

Érkezett: 2020. 05. 25. ▪ Received: 25. 05. 2020. ▪ https://doi.org/10.14382/epitoanyag-jsbcm.2021.5

Abstract

In this research work, monocrystalline Fe-doped $GdMnO_3$ ceramics specimens were prepared through solid-state reaction technique, several characterization methods, for instance, Scanning Electron Microscopy (SEM), X-Ray Diffraction (XRD), Energy Dispersive Spectroscopy (EDX) and Vibrating Sample Magnetometer (VSM) were used to investigate the topographical, structural and magnetic behaviours of the produced samples. All the samples show a single phase which confirmed by XRD and SEM. Magnetic properties of all the prepared samples at the low temperature (10 K) showed antiferromagnetic behaviour with a small difference in magnetization. The slight change in magnetic characteristics could probably occur because of small lattice structural distortion. Fe-doped $GdMnO_3$ could be a material of choice for multiferroic application showing a superior antiferromagnetic property.

Keywords: multiferroic materials, doping, $GdMnO_3$ ceramics, solid-state reaction, magnetic properties
Kulcsszavak: multiferroikus anyagok, adalékolás, $GdMnO_3$ kerámiák, szilárdfázisú reakció, mágneses tulajdonságok

Jamal-Eldin. F. M. IBRAHIM
is a lecturer at the University of Bahri, Khartoum, Sudan, he graduated from Marmara University, Istanbul, Turkey, Institute of Pure and Applied Sciences, Department of Metallurgical and Materials Engineering, for the time being, he is a PhD student at the University of Miskolc, Institute of Ceramics and Polymer Engineering, under supervision of Prof. L. A. Gömze.

Ayhen MERGEN (deceased)

Umut PARLAK
is Research assistant in Metallurgical and Materials Engineering at Marmara University (Istanbul/Turkey), he graduated from Gebze Technical University (Gebze/Turkey), recently, he is a PhD student at Jülich Research Centre (PGI-6) and Duisburg-Essen University.

Emese KUROVICS
is graduated from the University of Miskolc, Department of Ceramics and Silicate Engineering as a material engineer, where she actually continues her study as PhD student under supervision of Prof. L. A. Gömze.

Mohammed TIHTIH
Is a lecturer at the Sidi Mohamed Ben abdellah University, Morocco, he graduated from Faculty of sciences Dhar El Mahraz, Fez, Morocco, Department of Physics, for the time being, he is a PhD student in the University of Miskolc, Institute of Ceramics and Polymer Engineering, under supervision of Prof. L. A. Gömze

László A. GÖMZE
is a professor and establisher of the Department of Ceramics and Silicate Engineering at the University of Miskolc, Hungary. He is author and coauthor of 2 patents, 6 books and more than 300 scientific papers. Recently, he is the chair of the International Organization Board of ic-cmtp5 the 5th International Conference on Competitive Materials and Technological Processes (2018).

1. Introduction

The research topics in ceramic materials generally [1-8] and advanced ceramic particularly [9-12] are becoming more popular. After Landau and Lifshitz revealed theoretically in the early 1960s, the thermodynamic potential energy contains coupled magnetic and electric components that can influence each other [13], a flurry of research about multiferroics has been triggered up to now [14-18]. Although these materials are interesting and worth studying, the first dilemma is that multiferroics are very rare [19-20]. Secondly, their coupling of multiferroic properties is often too small for the application or appears only at low temperatures [21]. To overcome these difficulties, large efforts have been made to find new single-phase multiferroics as well as to enhance multiferroic couplings with heterogeneous structures of a ferromagnetic and a ferroelectric components [22-23].

The rare-earth manganites perovskite materials have drawn huge attention recently due to the coupling of (anti) ferromagnetic and ferroelectric orders in the same phase [24-27]. This behaviour enables this material to be used in future information-technology devices in which data can be transfer through the applied electric fields to the magnetic memory elements [28-29]. $REMnO_3$ can be found either in hexagonal or orthorhombic perovskite structure; generally, the orthorhombic $REMnO_3$ shows multiferroic behaviour since its magnetic phase can be controlled by an applied electric field at low temperature [30-31].

In this study, we partially substitute Fe cations in $GdMnO_3$ (GMO) compound. Single-phase $GdMn_{1-x}Fe_xO_3$ compounds were prepared by solid-state reaction route. Since GMO compounds are multiferroic compounds, Fe-doped GMO materials could be fascinating ceramic materials because of the existence of ferromagnetism characteristic of Mn moments and distortion of the lattice, which can improve the dipole ordering.

2. Experimental methods

2.1 Synthesis of $GdMn_{1-x}Fe_xO_3$

A single-phase $GdMn_{1-x}Fe_xO_3$ (x= 0.2 and 0.8) ceramic in a powder form were prepared through conventional solid-state synthesis route (*Fig. 1*). Gd_2O_3 (99.9%; Alfa Aesar), Mn_2O_3 (98%; Alfa Aesar) and Fe_2O_3 (99.9%; Alfa Aesar) were used as reactants. An appropriate amount of these powders were milled and mixed in ethanol in a plastic container using zirconium balls for 6 hours. Two different compositions were prepared; $GdMn_{1-x}Fe_xO_3$ where x= 0.2 and 0.8. The slurry was then dried by evaporating the ethanol at 100 °C for 24 h. The resultant powders were initially calcined at 600 °C for 10 h followed by cooling to room temperature. After grinding, the produced powders were heat-treated at different temperatures between 1000-1350 °C for 10 h with a heating and cooling rate of 300 °C/h to observe the phases development. Powders were also used to make pellets, which were used to produce dense ceramics. Pellets with 10 mm in diameter and 2 mm thickness were prepared by a compaction machine using a pressure of 10 MPa. Sintering was performed at 1350 °C for 20 h with a heating and cooling rate of 120 °C/h. Calcination and sintering studies were made using a high-temperature programmable furnace [32]. The fired specimens were characterized by different techniques like XRD and SEM. Besides, the magnetic characteristic of the Fe-doped $GdMnO_3$ samples ($GdMn_{1-x}Fe_xO_3$) were also investigated.

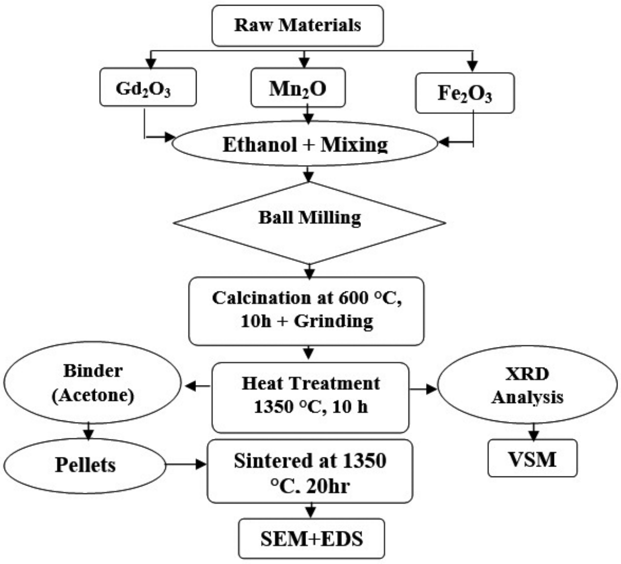

Fig. 1 Flow diagram for the preparation of $GdMn_{1-x}Fe_xO_3$ ceramics
1. ábra A GdMn1-xFexO3 kerámiák készítésének folyamata

2.2 Characterization

The prepared samples were characterized by a Bruker D2 PHASER X-ray diffractometer (XRD) operated in the Bragg-Brentano geometry and the tested samples were examined in 2θ range of 10-70 ° with a scanning rate of 1°/min and a step size of 0.01016 ° using CuKα radiation (λ= 1.54184 Å). For computer-based examination, DIFRACT measurement program was used. Surface morphology investigation of the produced samples was carried out using scanning electron microscopy (SEM, JEOL5910 LV) and surface analyses of the samples were carried out by energy-dispersive X-ray spectrometer (EDX). The fractured surface of the samples were coated with gold by SC7680 Super Coater before SEM analysis. Gold-coated fracture surfaces of the produced samples were investigated with different magnification values using secondary and back-scattered electrons. Also, the magnetic properties of the Fe-doped $GdMnO_3$ samples $GdMn_{1-x}Fe_xO_3$ at low temperature (10 K) were investigated using the vibrating sample magnetometer (VSM) and magnetization of the samples as a function of the magnetic field (M–H) was obtained.

3. Results and discussion

3.1 Structures

Fig. 2 shows the XRD patterns of undoped and B-site doped $GdMn_{1-x}Fe_xO_3$ (x= 0.2, 0.8) ceramics carried out at ambient temperature. All the samples show single-phase perovskite structure without any traces of impurities since there is a complete matching and no additional peaks were observed (*Fig. 3* and *4*). This indicates that Fe doping even at the high amount (x=0.8) doesn't result in a second phase formation and completely dissolves in the lattice giving a substitutional solid solution. The most significant notice to be mentioned here is that a close investigation of the peaks reveals a shift in the peak positions to the right side with increased doping concentration. This effect can be obtained due to the decrees in the lattice parameters. Thus the substitution of Mn by Fe causes a decrease in the volume of the unit cell since the atomic size of Fe with a radius (1.17 Å) is smaller than that of Mn with a radius (1.79 Å). The decrease in the unit cell volume with increasing the doping concentration leads to a unit cell distortion that may change the crystal structure. This change might be a significant factor for the materials' magnetic properties. DIFRACT.measurement programme was used to calculate the unit cell's lattice parameters and volume (*Table 1*). Undoped $GdMnO_3$ sample has an approximate lattice parameter with the theoretical value obtained from the PDF file (PDF No: 74-1477). However, when Fe's concentration increased, the lattice parameter decreased due to the smaller ionic radius of Fe (1.17 Å) than Mn (1.79 Å).

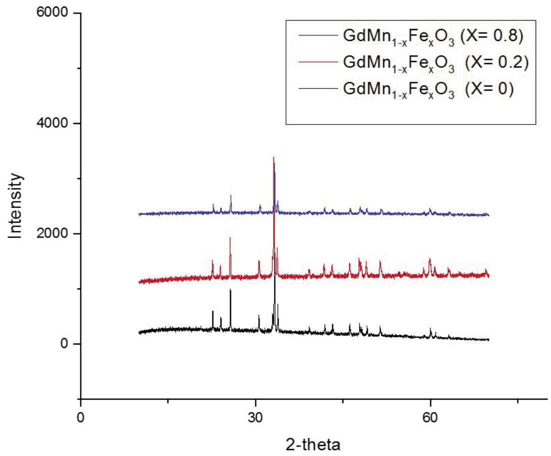

Fig. 2 Room temperature XRD patterns of $GdMn_{1-x}Fe_xO_3$ ceramics compounds (x= 0, 0.2 and 0.8) heat treated at 1350 °C for 24 h
2. ábra 1350°C-on 24 órán át hőkezelt $GdMn_{1-x}Fe_xO_3$ kerámiák XRD mintázata (x = 0; 0,2 és 0,8) szobahőmérsékleten

Composition	a (Å)	b (Å)	c (Å)	Volume (Å)³	Space group
$GdMnO_3$	5.31	5.84	7.43	230.41	Pnma
$GdMn_{0.8}Fe_{0.2}O_3$	5.316	5.679	7.611	229.77	Pnma
$GdMn_{0.2}Fe_{0.8}O_3$	5.3	5.6	7.62	226.16	Pnma

Table 1 Lattice parameters resulted from refinement procedure of powder XRD pattern of $GdMn_{1-x}Fe_xO_3$ ceramics compound (x=0.2, 0.8)
1. táblázat A rácsparaméterek a $GdMn_{1-x}Fe_xO_3$ kerámia alkotók XRD mintázatából adódtak (x = 0,2; 0,8)

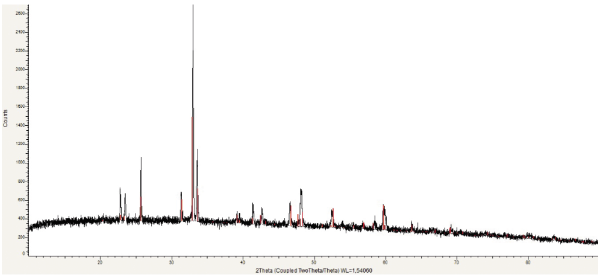

Fig. 3 XRD pattern for GdMn$_{1-x}$Fe$_x$O$_3$ ceramics sample at (x= 0.2)
3. ábra A GdMn$_{1-x}$Fe$_x$O$_3$ kerámia XRD mintája (x = 0,2)

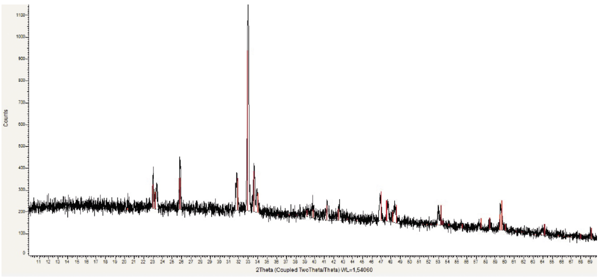

Fig. 4 XRD pattern for GdMn$_{1-x}$Fe$_x$O$_3$ ceramics sample at (x= 0.8)
4. ábra A GdMn$_{1-x}$Fe$_x$O$_3$ kerámia XRD mintája (x = 0,8)

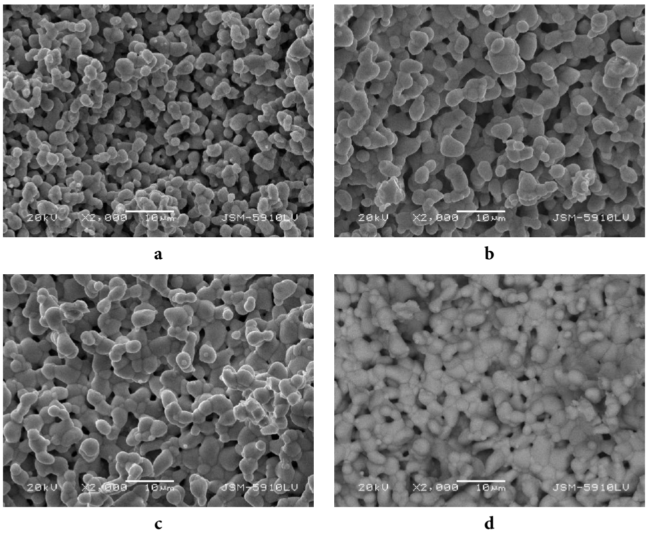

Fig. 5 SEM micrographs of Fe-doped GdMnO$_3$ samples at ×2.000 a) SEI of GdMn$_{0.8}$Fe$_{0.2}$O$_3$, b) BEI of GdMn$_{0.8}$Fe$_{0.2}$O$_3$, c) SEI of GdMn$_{0.2}$Fe$_{0.8}$O$_3$ and d) BEI of GdMn$_{0.2}$Fe$_{0.8}$O$_3$ samples (GdMn$_{1-x}$Fe$_x$O$_3$ ceramics where x= 0.2 and x= 0.8)
5. ábra Fe adalékolt GdMnO$_3$ minták SEM felvételei 2000x nagyítással a) GdMn$_{0.8}$Fe$_{0.2}$O$_3$ SEI, b) GdMn$_{0.8}$Fe$_{0.2}$O$_3$ BEI, c) GdMn$_{0.2}$Fe$_{0.8}$O$_3$ SEI és d) GdMn$_{0.2}$Fe$_{0.8}$O$_3$ BEI (GdMn$_{1-x}$Fe$_x$O$_3$ kerámiák, ahol x = 0,2 és x = 0,8)

3.2 Scanning electron microscopy (SEM) and EDS investigation of GdMn$_{1-x}$Fe$_x$O$_3$

Fig. 5 shows secondary and backscattered electron micrographs of the GdMn$_{0.8}$Fe$_{0.2}$O$_3$ and GdMn$_{0.2}$Fe$_{0.8}$O$_3$. In addition, *Fig. 6* shows larger magnifications of the same materials. SEM micrographs reveal that there is no second phase or impurity in the microstructure, as observed in the XRD. Backscattered electrons do not show any phase-contrast indicating no other second phases. The grain sizes in x= 0.2 and x= 0.8 samples were in the range of 0.7-5 µm and 0.8-4.6 µm respectively, showing that the grains sizes do not change significantly with Fe-doping.

EDS analysis taken from grains shows that they were near to the theoretical values (*Fig. 7*). While *Fig. 7-a* gives the EDS analysis of Gd$_{0.8}$Eu$_{0.2}$MnO$_3$, *Fig. 7-b* gives the EDS of Gd$_{0.2}$Eu$_{0.8}$MnO$_3$. The weight percentages obtained from EDS results were near to the calculated values. No other peaks or impurities were detected in the EDS. Au and Pd were due to coating made on the samples.

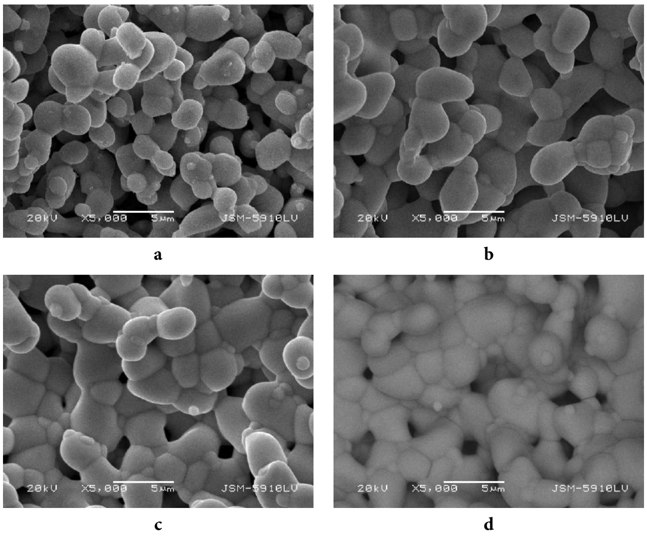

Fig. 6 SEM micrographs of Fe-doped GdMnO$_3$ samples at ×5.000 a) SEI of GdMn$_{0.8}$Fe$_{0.2}$O$_3$, b) BEI of GdMn$_{0.8}$Fe$_{0.2}$O$_3$, c) SEI of GdMn$_{0.2}$Fe$_{0.8}$O$_3$ and d) BEI of GdMn$_{0.2}$Fe$_{0.8}$O$_3$ samples (GdMn$_{1-x}$Fe$_x$O$_3$ ceramics where x= 0.2 and x= 0.8)
6. ábra Fe adalékolt GdMnO$_3$ minta SEM felvételei 5000x nagyítással a) GdMn$_{0.8}$Fe$_{0.2}$O$_3$ SEI, b) GdMn$_{0.8}$Fe$_{0.2}$O$_3$ BEI, c) GdMn$_{0.2}$Fe$_{0.8}$O$_3$ SEI és d) GdMn$_{0.2}$Fe$_{0.8}$O$_3$ BEI (GdMn$_{1-x}$Fe$_x$O$_3$ kerámiák, ahol x = 0,2 és x = 0,8)

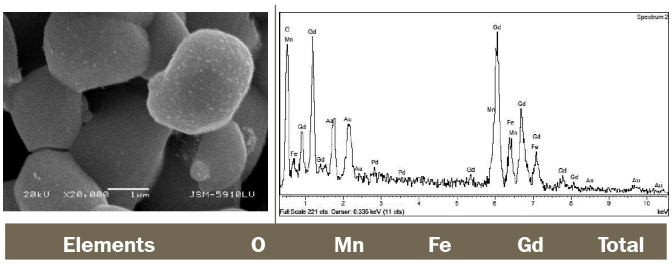

Elements	O	Mn	Fe	Gd	Total
Wt (%)	26.19	1.52	8.20	64.08	100.00
Calculated (W %)	18.43	16.88	4.289	60.395	100.00

a

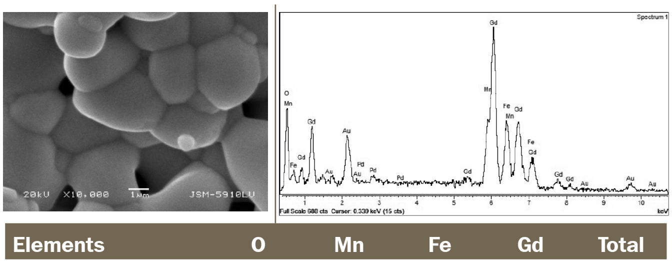

Elements	O	Mn	Fe	Gd	Total
Wt (%)	14.14	8.90	11.31	65.65	100.00
Calculated Wt (%)	18.39	4.21	17.12	60.27	100.00

b

Fig. 7 EDS analysis Fe-doped GdMnO$_3$ samples a) EDS analysis of GdMn$_{0.8}$Fe$_{0.2}$O$_3$ and b) EDS analysis of GdMn$_{0.2}$Fe$_{0.8}$O$_3$ sample (Tables show the weight fractions of the elements found by calculation from EDS results)
7. ábra Fe-adalékolt GdMnO$_3$ minták EDS-elemzése a) GdMn$_{0.8}$Fe$_{0.2}$O$_3$ és b) GdMn$_{0.2}$Fe$_{0.8}$O$_3$ (A táblázat a számítással és az EDS-eredmények alapján meghatározott elemek tömegarányát mutatja)

3.3 Magnetic properties

Fig. 8 shows magnetic field-dependent magnetization at low temperature (10K) for $GdMn_{1-x}Fe_xO_3$ (x=0.2, 0.8) ceramics. Both samples show antiferromagnetic behaviour at 10K with small differences. The saturation magnetization (M_s) for the sample at x= 0.8 appears higher with a value of about 60 emu/g, while the sample at x=0.2 shows slightly lower M_s with a value of about 58 emu/g. The slight enhancement in magnetization might be attributed to the distorted spiral magnetic ordering caused by the doping of Fe element. With increasing Fe concentration, the interatomic distance of Fe–O decreases, which leads to improvement in exchange interaction between Fe–*RE* , therefore enhance the magnetization [33].

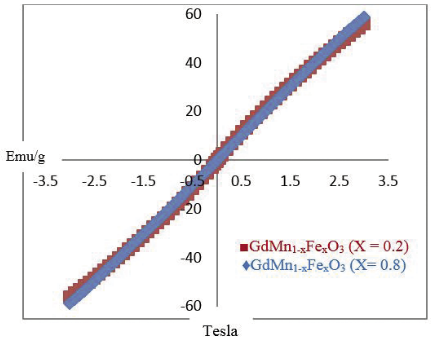

Fig. 8 The magnetic hysteresis loops of $GdMn_{1-x}Fe_xO_3$ ceramics compound (0.2 and 0.8) sintered at 1350 °C

8. ábra 1350°C-on szinterelt $GdMn_{1-x}Fe_xO_3$ kerámia alkotók (0,2 és 0,8) mágneses hiszterézis hurkjai

4. Conclusion

$GdMn_{1-x}Fe_xO_3$ (x= 0, 0.2, 0.8) samples show single-phase orthorhombic crystal structure with space group Pnma as confirmed by XRD investigation. Increasing the doping concentration leads to decreased lattice parameters (basically, b and c while a remains almost constant). Due to the Fe dopant element's small atomic radius, a decrease of the overall lattice volume has been observed. SEM examination reveals the synthesis of pure phase with no other impurities since the backscattered electrons micrograph does not show any phase contrast. EDS results of the produced samples show a close value between the experimental weight percentages and the calculated one, also no other peaks were detected in the EDS results, which is a strong indication for the formation of single-phase. The magnetic hysteresis loops of $GdMn_{1-x}Fe_xO_3$ (x= 0, 0.2, 0.8) carried out at low-temperature (10K) exhibit the antiferromagnetic characteristic in both samples, with only slight differences in the Ms.

Acknowledgements

Great thanks to Marmara University (Turkey) and the University of Miskolc (Hungary) for their support in this work.

References

[1] L. A. Gömze – L. N. Gömze (2009): Építőanyag–JSBCM **61** (2) 38 http://dx.doi.org/10.14382/epitoanyag-jsbcm.2009.7

[2] L. A. Gömze – L. N. Gömze – N. S. Kulkov – L. I. Shabalin – I. Gotman – F. Pedraza – G. L. Lecomte – T. Mayorova – E. Kurovics – A. Hamza (2015): Építőanyag–JSBCM **67** (4) 143 http://dx.doi.org/10.14382/epitoanyag-jsbcm.2015.24

[3] Gömze, L. A., et al. 2018 Építőanyag–JSBCM **70** (1) 8. https://doi.org/10.14382/epitoanyag-jsbcm.2018.2

[4] Kurovics, E. – S. N. Kulkov – L. A. Gömze: Építőanyag–JSBCM **70** (1) 3 https://doi.org/10.14382/epitoanyag-jsbcm.2018.1

[5] S. Kulkov et al 2014 Építőanyag–JSBCM 66 (1) 1. http://dx.doi.org/10.14382/epitoanyag-jsbcm.2014.1

[6] N. L. Savchenko, et al. Építőanyag–JSBCM **66** (2) 44 http://dx.doi.org/10.14382/epitoanyag-jsbcm.2014.9

[7] O. B. Kotova, et al 2019 **Építőanyag**–JSBCM 71 (4) 125 https://doi.org/10.14382/epitoanyag-jsbcm.2019.22

[8] A. Apkaryan – S. N. Kulkov – L. A. Gömze 2014 Építőanyag–JSBCM **66** (2) 38. http://dx.doi.org/10.14382/epitoanyag-jsbcm.2014.8

[9] M. Tihtih et al 2019 Építőanyag–JSBCM **71** (6) 190. https://doi.org/10.14382/epitoanyag-jsbcm.2019.33

[10] A. Y. Buzimov et al 2017 IOP Conf. Ser.: Mater. Sci. Eng. 175 012033 https://doi:10.1088/1757-899X/175/1/012033

[11] A. Y. Buzimov et al 2017 J. Phys.: Conf. Ser. 790 012004 https://doi:10.1088/1742-6596/790/1/012004

[12] P. David, Jr Penaloza 2019 **Építőanyag**–JSBCM 71 (3) 74 https://doi.org/10.14382/epitoanyag-jsbcm.2019.13

[13] L. D. Landau – E. M. Lifshitz: Statistical Physics." Course of Theoretical Physics 5 (1980): 396-400.

[14] Eerenstein et al, 2006 nature 442 (7104) 759. https://doi.org/10.1038/nature05023

[15] Vopson, M Melvin, 2015 „Fundamentals of multiferroic materials and their possible applications." Critical Reviews in Solid State and Materials Sciences 40 (4) 223.

[16] L. W. Martin – R. Ramesh 2012 Acta Materialia 60 (6-7) 2470. https://doi.org/10.1016/j.actamat.2011.12.024

[17] T. Zhao et al 2006 Nature materials 5(10) 829. https://doi.org/10.1038/nmat1731

[18] Kim et al 2005 Materials Letters 59 (29-30) 4006. https://doi.org/10.1016/j.matlet.2005.07.050

[19] Lone et al. 2019 Nanoscale research letters 14 (1) 1 https://doi.org/10.1186/s11671-019-2961-7

[20] Nan et al 2019 National Science Review 6 (4) 620. https://doi.org/10.1093/nsr/nwz093

[21] J. F. Scott 2013 NPG Asia Materials 5(11) 72. https://doi.org/10.1038/am.2013.58

[22] W Prellier et al 2005 Journal of Physics: Condensed Matter 17(30) R803. https://doi:10.1088/0953-8984/17/30/R01

[23] L. W. Martin – D. G. Schlom 2012 Current Opinion in Solid State and Materials Science. 16 (5).199. https://doi.org/10.1016/j.cossms.2012.03.001

[24] M. Mochizuki – N. Furukawa 2009 Physical Review B. 80(13):134416 https://doi.org/10.1103/PhysRevB.80.134416

[25] C. Dubourdieu et al 2007: Philosophical magazine letters 87(3-4) 203. https://doi.org/10.1080/09500830601137173

[26] G. Lalitha – P. V. Reddy 2008: Journal of magnetism and magnetic materials. 320 (5) 754 https://doi.org/10.1016/j.jmmm.2007.08.014

[27] P. P. Rout et al 2012: Physica B: Condensed Matter 407(12) 2072. https://doi.org/10.1016/j.physb.2012.02.007

[28] M. Barthélémy – A. Bibes 2008: Nat. Mater. (7) 425 https://doi: 10.1038/nmat2189.

[29] Z. Surowiak et al Archives of acoustics. 33 (2) 243

[30] Y. W. Windsor et al 2014: Physical review letters. 113 (16) 167202. https://doi.org/10.1103/PhysRevLett.113.167202

[31] K. H. Wu et al 2010: Thin Solid Films 518 (8) 2275. https://doi.org/10.1016/j.tsf.2009.09.089

[32] J. F. M. Ibrahim et al 2017: Advanced Ceramics Progress 3 (4) 1. 10.30501/ACP.2017.90758

[33] Y. J. Zhang et al 2010: Journal of Magnetism and Magnetic Materials. 322 (15) 2251. https://doi.org/10.1016/j.jmmm.2010.02.020

Ref.:
Ibrahim, Jamal Eldin F. M. – **Mergen**, Ayhan – **Parlak**, Umut – **Kurovics**, Emese – **Tihtih**, Mohammed – **Gömze**, László A.: *Synthesis and characterization of iron-doped $GdMnO_3$ multiferroic ceramics*
Építőanyag – Journal of Silicate Based and Composite Materials, Vol. 73, No. 1 (2021), 24–27. p.
https://doi.org/10.14382/epitoanyag-jsbcm.2021.5

An investigation on the physical, mechanical and thermal properties of dune sand mortars lightened by expanded polystyrene beads (EPS)

Ouided HERIHIRI
Lecturer at the Department of Civil Engineering, University of Medea, Algeria. Her research interests include lightweight concrete technology, reuse of wastes.

Abdelhamid GUETTALA
Professor at the Department of Civil Engineering, University of Biskra, Algeria. His research interests include, concrete technology, reuse of local materials.

Benchaa BENABED
Professor at the Department of Civil Engineering, University of Laghouat, Algeria. His research interests include self-compacting concrete technology, reuse of local materials, rheology and durability of cement-based materials.

Ouided HERIHIRI ▪ Department of Civil Engineering, University of Medea 26000, Algeria
▪ Civil Engineering Research Laboratory, University of Biskra 07000, Algeria
Abdelhamid GUETTALA ▪ Civil Engineering Research Laboratory, University of Biskra 07000, Algeria
Benchaa BENABED ▪ Civil Engineering Research Laboratory (LRGC),
University of Laghouat 03000, Algeria ▪ b.benchaa@lagh-univ.dz

Érkezett: 2020. 04. 25. ▪ Received: 25. 04. 2020. ▪ https://doi.org/10.14382/epitoanyag-jsbcm.2021.6

Abstract

As the idea of sustainable development has been involved in all fields including construction and civil engineering, a huge amount of researches has focused on reducing energy use and protecting the environment, while at the same time ensuring the comfort of inhabitant. Taking on this viewpoint, the current work focuses on replacing natural materials with recycled and synthetic materials, to produce a new eco-material that satisfies the binary concept; minimizing cost and constructing light elements with complex geometry that promotes architectural innovation. The present work aims to mix design and study a mortar based on mixture of fine siliceous dune sand and crushed limestone sand lightened by expanded polystyrene (EPS). Sand was substituted by EPS with percentages of 0, 5, 10, 15, 20, 25 and 100%. The physical, mechanical and thermal properties of composite mortars were assessed according to the dry density, compressive strength, flexural strength, porosity, and conductivity. The obtained results show that, the use of EPS decreases the mechanical properties and the density of mortars. However, the thermal properties of mortars incorporating EPS were improved and meet the requirement for lightweight concrete constructions and insulation applications.

Keywords: EPS, dune sand, crushed sand, physic-mechanical properties, porosity, thermal properties

Kulcsszavak: EPS, dűne homok, zúzott homok, fizikai-mechanikai tulajdonságok, porozitás, hőtani tulajdonságok

1. Introduction

Concrete is the most widely used material in building construction despite its relatively high weight and limited thermal performance in which thermal conductivity ranges between 1.4 and 3.6 W/mK [1-3]. Lightweight concrete (LWC) offers a considerable advantage in terms of its unit weight which encourages its use in the construction industry where savings made in the weight of structures are a major factor [4]. Several researchers have exploited natural, artificial and recycled lightweight aggregates in order to enhance their importance in modern construction [5]. Expanded polystyrene (EPS) is one of the artificial lightweight aggregates that provide concrete lightening, and a wide range of density choices and is used in thermal insulation. The introduction of this material therefore contributes to the efficient management of solid waste while saving landfills, conserving natural resources and protecting the environment [6]. Herki et al [7] Examined the effect of using EPS waste and fly ash in concrete. The results showed that the compressive strength and ultrasonic velocity decreases with increasing amounts of EPS and fly ash in the concrete. Ferrandiz-Mas et al [8] investigated the effect of EPS on the thermal conductivity of lightweight mortars; the results showed that the increase in the percentage of EPS beads decreases the thermal conductivity, thus increasing the thermal insulation. Sayadi et al [9] found that the strength of lightweight concrete made with EPS beads decreases as the amount of replacement EPS increases. Ali et al [10] have carried out some tests on concretes made of polyethylene balls; the results showed that regardless of the EPS balls content, the shrinkage of EPS concrete is greater than that of the control concrete. In the context of sustainable development, the Algerian Minister of Housing and Urban Planning has banned the exploitation of river and sea sand, as a justified way to preserve the environment; this is a major environmental challenge due to the increasing need for sand. In order to balance the country's need for sand in construction field and the preservation of the environment, researchers have started to introduce new ideas and innovative solutions for this complicated problem in one hand. On the other hand, the improved thermal performance of lightweight aggregate concrete is considered as the most appropriate, particularly in reducing the energy used in heating and air conditioning of buildings. Among the steps suggested by researchers is to use the quarry limestone crushed sand and to evaluate the economy of the aggregates sector. The approach alone, however, cannot satisfy the growing demand for development programs of construction projects. Nevertheless, the search for other alternatives to deal with the lack of materials especially the sand remains increasingly important. Recently, a shift in research towards new construction materials has taken place through the reuse of local materials for the construction of high-performance concrete from a mechanical and economic point of view as well as its durability. A local available dune sand which covers more than 60% of the Algerian territory is practically unexploited until now [11]. Many researches have been done on the use of dune sand in the field of construction in Algeria, due to the availability of this material in huge quantities especially in the southern zones [12-16]. The main objective of this work is to investigate the effect of EPS beads and plasticizer on the properties of mortar made with a mixture sand of dune and crushed sand, in order to meet the concern of preserving the natural resources, and enhance the thermal insulation of buildings. The physical, mechanical and thermal properties of mortar were evaluated according the dry density, compressive, flexural strength, porosity and thermal conductivity.

2. Experimental program

2.1 Material

2.1.1 Cement

The cement used in this work is a Portland Limestone Cement of type CPJ CEM/II which conforms to the standard EN 197-1:2000 [17]. Its specific density is 3.1 g/cm^3 and its Blaine specific surface area is 3100 cm^2/g.

2.1.2 Sand

As fine aggregates, a mixture of 44% of siliceous dune sand (DS) and 56% limestone crushed sand (CS) were used. The physical properties and sieve analysis results of these sands are given in *Table 1* and *Fig. 1* respectively.

Physical properties	DS	CS
Apparent density (kg/m^3)	1440	1530
Absolute density (kg/m^3)	2610	2630
Finesse modulus	0.74	3.88
Sand equivalent (%)	62	88
Absorption coefficient (%)	1	2
Compactness (%)	54.9	58.1
Porosity (%)	45.1	41
Empty index	0.82	0.72

Table 1 Physical properties of sand used
1. táblázat A felhasznált homok fizikai tulajdonságai

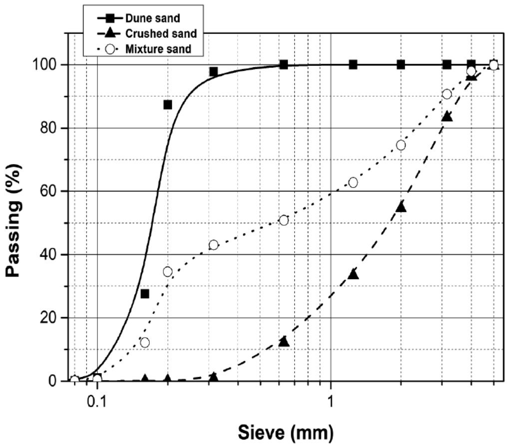

Fig. 1 Particle size distribution of sand used
1. ábra A felhasznált homok szemcseméret eloszlása

2.1.3 Expanded polystyrene (EPS)

The manufacture of polystyrene is obtained by polymerizing the basic product, which is styrene. The EPS balls with diameters ranging from 1.5 to 4 mm were used to substitute sand by percentage of 0, 5, 15, 25, 50, 75 and 100 % to lighten the mortar. The properties of the EPS balls used are given in *Table 2.*

Properties	Value
Particles' size (mm)	1.5 - 4
Absolute density (kg/m^3)	28
Apparent density (kg/m^3)	18
Dry thermal conductivity (W/m.K)	0.045

Table 2 Properties of EPS
2. táblázat EPS tulajdonságai

2.1.4 Plasticizer

A plasticizer with a specific gravity of 1.04 ± 0.01 g/cm^3, solid content of 35% and pH of 7.9, was used to ensure the suitable workability of mortar mixtures.

2.2 Mix proportions and mixing procedure

To assess the effect of EPS on the physical, mechanical and thermal properties of lightweight mortar, seven mixtures were prepared. In order to determine the quantity required for each ingredient of lightweight mortar, the general method is used according to the standard EN 196-1 [18]. Cement/sand (S/C) ratio is maintained constant (1/3). Sand was substituted by EPS with percentages of 0, 5, 10, 15, 20, 25 and 100%. In order to reach suitable workability, varying amounts of plasticizer (PL) and water/cement (W/C) ratio were used. The mixture proportions of all lightweight mortar mixes are given in *Table 3.*

Mixtures		1	2	3	4	5	6	7
Cement (kg/m^3)		450	450	450	450	450	450	450
Sand (kg/m^3)		1302.50	1237.38	1107.13	976.88	651.25	325.63	0.00
EPS (%)		0	5	15	25	50	75	100
EPS (kg/m^3)		0.00	0.82	2.45	4.09	8.17	12.26	16.34
W/C	*	0.55	0.5	0.48	0.44	0.38	0.33	0.27
	**	0.5	0.47	0.43	0.4	0.34	0.29	0.26
PL (%)	*	0.5	0.5	0.5	0.5	0.5	0.5	0.5
	**	1	1	1	1	1	1	1

Table 3 Mix proportions of different EPS mortars
3. táblázat Habarcs keverékek összetétele

The mixing procedure for making control mortar mixtures takes three steps. Firstly, the cement and sand were mixed for 1 min, and then 80% of the mixing water was added and mixed for 1 min. The remaining 20% of water containing the PL was then added and mixed for 1 min. Finally, the procedure continued for another 2 min. For the mixture containing EPS, with an additional mixing time of 2 min.

2.3 Testing

- The workability was measured according to the standard NF P 15-437 [19].
- The air content in the mortars was measured by aerometer according to the standard NF P 18-353 [20].
- The dry density of the composites was measured according to the standard NF P18-435[21].
- The flexural strength and compressive strength are measured 28 days according to ASTM C348 [22] and ASTM C349 [23] standards, respectively.
- The measurements of the thermal properties were carried out according to the standard ISO 8497-1 [24].
- The porosity accessible to water was measured according to standard NFEN18-459 [25].
- The dynamic elastic modulus of composites was determined at 28 days, using the ultrasonic pulse velocity (UPV) test according the standard ASTM C597-97 [26].
- To understand the developing of microstructure of hardened mixtures, a scanning electron microscopy analysis (SEM) was performed.

3. Results and Discussion

3.1 Fresh properties

3.1.1 Workability

Table 3 shows that the values of the W/C ratio decrease with the increase in the dosage of EPS beads, due to the polystyrene properties, it is a material that does not absorb water through a closed cellular structure [27]. These results are confirmed by the studies carried out by Bengin et al [28]. Kim et al [29] investigated the effect of polystyrene on the workability of lightweight mortars; and found that the increase in polystyrene content causes an increase in workability. Madandoust et al [30] showed that the use of EPS decreased the demand for high range water reducer, while higher slump flow was achieved. The plasticizer was added to the mixture in order to improve the consistency class of mortar with the fluidity time less than 10 s. The optimization of the percentage of PL consists in developing the best characteristics of mortar at the fresh state to ensure better performance at the hardened state. In this study, two percentages of PL were used; 0.5% and 1% by weight of cement.

Fig. 2 shows the variation of the workability of mortars with different percentages of EPS. As shown in *Fig. 2*, the flow time for all mixes was between 7 and 11 s, which indicates good consistency and compliance with flow time limitation so that requirement is less than 10 s in order to have a similar fluidity. It was noted that, mortars with 1% of PL have a high fluidity compared to those with 0.5% of PL [31]. For visual control, the setting is easy without any tendency to segregation or bleeding for the high percentages of EPS beads. This is due to the increase in the percentage of EPS, which is characterized by a hydrophobic behavior.

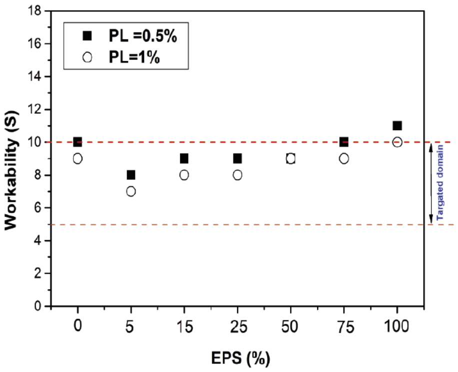

Fig. 2 *Workability of mortars made with different EPS contents*
2. ábra *Különböző EPS tartalommal készített habarcsok bedolgozhatósága*

3.1.2 Air content

The variation of the air content of the composite as a function of the EPS content, is illustrated in *Fig. 3*. According to this figure, the air content of mortars with EPS is more important than that of reference mortar with 0% of EPS. Up to 15% of EPS substitution, the air content increases with increasing the EPS content from 6.2% for mortar with 0% of EPS to 9.1% for mortar with 100% of EPS. However, the incorporation of 5% of EPS decreases the air content in the mixture by 20% compared to the control mortar. The decrease is due to the increase in compactness of the composite, it can be confirmed by the results of the workability test of this mixture. These results seem to be similar for the both plasticizer percentages used. The increase in the air content is explained by the increase in porosity, which can be attributed to the morphology of EPS, which is characterized by a hydrophobic nature. This explains that the EPS composite is less compact , and therefore it is more porous compared to the control mortar and that EPS balls can trap air, thus significantly increasing the air volume in composites. Increasing the air content in fresh mixture is practically identical with increasing the porosity of the composite at hardened state to the detriment of mechanical strength and the durability of the composite in general.

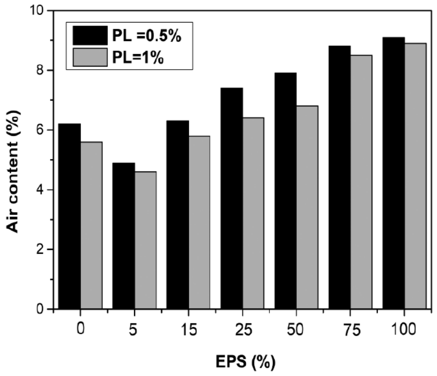

Fig. 3 *Air content of mortars made with different EPS contents*
3. ábra *Különböző EPS tartalommal készített habarcsok levegőtartalma*

3.2 Hardened properties

3.2.1 Density

The evolution of the density of the composite with various EPS content is given in *Fig. 4*; the figure shows that the density varies from 2227.5 kg/m^3 to 944.01 kg/m^3 for mixtures with 1% of PL. For the control mortar, the density was 2204.98 kg/m^3, and it decreased to 962.66 kg/m^3, when incorporating 100 % of EPS and 0.5% of PL in the mixture. This low density can also facilitate the implementation of concrete in construction sites [32]. In addition, the decrease in the density is related to the increase of the air content in the matrix, which increases with the increase of EPS content [33-35]. Therefore, the substitution of sand by EPS has a negative effect on the density of the all mixtures, whereas the increase in the percentage of plasticizer causes an increase in density. These results were expected because the density of EPS is lower than that of the control mixture.

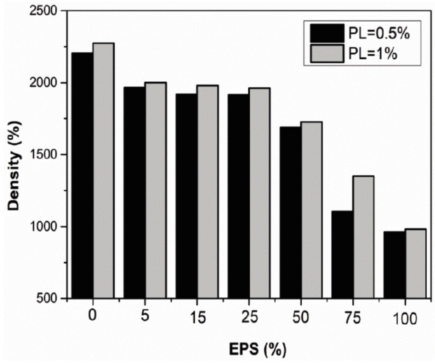

Fig. 4 Density of mortars made with different EPS contents
4. ábra Különböző EPS tartalommal készített habarcsok sűrűsége

3.2.2 Compressive Strength

The variation of the compressive strength of the mixtures with different substitution rates of EPS is shown in *Fig. 5*. From the figure, it can be seen that the compressive strength considerably decreases with the increase in the content of EPS, but it remains acceptable, even for mortars with a content of 100% of EPS as used in semi-solid insulators manufacture.

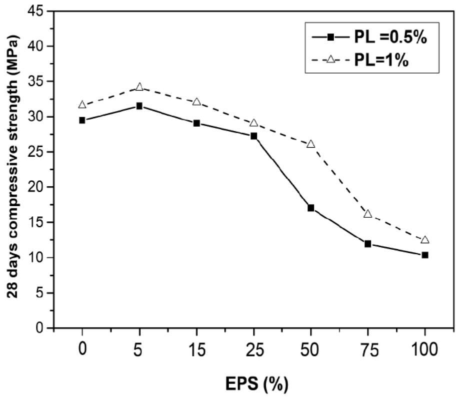

Fig. 5 Compressive strength at 28 days of mortars made with different EPS contents
5. ábra Különböző EPS tartalommal készített habarcsok 28 napos nyomószilárdsága

The compressive strength of mortar with 100% of EPS decreases from 31.58 MPa to 12.4 MPa and from 29.47 MPa to 10.34 MPa, compared to the control mixture, when using 1% and 0.5% of PL respectively. This reduction in strength is attributed to the stiffness of polystyrene, which is much lower compared to that of natural aggregates on one hand. On the other hand, the porosity percentage of the produced composites increases with the increase of the percentage of the EPS balls [36, 37]. However, a slight increase in the compressive strength of mortars is noted with the incorporation of 5% of EPS; this is due to the decrease in the W/C ratio as well as to the small percentage of the porosity of mixture.

3.2.3 Flexural tensile strength

Fig. 6 shows the 28 days flexural tensile strength of mortars made with different percentages of EPS. It is found that, the flexural strength of mortar decreases when adding EPS. for example, the flexural strength decreases from 4.51 to 2.79 MPa for mortars with EPS content of 0% and 100% respectively, which represents a reduction rate of about 40%, whatever the percentage of PL used. This decrease in the flexural strength is probably due to the microstructure of mortar, which is characterized by high porosity and low adhesion between the EPS beads and the cement paste [38, 39]. These results are similar to those previously obtained by some authors on lightweight aggregate-based mortars [36, 37]

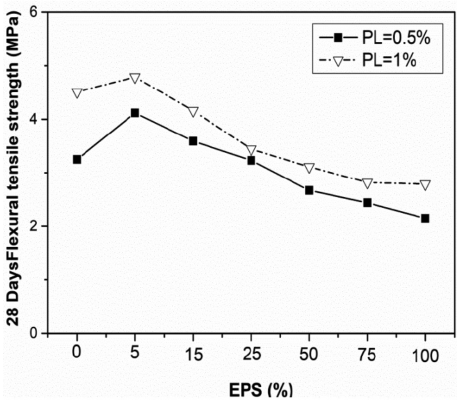

Fig. 6 Flexural tensile strength at 28 days of mortars made with different EPS contents
6. ábra Különböző EPS tartalommal készített habarcsok 28 napos hajlító-húzószilárdsága

3.2.4 Dynamic modulus of elasticity

Fig. 7 shows the evolution of the dynamic modulus of elasticity at 28 days of the composites as a function of the EPS content. The figure illustrates that the modulus of elasticity of mortar varies in the same way as the flexural tensile strength and decreases with the increase of EPS content. The reduction rate of dynamic modulus of elasticity is about 85% when incorporating 100% of EPS in mixture compared to that with 0% of EPS, whatever the percentage of PL used. The weak bond between the matrix and the EPS balls may have contributed to this reduction. In addition, the presence of air bubbles in the matrix may accentuated this reduction. The waves must pass through these air bubbles in order to be propagated in the cement paste [40]. This highlights the capacity to mitigate the ultrasonic waves as well as the damping of vibrations, which indicates the good sound insulation behavior.

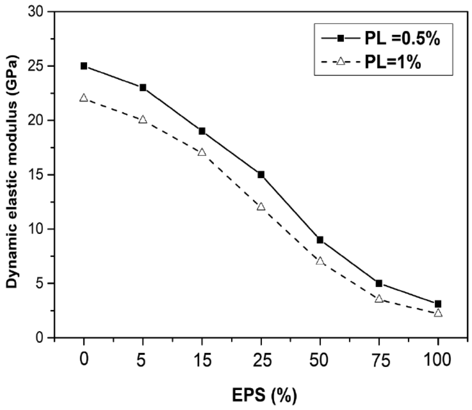

Fig. 7 *Dynamic modulus of elasticity of mortars made with different EPS contents*
7. ábra *Különböző EPS tartalommal készített habarcsok dinamikus rugalmassági modulusa*

3.2.5 Porosity

Fig. 8 shows the porosity accessible to water of different mortar mixtures as function of EPS aggregates percentages. From this figure, it can be noticed that, the two series of composites have the same behavior of the evolution of porosity versus the incorporated volume of EPS; the porosity of mixtures increases as the EPS content increases. For example, for mixtures with 0.5% of PL, the porosity increases from 8% to 27% when the EP S content increases from 0% to 100%. For composites with 1% of PL, the porosity varies from 7% to 24% when the EPS content varies from 0% to 100%. This increase is due to the low adhesion between the cement matrix and the EPS beads, which are characterized by hydrophobic nature in which the alveolus-shape cells are closed and remove of a part of the matrix resulting in a more complex porous structure [12]. These results are similar to those found by other researchers [41, 42]. G. Babu and S. Babu [43] studied the effect of EPS content on the porosity of concrete. The results showed an increase in porosity with the inclusion of high EPS content compared to control mixtures.

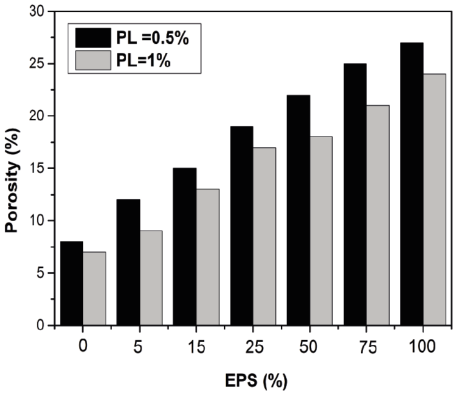

Fig. 8 *Porosity of mortars made with different EPS contents*
8. ábra *Különböző EPS tartalommal készített habarcsok porozitása*

3.3 Thermal properties

The results of the thermal properties: conductivity, diffusivity, effusivity and resistance of composites with different EPS proportions are shown in *Figs. 9, 10, 11* and *12* respectively.

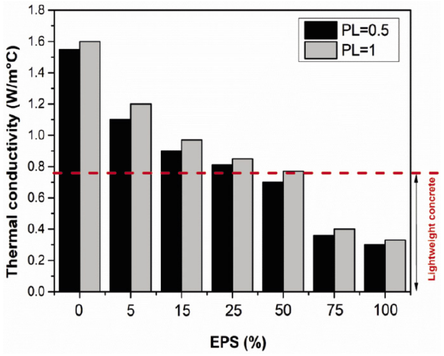

Fig. 9 *Thermal conductivity of mortars made with different EPS contents*
9. ábra *Különböző EPS tartalommal készített habarcsok hővezető képessége*

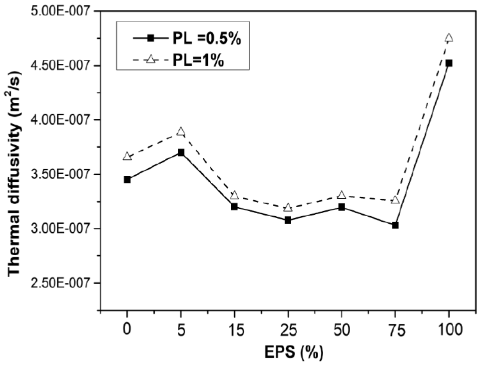

Fig. 10 *Thermal diffusivity of mortars made with different EPS contents*
10. ábra *Különböző EPS tartalommal készített habarcsok hőterjedési képessége*

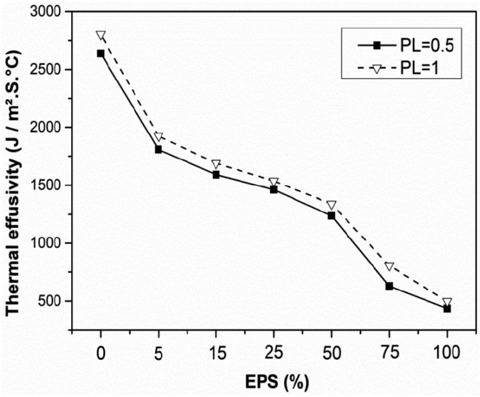

Fig. 11 *Thermal effusivity of mortars made with different EPS contents*
11. ábra *Különböző EPS tartalommal készített habarcsok hőkibocsátó képessége*

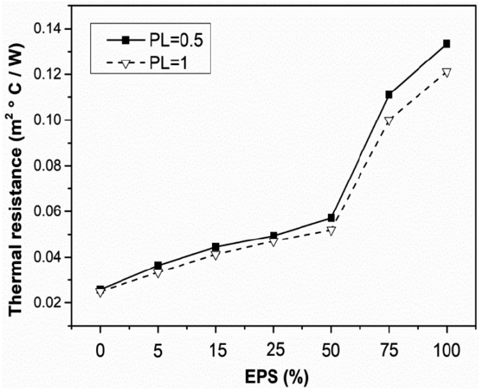

Fig. 12 *Thermal resistance of mortars made with different EPS contents*
12. ábra *Különböző EPS tartalommal készített habarcsok termikus ellenállása*

Fig. 9 shows the thermal conductivity variation of composites with different EPS contents. It can noted that the thermal conductivity of mortar decreases with the increase in the percentage of EPS beads compared to that of the composite control. This corresponds to a reduction of about 80% for the composite with 100% of EPS compared to the composite without EPS. This reduction in thermal conductivity is due to the morphology of EPS, which represents an amorphous structure and its low thermal conductivity is 0.4 W/m˚C compared to natural aggregates that represent a crystalline structure and a thermal conductivity more than 1.5 W/m˚C [44]. The RILEM recommendations reported that all mixtures studied, except the control, are classified in the "class II" of lightweight concrete of construction and insulation, based on their range of thermal conductivity less than 0.75 $Wm^{-1}k^{-1}$ [45]. Laoubi et al [46] found that the conductivity of the lightweight plaster decreased with the increase in the quantity of EPS, due to the insulating effect of the EPS.

Figs. 10 and *11* show the results of the thermal diffusivity and the thermal effusivity of the different composites. It is observed that, the diffusivity and effusivity values are in the range between (3.454 – 4.743) × 10^{-7} m/s^2 and (2637.244 - 435.592) J/m^{2}s°C respectively. From this result, it can be concluded that, the incorporation of EPS beads decreases these parameters, due to the insulating effect of the EPS beads, which makes the produced composite more efficient thermally.

The results of thermal resistance of mortars with different percentages of EPS is shown in *Fig. 12*. The figure reveals the positive effect of adding EPS beads in improving the thermal resistance of composites. For control mortar, thermal resistance is 0.026 m^2°C/W which increases to 0.133 m^2°C/W for mortar prepared with 100% of EPS and 0.5 % of PL. According to the standard NFP 75-101 [47], if the thermal resistance of product is at least equal to 0.50 m^2°C/W, it can be classified as a good thermal insulator in the building. This classification shows that all mortars were belonged to the NFP 75-101 limitation standard.

3.4 Microstructure analysis using SEM

The analysis of the specimens' morphology was carried out using a scanning electron microscopy (SEM) in order to highlight the interaction between cement-aggregates zones and the eventual changes of the microstructure of the composites within the incorporation different EPS contents. *Fig. 13* shows some SEM images for samples of EPS composite mortars after 28 days of maturity.

Fig. 13 a shows that the specimen has an alveolar structure of the EPS beads, which explains the lightness of the produced composites. *Figs. 13 b, c* show a poor adhesion of interfacial transition zone (ITZ) between cement-aggregates, which can significantly reduce the strength. This may be because that EPS beads have surface electrostatic charges that move the paste on EPS ball-paste contact area and known as the aggregate paste interaction.

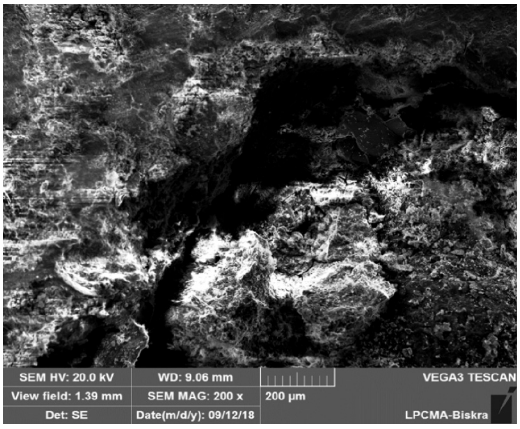

Fig. 13.a *SEM appearance of the porous EPS beads structure*
13a. ábra *A porózus EPS szerkezetének felépítése pásztázó elektronmikroszkópos felvételen*

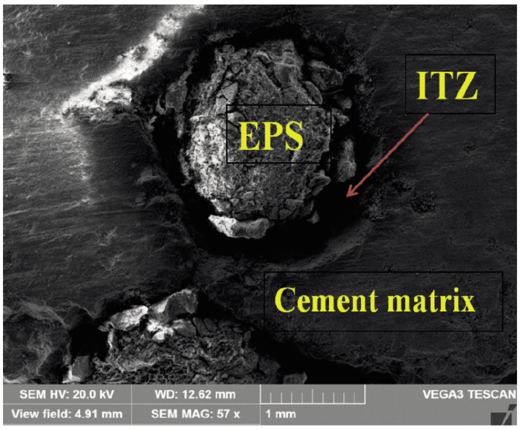

Fig. 13.b *Interfacial transition zone between EPS beads and the cement matrix*
13b. ábra *Felületi átmeneti zóna az EPS gyöngyök és a cementmátrix között*

Fig. 13 d reveals that, the adhesion between EPS and the cement matrix is weak; this is because the EPS beads form agglomerations. The analysis of the interface "cement-aggregate" showed the bad adhesion between the EPS and the cement matrix. Indeed, some gaps have been observed between these two components as shown in *Fig. 13 e*. The incorporation of EPS beads seems affect the total pore volume in the mixture, which results in high porosity and producing a more complex pore network in the composite.

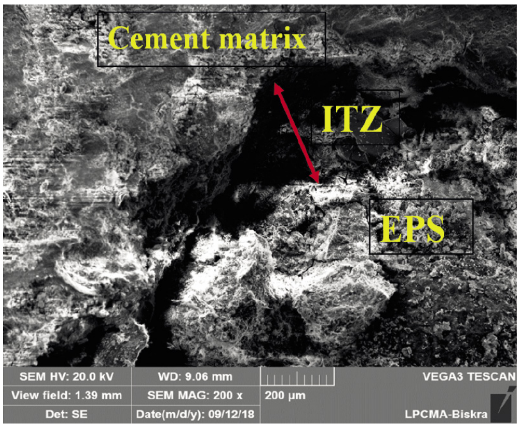

Fig. 13.c *Interfacial transition zone EPS beads and the cement matrix*
13 c. ábra *Felületi átmeneti zóna az EPS gyöngyök és a cementmátrix között*

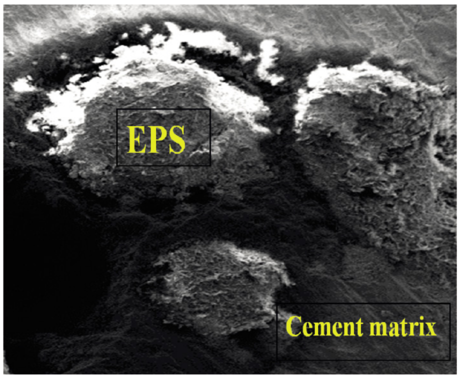

Fig. 13.d SEM observation of the grouping of EPS beads in the mass of the cement matrix
13d. ábra Pásztázó elektronmikroszkópos felvételen az EPS gyöngyök csoportosulása a cement mátrixban

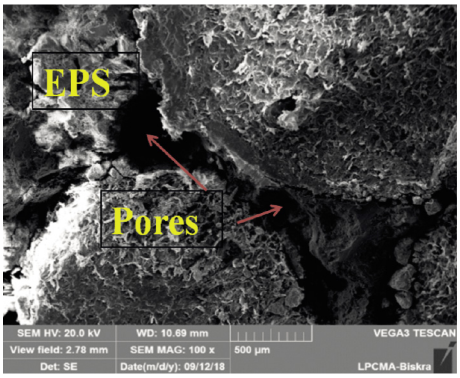

Fig. 13.e Interfacial transition zone EPS beads and the cement matrix
13.e ábra Felületi átmeneti zóna az EPS gyöngyök és a cementmátrix között

3.5 Relationships between the properties of ESP composites

The relationship between the compressive strength and density is illustrated in *Fig. 14*. The figure indicates that the compressive strength of composite decreases proportionally with density; the decrease in compressive strength of the EPS composite is associated with a decrease in density with a good coefficient of correlation ($R^2 > 0.8$). This decrease was about 60% for both strength density. In this aspect, Sayadi et al [9] have found that the evolution of the compressive strength of concretes and mortars decreases with the increase of polystyrene substitution. An improvement of the resistance is obtained for the substitution of 5% in EPS; it is related to the decrease of the percentage of the density of this composite.

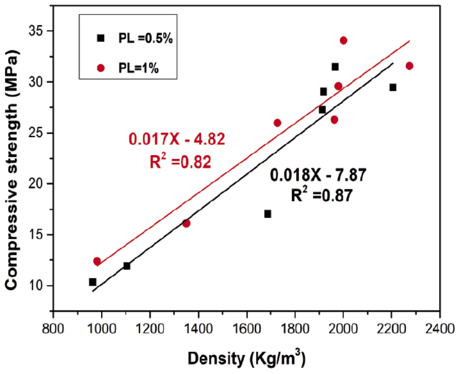

Fig. 14 Correlation between compressive strength and density of EPS composites
14. ábra EPS kompozitok nyomószilárdságának és sűrűségének összefüggése

Fig. 15 shows the correlation established between the compressive strength and thermal conductivity. According to this figure, it is noted that, a decrease in the compressive strengths is associated with a decrease in thermal conductivity. A good non-linear correlation for all mixtures ($R^2 > 0.9$) is found between the two properties.

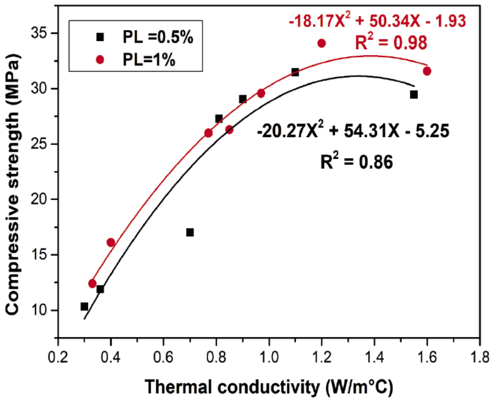

Fig. 15 Correlation between compressive strength and thermal conductivity of EPS composites
15. ábra EPS kompozitok nyomószilárdságának és hővezető képességének összefüggése

Figs. 16 and *17* illustrate the relationship between the thermal conductivity, density and porosity for all mixtures, respectively. It can be seen that, a good linear correlation is therefore observed between the parameters studied with high coefficients of correlation.

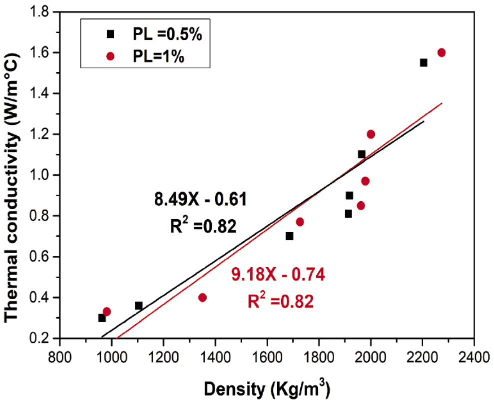

Fig. 16 Correlation between thermal conductivity and density of EPS composites
16. ábra EPS kompozitok hővezető képességének és sűrűségének összefüggése

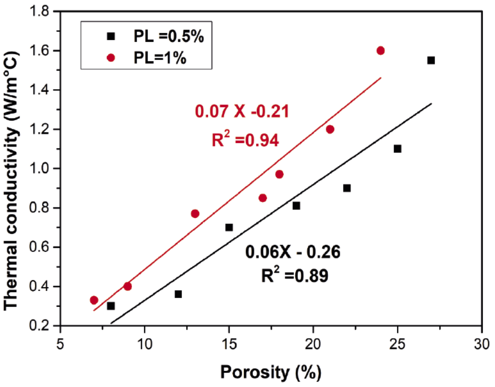

Fig. 17 Correlation between thermal conductivity and porosity of EPS composites
17. ábra EPS kompozitok hővezető képességének és porozitásának összefüggése

4. Conclusions

The present experimental study investigated the physic-mechanical and thermal performances of dune sand mortars containing EPS as aggregate, the following conclusions can be drawn:

- The incorporation of EPS beads as aggregate improved the workability of mortar.
- An increase in the percentage of EPS beads is accompanied by the increase of the air content of the composites, which increases the voids inside the matrix and consequently increases its porosity.
- The compressive strength and flexural tensile strength decreased as the quantity of EPS beads increased, except the mixture with 5% of EPS that gives the best mechanical performance compared to other mixtures.
- The modulus of elasticity of the composites lightened by EPS relatively decreases according to the increase in the percentage of EPS, which means greater deformability in the reference matrices and therefore less risk cracking.
- The increase of EPS percentages of substitution up to 50% decreased significantly the density of the composites.
- The microstructure analysis showed that the use of EPS in mixtures caused an increase in porosity as well as a weak adhesion zone between cement and aggregate.
- The thermal properties of all mixtures are significantly decreased by the addition of the EPS; it was possible to obtain a thermal conductivity equal to 0.30 $Wm^{-1}°C^{-1}$ for when 100% of EPS is used. It should be noted that the obtained values of the thermal conductivity meet the RILEM recommendations, which suggest a coefficient of thermal conductivity less than 0.75 $Wm^{-1}°C^{-1}$ for lightweight concrete construction and insulation applications.
- Finally, the EPS composites could be the subject of several applications, and can be used to reduce the heat transfer and thus to save energy.

Acknowledgments

The authors are very grateful to the head of the department of civil engineering and staff of the civil engineering laboratory of University of Medea, for their assistance in carrying out this experimental work. The staff of the Laboratory of the National Center for Integrated Research and Studies in Building (CNERIB) is warmly thanked for the thermal properties measurements.

References

[1] Ouldkhaoua, Y., Benabed, B., Abousnina, R., Kadri, E., Khatib, J. (2020) Effect of using metakaolin as supplementary cementitious material and recycled CRT funnel glass as fine aggregate on the durability of green self-compacting concrete. Construction and Building Materials. 235, 117802. https://doi.org/10.1016/j.conbuildmat.2019.117802

[2] Thienel, K.C., Haller, T., Beuntner, N. (2020) Lightweight concrete–from basics to innovations. Materials. 13, 1120. https://doi.org/10.3390/ma13051120

[3] Yang, K.H., Mun, J.H., Kim, S.J., Lee, H.J. (2020) Flexural behavior of two-span lightweight aggregate concrete T-beams. ACI Structural Journal. 117, pp. 267-276. https://doi.org/10.14359/51721368

[4] Vakhshouri, B., Nejadi, S. (2018) Review on the mixture design and mechanical properties of the lightweight concrete containing expanded polystyrene beads. Australian Journal of Structural Engineering. 19, pp. 1-23. https://doi.org/10.1080/13287982.2017.1353330

[5] Fenyvesi, O., Jankus, B., (2015) Opportunities in recycling AAC waste as aggregate for lightweight concrete. Építőanyag – Journal of Silicate Based and Composite Materials. 67, pp. 66–70. http://dx.doi.org/10.14382/epitoanyag-jsbcm.2015.11

[6] Ouldkhaoua, Y., Benabed, B., Abousnina, R., Kadri, E. (2019) Rheological properties of blended metakaolin self-compacting concrete containing recycled CRT funnel glass aggregate, Epitoanyag-Journal of Silicate Based & Composite Materials. 71, pp. 154–161. https://doi.org/10.14382/epitoanyag-jsbcm.2019.27

[7] Herki, B., Khatib, J., Negim, E. (2013) Lightweight concrete made from waste polystyrene and fly ash. World Applied Sciences Journal. 21, pp. 1356-1360. https://doi.org/10.5829/idosi.wasj.2013.21.9.20213

[8] Ferrándiz-Mas, V., Bond, T., García-Alcocel, E., Cheeseman, C.R. (2014) Lightweight mortars containing expanded polystyrene and paper sludge ash. Construction and Building Materials. 61, pp. 285-292. https://doi.org/10.1016/j.conbuildmat.2014.03.028

[9] Sayadi, A.A., Tapia, I.V., Neitzert, T.R., Clifton, G.C. (2016) Effects of expanded polystyrene (EPS) particles on fire resistance, thermal conductivity and compressive strength of foamed concrete. Construction and building materials. 112, pp. 716-724. https://doi.org/10.1016/j.conbuildmat.2016.02.218

[10] Ali, M., Maslehuddin, M., Shameem, M., Barry, M. (2018) Thermal-resistant lightweight concrete with polyethylene beads as coarse aggregates. Construction and Building Materials. 164, pp. 739-749. https://doi.org/10.1016/j.conbuildmat.2018.01.012

[11] Benabed, B. (2018) Effect of combined use of crushed sand and Algerian desert dune sand on fresh properties and strength of self-compacting concrete. Epitoanyag-Journal of Silicate Based & Composite Materials. 70, pp. 155-167. https://doi.org/10.14382/epitoanyag-jsbcm.2018.29

[12] Laoubi, H., Djoudi, A., Dheilly, R., Bederina, M., Goullieux, A., Quéneudéc, M. (2019) Durability of a lightweight construction material made with dune sand and expanded polystyrene. Journal of Adhesion Science and Technology. 33, pp. 2157-2179. https://doi.org/10.1080/01694243.2019.1637091

[13] Bédérina, M., Khenfer, M., Dheilly, R., Quéneudec, M. (2005) Reuse of local sand: effect of limestone filler proportion on the rheological and mechanical properties of different sand concretes. Cement and concrete Research. 35, pp. 1172-1179. https://doi.org/10.1016/j.cemconres.2004.07.006

[14] Bouziani, T., Benmounah, A., Bederina, M., Lamara, M. (2011) Effect of marble powder on the properties of self-compacting sand concrete. The Open Construction and Building Technology Journal. 5, pp. 25-29. https://doi.org/10.2174/1874836801105010025

[15] Bouziani, T., Bederina, M., Hadjoudja, M. (2012) Effect of dune sand on the properties of flowing sand-concrete (FSC). International Journal of Concrete Structures and Materials. 6, pp. 59-64. https://doi.org/10.1007/s40069-012-0006-z

[16] Damene, Z., Goual, M., Houessou, J., Dheilly, R., Goullieux, A., Quéneudec, M. (2018) The use of southern Algeria dune sand in cellular lightweight concrete manufacturing: effect of lime and aluminium content on porosity, compressive strength and thermal conductivity of elaborated materials. European Journal of Environmental and Civil Engineering. 22, pp. 1273-1289. https://doi.org/10.1080/19648189.2016.1256233

[17] BS 197-1. (2000) Cement–Part 1: Composition, specifications and conformity criteria for common cements. British Standards Institution.

[18] N. EN, 196-1 (2003) Cements and lime, French Association for Standardization (AFNOR), Paris, 2003.

[19] P. NF, P 15-437 (1987) Hydraulic binders, testing technics. Characterization of cements by fluidity measurement under mortar vibration.

[20] N. EN, 12350-7 (2001) Fresh concrete testing-Part 7.

[21] P 18-435 (2001) Hardened concrete testing - Part 7: Bulk density of concrete.

[22] C. ASTM, 348 (2000) Standard Test Method for Flexural strength of hydraulic-cement mortars. Annual book of ASTM standards 4, pp. 221-226.

[22] C. ASTM, 349-97 (2002) Standard Test Method for Compressive Strength of Hydraulic-Cement Mortars (Using Portions of Prisms Broken in Flexure), Annual book of ASTM 4.

[23] De Ponte, F., Klarsfeld, S. (2002) Conductivité thermique des isolants. Techniques de l'ingénieur. , traité Mesures et Contrôle - Doc. R 2 930.

[24] P. NFP 18-459 (2010) Hardened concrete testing, porosity and bulk density.

[25] C. ASTM 597 (2009) Standard test method for pulse velocity through concrete, ASTM International, West Conshohocken, PA.

[26] Tang, W.C., Lo, Y., Nadeem, A. (2008) Mechanical and drying shrinkage properties of structural-graded polystyrene aggregate concrete. Cement and Concrete Composites. 30, pp. 403-409. https://doi.org/10.1016/j.cemconcomp.2008.01.002

[27] Herki, B. (2017) Absorption characteristics of lightweight concrete containing densified polystyrene. Civil Engineering Journal. 3, pp. 594-609. https://doi.org/10.28991/cej-2017-00000115

[28] Kim, H.K., Jeon, J.H., Lee, H.K. (2012) Workability, and mechanical, acoustic and thermal properties of lightweight aggregate concrete with a high volume of entrained air. Construction and Building Materials. 29, pp. 193-200. https://doi.org/10.1016/j.conbuildmat.2011.08.067

[29] Madandoust, R., Ranjbar, M.M., Mousavi, S.Y. (2011) fresh properties of self-compacted lightweight concrete containing expanded polystyrene. Construction and Building Materials. 25, pp. 3721-3731. https://doi.org/10.1016/j.conbuildmat.2011.04.018

[30] Kan, A., Demirboğa, R. (2007) Effect of cement and EPS beads ratios on compressive strength and density of lightweight concrete. Indian Journal of Engineering and Materials Sciences. 14, pp. 158-162

[31] Tasdemir, C., Sengul, O., Tasdemir, M.A. (2017) A comparative study on the thermal conductivities and mechanical properties of lightweight concretes. Energy and Buildings. 151, pp. 469-475. https://doi.org/10.1016/j.enbuild.2017.07.013

[32] Rahmani, E., Dehestani, M., Beygi, M.H.A., Allahyari, H., Nikbin, I.M. (2013) On the mechanical properties of concrete containing waste PET particles. Construction and Building Materials. 47, pp. 1302-1308. https://doi.org/10.1016/j.conbuildmat.2013.06.041

[33] Saikia, N., De Brito, J. (2014) Mechanical properties and abrasion behaviour of concrete containing shredded PET bottle waste as a partial substitution of natural aggregate. Construction and building materials. 52, pp. 236-244. https://doi.org/10.1016/j.conbuildmat.2013.11.049

[34] Allahverdi, A., Azimi, S.A., Alibabaie, M. (2018) Development of multi-strength grade green lightweight reactive powder concrete using expanded polystyrene beads. Construction and Building Materials. 172, pp. 457-467. https://doi.org/10.1016/j.conbuildmat.2018.03.260

[35] Nikbin, I.M., Golshekan, M. (2018) The effect of expanded polystyrene synthetic particles on the fracture parameters, brittleness and mechanical properties of concrete. Theoretical and Applied Fracture Mechanics. 94, pp. 160-172. https://doi.org/10.1016/j.tafmec.2018.02.002

[36] Kuhail, Z., Shihada, S. (2003) Mechanical properties of polystyrene-lightweight concrete. Journal of Islamic University of Gaza. 11, pp. 93-114

[37] Sohel, K.M.A., Al-Jabri, K., Zhang, M.H., Richard Liew, J.Y. (2018) Flexural fatigue behavior of ultra-lightweight cement composite and high strength lightweight aggregate concrete. Construction and Building Materials. 173, pp. 90-100. https://doi.org/10.1016/j.conbuildmat.2018.03.276

[38] Aboul-Nour, L.A., Zaghlal, A., Yahia, M., Malek, K.A. (2020) Flexural behavior of structural lightweight concrete beam. International Journal of Civil Engineering and Technology. 11, pp.329-339

[39] Assaad, J.J., El Mir, A. (2020) Durability of polymer-modified lightweight flowable concrete made using expanded polystyrene. Construction and Building Materials. 249, 118764. https://doi.org/10.1016/j.conbuildmat.2020.118764

[40] Dixit, A., Dai Pang, S., Kang, S.H., Moon, J. (2019) Lightweight structural cement composites with expanded polystyrene (EPS) for enhanced thermal insulation. Cement and Concrete Composites. 102, pp. 185-197. https://doi.org/10.1016/j.cemconcomp.2019.04.023

[41] Koksal, F., Mutluay, E., Gencel, O. (2020) Characteristics of isolation mortars produced with expanded vermiculite and waste expanded polystyrene. Construction and Building Materials. 236, 2020, 117789. https://doi.org/10.1016/j.conbuildmat.2019.117789

[42] Babu, K.G., Babu, D.S. (2003) Behaviour of lightweight expanded polystyrene concrete containing silica fume. Cement and Concrete Research. 33, pp. 755-762. https://doi.org/10.1016/S0008-8846(02)01055-4

[43] Remesar, J.C., Simon, F., Vera, S., Lopez, M. (2020) Improved balance between compressive strength and thermal conductivity of insulating and structural lightweight concretes for low-rise construction. Construction and Building Materials. 247, 118448. https://doi.org/10.1016/j.conbuildmat.2020.118448

[44] RILEM. (1970) Commission des bétons légers. Terminologie et définition. Matériaux et construction Terminology and definition. Materials and Construction. pp. 60-69.

[45] Laoubi, H., Bederina, M., Djoudi, A., Goullieux, A., Dheilly, R.M., Queneudec, M. (2018) Study of a new plaster composite based on dune sand and expanded polystyrene as aggregates. The Open Civil Engineering Journal. 12, pp. 4016412. https://doi.org/10.2174/1874149501812010401

[46] NF P 75 101. Thermal Insulators for Building. October 1983.

Ref.:

Herihiri, Ouided – **Guettala**, Abdelhamid – **Benabed**, Benchaa: *An investigation on the physical, mechanical and thermal properties of dune sand mortars lightened by expanded polystyrene beads (EPS)*
Építőanyag – Journal of Silicate Based and Composite Materials, Vol. 73, No. 1 (2021), 28–36. p.
https://doi.org/10.14382/epitoanyag-jsbcm.2021.6

GUIDELINE FOR AUTHORS

The manuscript must contain the followings: title; author's name, workplace, e-mail address; abstract, keywords; main text; acknowledgement (optional)**; references; figures, photos with notes; tables with notes; short biography** (information on the scientific works of the authors).

The full manuscript should not be more than 6 pages including figures, photos and tables. Settings of the word document are: 3 cm margin up and down, 2,5 cm margin left and right. Paper size: A4. Letter size 10 pt, type: Times New Roman. Lines: simple, justified.

TITLE, AUTHOR

The title of the article should be short and objective.

Under the title the name of the author(s), workplace, e-mail address.

If the text originally was a presentation or poster at a conference, it should be marked.

ABSTRACT, KEYWORDS

The abstract is a short summary of the manuscript, about a half page size. The author should give keywords to the text, which are the most important elements of the article.

MAIN TEXT

Contains: materials and experimental procedure (or something similar), results and discussion (or something similar), conclusions.

REFERENCES

References are marked with numbers, e.g. [6], and a bibliography is made by the reference's order. References should be provided together with the DOI if available.

Examples:

Journals:

[6] Mohamed, K. R. – El-Rashidy, Z. M. – Salama, A. A.: In vitro properties of nano-hydroxyapatite/chitosan biocomposites. *Ceramics International.* 37(8), December 2011, pp. 3265–3271, http://doi.org/10.1016/j.ceramint.2011.05.121

Books:

[6] Mehta, P. K. – Monteiro, P. J. M.: Concrete. Microstructure, properties, and materials. *McGraw-Hill*, 2006, 659 p.

FIGURES, TABLES

All drawings, diagrams and photos are figures. The **text should contain references to all figures and tables**. This shows the place of the figure in the text. Please send all the figures in attached files, and not as a part of the text. **All figures and tables should have a title.**

Authors are asked to submit color figures by submission. Black and white figures are suggested to be avoided, however, acceptable.

The figures should be: tiff, jpg or eps files, 300 dpi at least, photos are 600 dpi at least.

BIOGRAPHY

Max. 500 character size professional biography of the author(s).

CHECKING

The editing board checks the articles and informs the authors about suggested modifications. Since the author is responsible for the content of the article, the author is not liable to accept them.

CONTACT

Please send the manuscript in electronic format to the following e-mail address: femgomze@uni-miskolc.hu and epitoanyag@szte.org.hu or by post: Scientific Society of the Silicate Industry, Budapest, Bécsi út 122–124., H-1034, HUNGARY

We kindly ask the authors to give their e-mail address and phone number on behalf of the quick conciliation.

Copyright

Authors must sign the Copyright Transfer Agreement before the paper is published. The Copyright Transfer Agreement enables SZTE to protect the copyrighted material for the authors, but does not relinquish the author's proprietary rights. Authors are responsible for obtaining permission to reproduce any figure for which copyright exists from the copyright holder.

Építőanyag – *Journal of Silicate Based and Composite Materials* allows authors to make copies of their published papers in institutional or open access repositories (where Creative Commons Licence Attribution-NonCommercial, CC BY-NC applies) either with:

- placing a link to the PDF file at **Építőanyag** – *Journal of Silicate Based and Composite Materials* homepage or
- placing the PDF file of the final print.

Építőanyag – *Journal of Silicate Based and Composite Materials*, Quarterly peer-reviewed periodical of the Hungarian Scientific Society of the Silicate Industry, SZTE.
http://epitoanyag.org.hu

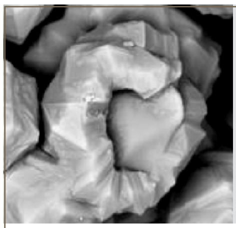

We are pleased to announce the organization of

ic-cmtp6

THE 6TH INTERNATIONAL CONFERENCE ON COMPETITIVE MATERIALS AND TECHNOLOGY PROCESSES

to be held in Hotel Palota in Miskolc-Lillafüred in May 3-7, 2021

The **ic-cmtp6** conference will be held in the wonderful palace of **Hotel Palota** in the exceptionally beautiful environment of **Beech Mountain** in **Miskolc-Lillafüred** in **Hungary**. In 2018 in the previous conference scientists had participated from **46** countries of **5** continents and the largest delegations have arrived from **Japan, Russian Federation, China, Czech Republic,** and **Korea**.

THE CONFERENCE SESSIONS

1. Advanced Ceramics and Nanoceramics
2. Advanced Composites and Nanocomposites
3. Advanced Materials for Bio- and Medical Applications
4. Advanced Materials for Extreme Applications
5. Advanced Nanomaterials and Nanocomposites
6. Advanced Optical Materials – Properties and Applications
7. Advanced Polymer-Clay Nanocomposites
8. Advanced Powder Metallurgy Materials
9. Advanced Processing and Characterization Methods for Nanocomposites
10. Bioelectronic Materials and Biosensors
11. Biomaterials Derived Ceramics and Nanocomposites
12. Clay Minerals and Organo-Clay Complexes
13. CO2 Capture and Fixing Materials and Methods
14. Glasses and Related Competitive Materials
15. Graphene – Properties and Applications
16. Hetero-Modulus and Hybrid Materials
17. Intelligence and Smart Materials – Structures, Properties and Applications
18. Interface as a Functional Material – Behavior, Function and Application
19. Light Weight Materials with Predesigned and Controlled Nanostructur
20. Materials and Methods to Capture and Fixing Radioactive Pollutants from Waters and Soils
21. Materials for Membranes and Catalysts
22. Materials for Biological Systems and Health
23. Materials for Energy Saving and Conservation
24. Materials for Harvesting Renewable Energy
25. Materials for Sensors and Actuators
26. Materials with Extreme Dynamic Strength
27. Mechanical Properties and Processing Technology of Advanced Materials
28. Minerals for Environmental and Medical Application
29. Nanomaterials Applied to Biomedical Applications and Nanomedicine
30. Nanomaterials for Electronic and Electrotechnical Applications
31. Novel Synthesis and Processing Technology
32. Polymer Derived Ceramics and Advanced Nanocomposites
33. Processing and Properties of Silicate Ceramics
34. Sol-Gel Technology in Materials Processing
35. Testing and Characterization of Materials – Methods, Equipment and Uncertainties
36. Traditional Ceramics and Building Materials
37. Traditional Ferrous and Nonferrous Metals

In case of pandemic quarantine of COVID-19 or other force majeure situation the conference ic-cmtp6 will be held in the same place in October 4-8, 2021.

Registration and further information: www.ic-cmtp6.eu